Optimizing Chemogenetic Ablation of Dopaminergic Neurons and Establishing Single-Cell Brain Dissociation Protocols for scRNA-seq in Adult Zebrafish

Herman Aishi Mbesha

Thesis submitted to the University of Ottawa in partial fulfillment of the requirements for the Master's degree in Biology

Department of Biology
Faculty of Science
University of Ottawa

ACKNOWLEDGMENTS

I would like to begin by expressing my deepest gratitude to my wonderful supervisor, Dr. Marc Ekker, for his invaluable guidance, mentorship, and unwavering support throughout my graduate studies. His vision, encouragement, and openness to new ideas created a stimulating and supportive environment that allowed me to grow not only as a researcher but also as a person.

I am also sincerely thankful to the members of the Ekker Lab, past and present, whose advice, encouragement, and camaraderie have been an essential part of my research journey. I am particularly grateful to Emily Yu, Michael Kalyn, and Ryan Lambert for their thoughtful discussions, assistance, and support in troubleshooting experiments. I am also indebted to Vishal Saxena, whose technical expertise and practical advice were instrumental in guiding me through key challenges in my project.

My heartfelt thanks also go to my TAC committee members, Dr. Marie-Andrée Akimenko and Dr. Bill Willmore, for their continued guidance throughout my graduate studies. Their evaluations of my progress and thoughtful recommendations helped me navigate challenges along the way and provided valuable perspective on how to strengthen my research direction.

Finally, I owe my deepest gratitude to my partner, Noëlle Buzohera, and to my family for their patience, love, and unwavering support throughout this journey. Their belief in me and constant encouragement provided the foundation I needed during the most challenging times. None of this work would have been possible without them.

ABSTRACT

Parkinson's disease (PD) is a progressive neurodegenerative disorder marked by the loss of midbrain dopaminergic neurons, producing motor and non-motor symptoms. Adult zebrafish (*Danio rerio*) offer unique advantages for studying both degeneration and regeneration, yet existing chemogenetic PD models are mostly larval and rely on immersion-based prodrug delivery, which yields incomplete or biased ablation.

This thesis aimed to establish an adult zebrafish PD model by combining nitroreductase (NTR)-activated prodrugs, metronidazole (MTZ), nifurpirinol (NFP), and ronidazole (RON) with cerebroventricular microinjection (CVMI) for brain-wide delivery. Dopaminergic neuron survival was quantified in the olfactory bulb, telencephalon, and diencephalon using tyrosine hydroxylase (TH) and cyan fluorescent protein (CFP), the latter expressed under regulatory elements of the dopamine transporter (DAT) promoter. Behavioural assays assessed locomotor and olfactory function at 1 and 7 days post-treatment.

No significant reductions in dopaminergic neuron counts or behavioural impairments were observed compared with vehicle controls. This outcome likely reflects multiple constraints: the low solubility and limited bioavailability of prodrugs, the modest catalytic efficiency of first-generation NTR, and possible rapid neuronal regeneration in adults. Technical factors such as autofluorescence and reliance on manual counts may also have masked subtle changes.

In parallel, this work piloted adult brain dissociation for single-cell RNA sequencing (scRNA-seq). While single-cell suspensions were obtained, viability assessment by microscopy proved insufficient, highlighting the need for quantitative approaches such as flow cytometry.

Overall, this thesis identifies key methodological limitations and outlines strategies, including NTR 2.0 transgenics, refined prodrug delivery, and optimized cell dissociation, that will enable robust adult zebrafish PD models for regenerative studies.

RÉSUMÉ

La maladie de Parkinson (PD) est un trouble neurodégénératif caractérisé par la perte de neurones dopaminergiques du mésencéphale, entraînant des symptômes moteurs et non moteurs. Le poisson-zèbre adulte (*Danio rerio*) présente des avantages uniques pour étudier à la fois la dégénérescence et la régénération; toutefois, les modèles chimiogénétiques existants de la PD sont principalement larvaires et reposent sur une administration des promédicaments par immersion, ce qui entraîne une ablation incomplète de neurones dopaminergiques.

Cette thèse visait à établir un modèle adulte de PD chez le poisson-zèbre en combinant des promédicaments activés par la nitroréductase (NTR), le métronidazole (MTZ), le nifurpirinol (NFP) et le ronidazole (RON) à la microinjection cérébroventriculaire (CVMI) afin d'assurer une distribution à l'ensemble du cerveau. La survie des neurones dopaminergiques a été quantifiée dans le bulbe olfactif, le télencéphale et le diencéphale à l'aide du marquage de la tyrosine hydroxylase (TH) et de la protéine fluorescente cyan (CFP), cette dernière étant exprimée sous le contrôle des éléments régulateurs du promoteur du transporteur de la dopamine (DAT).

Les fonctions locomotrices et olfactives ont été évaluées à 1 et 7 jours post-traitement. Aucune diminution significative du nombre de neurones dopaminergiques ni altération comportementale n'a été observée par rapport aux contrôles véhicule (DMSO 0,2 %). Ce résultat reflète probablement plusieurs contraintes, notamment la faible solubilité et la biodisponibilité limitée des promédicaments, l'efficacité catalytique modeste de la NTR de première génération, ainsi qu'une possible régénération neuronale rapide chez l'adulte.

En parallèle, ce travail a mis à l'essai la dissociation du cerveau adulte en vue du séquençage d'ARN unicellulaire (scRNA-seq). Bien que des suspensions monocellulaires aient

été obtenues, l'évaluation de la viabilité par microscopie s'est révélée insuffisante, soulignant la nécessité d'approches quantitatives telles que la cytométrie en flux.

Globalement, cette thèse met en évidence des limites méthodologiques clés et propose des pistes d'amélioration dont l'utilisation de lignées transgéniques NTR 2.0, l'optimisation de l'administration des promédicaments et le raffinement des protocoles de dissociation pour établir des modèles adultes robustes de la maladie de Parkinson chez le poisson-zèbre, adaptés à l'étude des mécanismes régénératifs.

TABLE OF CONTENTS

LIST OF FIGURES

LIST OF TABLES

LIST OF ABBREVIATIONS

6-OHDA	6-hydroxydopamine
ANOVA	analysis of variance
AO	acridine orange
BSA	bovine serum albumin
CFP	cyan fluorescent protein
CNS	central nervous system
COMT	catechol-O-methyltransferase
CRISPR	clustered regularly interspaced short palindromic repeats
CVF	cerebroventricular fluid
CVMI	cerebroventricular microinjection
DA	dopaminergic
DAT	dopamine transporter
DAPI	4′,6-diamidino-2-phenylindole
DJ-1	Parkinson's disease protein 7
DMSO	dimethyl sulfoxide
dpf	days post-fertilization
dpt	days post-treatment
EGFP	enhanced green fluorescent protein
EOPD	early-onset Parkinson's disease
ETC	electron transport chain
FBS	fetal bovine serum
GFP	green fluorescent protein
hpf	hours post-fertilization
IHC	immunohistochemistry
LRRK2	leucine-rich repeat kinase 2
MAO	monoamine oxidase
MO	morpholino (antisense oligonucleotide)
MPP^+	1-methyl-4-phenylpyridinium (toxic metabolite of MPTP)
MPTP	1-methyl-4-phenyl-1,2,3,6-tetrahydropyridine

MTZ	metronidazole
NAc	nucleus accumbens
NFP	nifurpirinol
NTR	nitroreductase
OB	olfactory bulb
PBS	phosphate-buffered saline
PBST	PBS with Tween-20
PD	Parkinson's disease
PFA	paraformaldehyde
PI	propidium iodide
PINK1	PTEN-induced kinase 1 (Parkinson's disease gene)
PRKN	Parkin (Parkinson's disease gene)
RON	ronidazole
ROS	reactive oxygen species
SN	substantia nigra
SNCA	α-synuclein (gene name for alpha-synuclein)
SNpc	substantia nigra pars compacta
TALEN	transcription activator-like effector nuclease
TH	tyrosine hydroxylase
VTA	ventral tegmental area

1. Introduction

1.1 Clinical and Neuropathological Overview of PD

Parkinson's disease is a progressive neurodegenerative disorder that predominantly manifests in later life with motor symptoms such as generalized slowing of movement (bradykinesia), resting tremors, rigidity, and postural instability. As the disease advances, these motor symptoms typically become more pronounced. However, the clinical picture of PD extends beyond motor dysfunction. Non-motor symptoms, including mood disorders, anosmia (loss of smell), hypersalivation, sleep disturbances, and gastrointestinal issues like constipation, often emerge years or even decades before the onset of apparent motor impairments. PD is currently the second most prevalent neurodegenerative disease after Alzheimer's disease (Antony et al., 2013). It is multifactorial, with both genetic and environmental contributors. Age remains the strongest risk factor, with prevalence estimates in industrialized nations hovering around 0.3% of the general population and approximately 1% among individuals over 60 years old (Sveinbjornsdottir, 2016).

The hallmark pathology of PD includes the presence of Lewy bodies, intracytoplasmic inclusions composed primarily of aggregated alpha-synuclein, and the progressive, selective degeneration of dopaminergic (DA) neurons, particularly within the substantia nigra pars compacta (SNpc) of the midbrain. Dopamine plays a crucial role in diverse cognitive and motor functions, including reward processing, learning, and movement control. Its depletion in PD underlies key clinical features such as tremors, rigidity, and bradykinesia (Tysnes & Storstein, 2017). Notably, clinical motor symptoms typically appear only after 50-80% of DA neurons are lost (Cheng et al., 2010), underscoring the stealthy progression of the disease. Meanwhile, a range

of non-motor symptoms, including anxiety, depression, fatigue, sleep and olfactory disturbances, are often observed and can precede motor onset by up to a decade (Sveinbjornsdottir, 2016).

Neuropathologically, Braak and colleagues (Braak et al., 2003, 2004) proposed a six-stage model of PD progression as shown in Figure 1. In the early, pre-symptomatic stages (stages 1-2), Lewy body pathology is first detected in the olfactory bulb and lower brainstem regions such as the medulla oblongata and pontine tegmentum. As the disease advances into stages 3-4, the pathology reaches midbrain areas, including the substantia nigra, typically corresponding with the emergence of clinical motor symptoms. In the later stages (5-6), more widespread involvement of the neocortex gives rise to complex cognitive and behavioural symptoms.

While most PD cases are idiopathic, approximately 10-15% report a family history, and 5% exhibit Mendelian inheritance patterns (Kouli et al., 2018). Genes associated with familial PD are designated with the PARK nomenclature and include several key loci implicated in protein degradation, mitochondrial dynamics, and oxidative stress responses. Despite advances in understanding the pathological features and genetic underpinnings of PD, the precise molecular and cellular mechanisms responsible for the loss of DA neurons remain unclear. As such, current treatments are largely palliative, aimed at alleviating symptoms rather than halting or reversing disease progression.

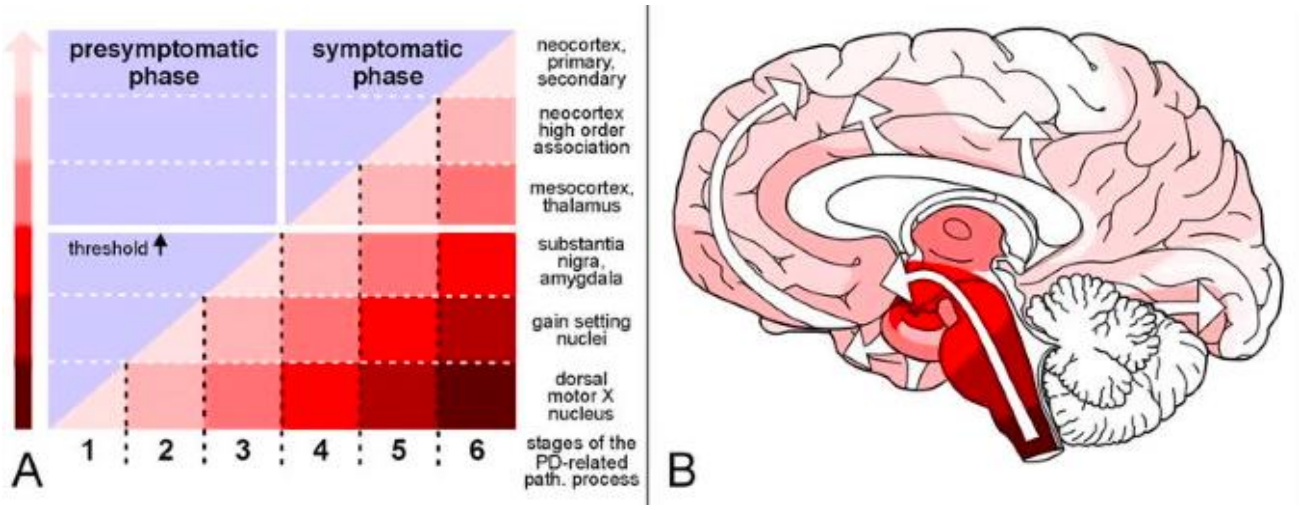

Figure 1. Schematic showing PD progression in six neuropathological stages. (**A)** The presymptomatic phase is marked by the appearance of inclusion bodies. In the symptomatic phase, the individual neuropathological threshold is exceeded (black arrow). The increasing slope and intensity of the colour indicate the growing severity of the pathology in vulnerable brain regions. (**B)** Diagram showing the ascending pathological process (white arrows). Adapted from (Braak et al., 2004).

1.2 Dopaminergic System and Its Relevance to PD

DA neurons form anatomically and functionally heterogeneous cell groups.(Gasiorowska et al., 2021). Immunohistochemistry (IHC) studies identified nine dopaminergic cell groups in the mammalian brain, primarily within the diencephalon, mesencephalon, and olfactory bulb (Björklund & Dunnett, 2007; Chinta & Andersen, 2005). In mammals, dopamine comprises 80% of the catecholamine content in the brain, establishing it as the predominant neurotransmitter of its kind. Its function is well conserved across nearly all animal species, from roundworms to humans. Tyrosine hydroxylase, a widely used marker for these cells, catalyzes the hydroxylation of tyrosine

to L-DOPA, which is then rapidly decarboxylated to dopamine by aromatic L-amino acid decarboxylase, as shown in Figure 2 (Musacchio, 1975).

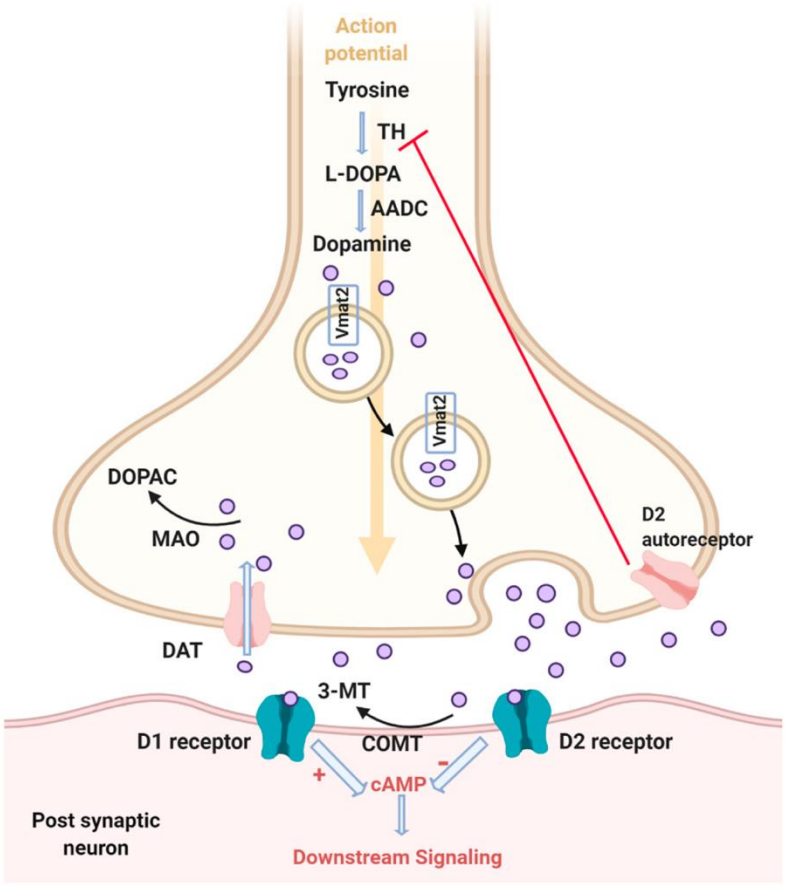

Figure 2. Dopamine signalling pathway. (Wang & Cao, 2021)

DA is packaged into vesicles by the vesicular monoamine transporter 2 (VMAT2) and transported to its cellular release sites. Once released, DA acts on two major families of receptors. Both G-protein coupled, D1-type and D2-type. The activation of D1-type receptors promotes synaptic plasticity and increases neuronal excitability, while activation of D2-type family receptors has the opposite effect. The postsynaptic effects of dopamine are regulated by the rate of

extracellular dopamine clearance. Regulators such as monoamine oxidase (MAO), catechol-O-methyltransferase (COMT), norepinephrine transporter and dopamine transporter (DAT) are responsible for the extracellular dopamine modulation. The latter, being the most efficient dopamine clearance mechanism, is used as another marker for DA neurons. By regulating the duration and amplitude of extracellular dopamine, DAT modulates the binding of dopamine to its receptor and thus influences behaviour.

Despite dopamine acting as a neurotransmitter in several neural circuits such as the olfactory bulb, retina and hypothalamus, most of the dopamine in the mammalian brain is produced by a subset of neurons located in the ventral midbrain, specifically the ventral tegmental area (VTA) and the substantia nigra (SN), the latter holding substantially more DA neurons. There are at least eight dopaminergic pathways in the brain (Björklund & Lindvall, 1984), but most of the dopamine in the brain is distributed via four pathways (Figure 3). The tuberoinfundibular pathway originates from the hypothalamus and three main projections stemming from dopaminergic neurons of the midbrain and projecting to the cortex, ventral and dorsal striatum. These projections form the mesocortical, mesolimbic, and nigrostriatal pathways, respectively.

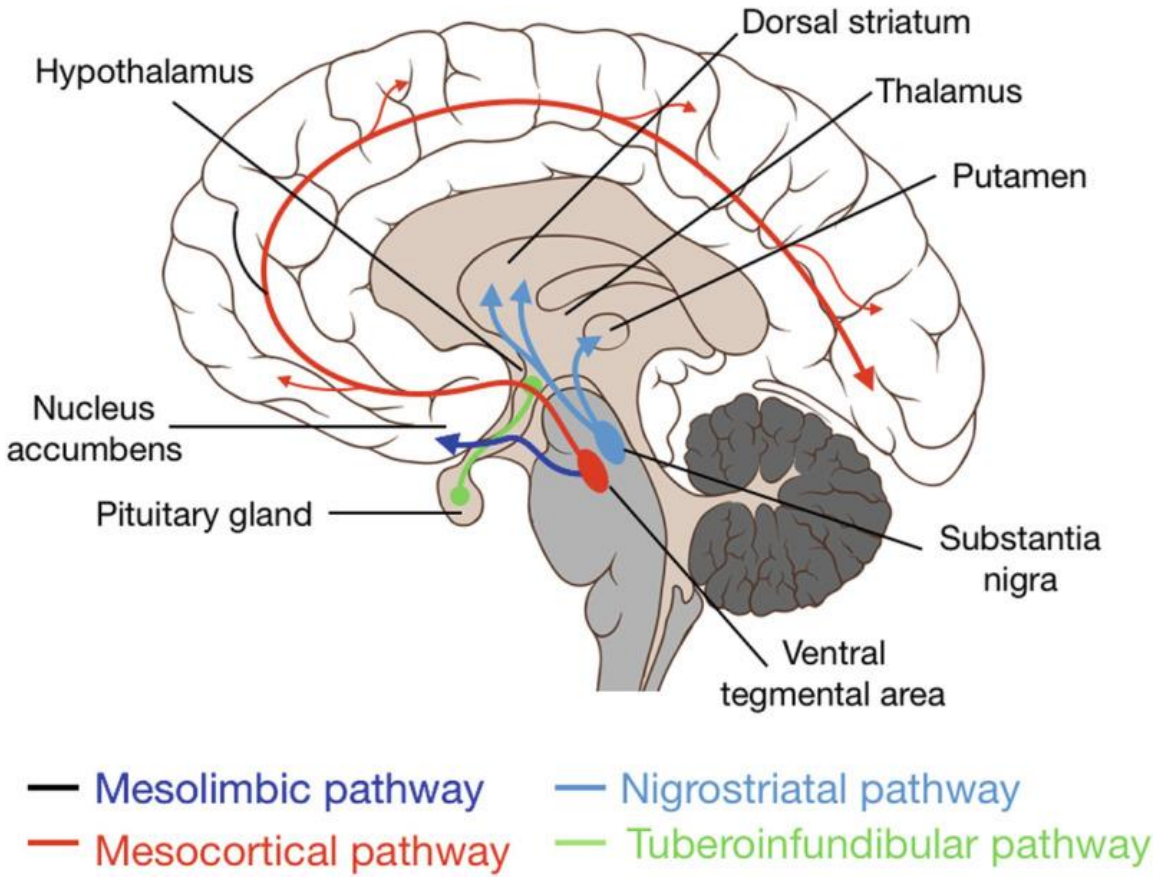

Figure 3. Main dopamine pathways in the brain. (Nummenmaa et al., 2022)

Tuberoinfundibular pathway: DA neurons originate in the arcuate nucleus of the hypothalamus and deliver dopamine to the pituitary gland. In this pathway, dopamine functions as a hormone rather than a neurotransmitter. It inhibits the release of prolactin from the anterior lobe of the pituitary gland. Prolactin is a protein secreted by the pituitary gland that enables maternal lactation(Grattan, 2015)

Mesocortical pathway: Closely associated with the mesolimbic pathways, it originates in the VTA and projects to the prefrontal cortex, which is highly involved in cognition, working memory and decision making. This pathway is believed to behave abnormally in individuals suffering from neuropsychiatric diseases such a schizophrenia. (Blaess et al., 2020)

Mesolimbic pathway: Originates in the VTA of the midbrain with projections to the nucleus accumbens (NAc) and amygdala.(Blaess et al., 2020). The NAc is in the ventral medial portion of the striatum. Dopamine primarily mediates feelings of pleasure and reward. Thus, rewarding or pleasurable stimuli such as food, copulation, drugs, etc., cause the release of dopamine from the VTA to the NAc, which creates a positive feeling that reinforces the behaviour. The amygdala is a key component of the limbic system and is associated with emotion. Given the nature of the cognitive sensations associated with this pathway, many theories have been proposed suggesting this pathway is involved in conditions such as addiction and depression. (Van den Heuvel & Pasterkamp, 2008)

Nigrostriatal pathway: Contains around 80% of dopamine in the brain. It is characterized by dopaminergic fibres projecting from the SNpc to the dorsal striatum, specifically the caudate and putamen. The DA neurons in this pathway stimulate purposeful movement. Given the implication in locomotion of DA neurons in this pathway, a reduction in their number can result in motor control impairments, including movement disorders such as PD.

1.2 Zebrafish as a Model for Parkinson's Disease

Zebrafish have been commonly used in developmental biology as a model organism. It is now emerging as a model for human diseases. Zebrafish (*Danio rerio*) are cheap and easy to sustain, breed transparent embryos in large amounts, and are easily manipulated by different methods, particularly genetic ones. In addition, zebrafish is a vertebrate species, meaning the findings obtained from zebrafish may be more applicable to humans than those derived from genetic models of invertebrates such as Drosophila melanogaster and Caenorhabditis elegans.

With its close neurofunctional and behavioural similarities to humans, the zebrafish has become an excellent model of neurodegenerative, neurodevelopmental, and neuropharmacological studies (Vaz et al., 2018). While there are some significant variations between the brain of the zebrafish and that of humans in terms of form and size, the overall organization shows similarity. When compared with their human counterparts, certain zebrafish brain regions show striking structural conservation and may share functional links (Figure 4) (Razali et al., 2021).

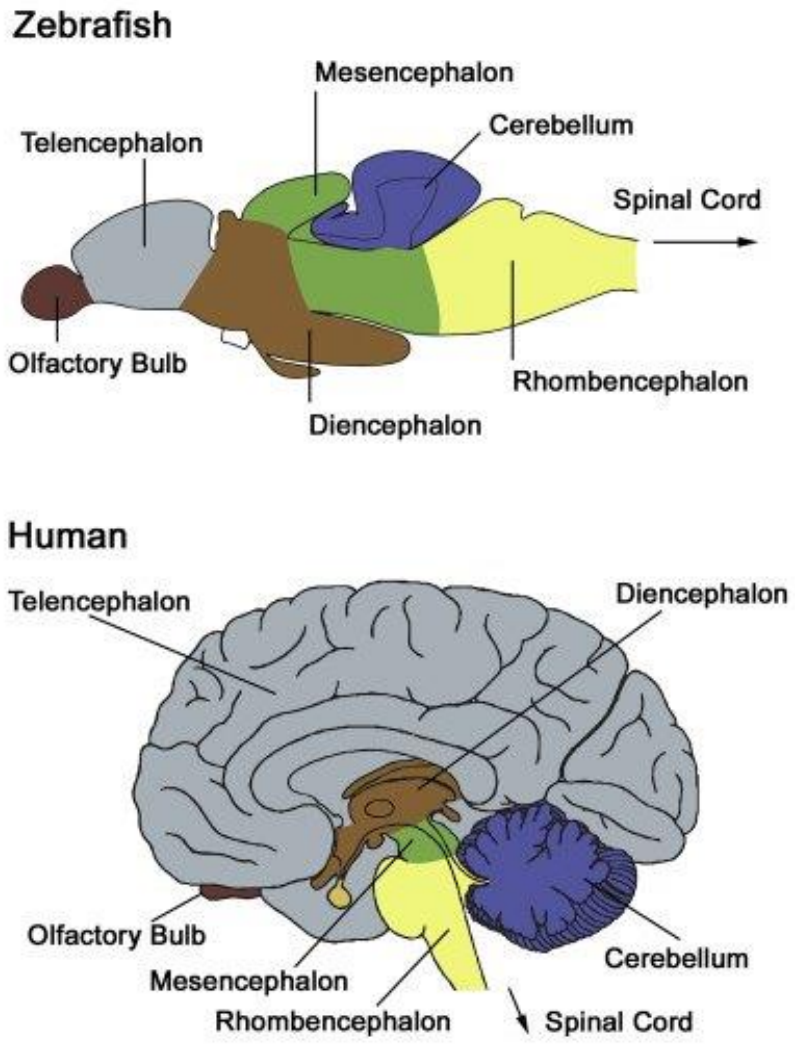

Figure 4. Conservation of CNS organization between human and zebrafish. (Bartel et al., 2020)

The earliest presence of DA neurons in the zebrafish embryo was detected at 19th hour post-fertilization (hpf) in the posterior tuberculum of ventral diencephalon, the region that is equivalent to human Substantia Nigra, and the cluster of these neurons was shown to project to ventral telencephalon, the zebrafish equivalent of human striatum (Figure 5). The whole process is believed to be the zebrafish equivalent of the nigrostriatal dopaminergic nervous system (Flinn et al., 2008), which is a feature that is undoubtedly important in PD pathology.

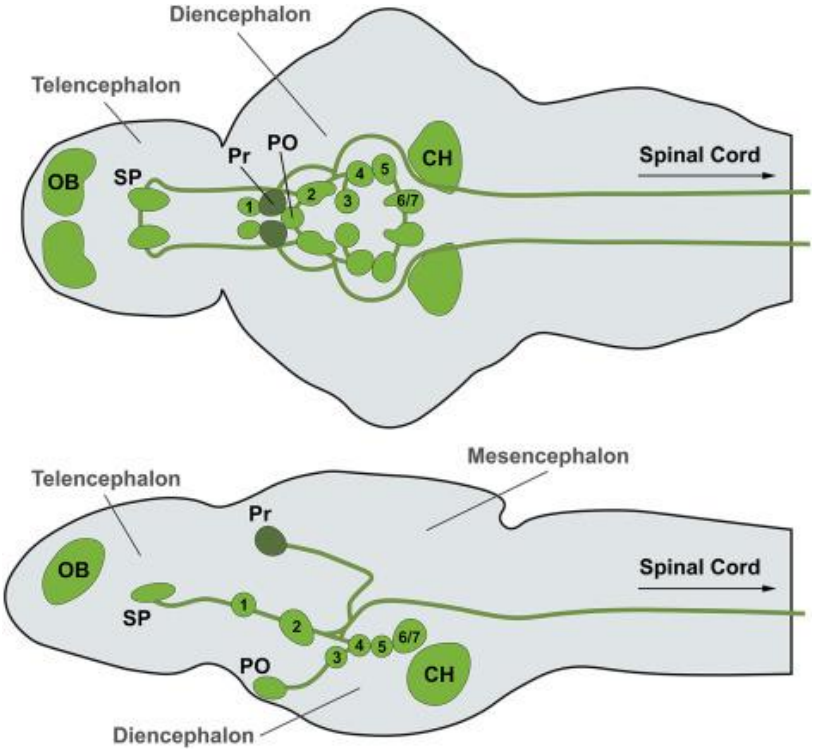

Figure 5. Major groups of dopaminergic neurons in zebrafish larvae 5 days post-fertilization. CH, caudal hypothalamus; OB, olfactory bulb; PO, preoptic area; Pr, pretectum; SP, subpallium. Neurons of DC2/4 that send axonal projections to the telencephalon are considered to be the anatomical homolog of the mammalian nigrostriatal system. (Bartel et al., 2020)

Aside from their neuro-functional similarity to humans, zebrafish demonstrate behaviours and phenotypes that mirror human conditions. For example, when exposed to neurotoxins, zebrafish show movement impairments such as reduced swimming speed and disorganized swimming patterns, changes that translate to bradykinesia-like symptoms observed in Parkinson's disease patients (Hughes et al., 2020).

In the genetic context, whole-genome sequencing has revealed that the zebrafish genome shares approximately 70 % overall similarity with the human genome, with roughly 80 % of the genes residing on the same chromosomes and in the same order, indicating conserved synteny between the two species (Howe et al., 2013).

Unlike mammals, adult zebrafish possess widespread neurogenesis and can regenerate neurons lost to injury or disease (Gemberling et al., 2013). This regenerative capacity depends on numerous proliferating ventricular progenitors, whereas the mammalian brain contains only a few such cells and therefore has a limited ability to generate new neurons in adulthood. Following dopaminergic neuron ablation, zebrafish activate intrinsic repair programs that involve signalling pathways such as Wnt, Notch, Sonic Hedgehog and immune-modulated cues, eventually leading to functional recovery (Godoy et al., 2020). Hence, an adult zebrafish model that reproduces PD-like dopaminergic neuron loss offers an exceptional opportunity to investigate the molecular mechanisms that control vertebrate neuron regeneration insights with clear therapeutic relevance.

To analyze these mechanisms at the cellular resolution, advanced transcriptomic tools such as single-cell RNA sequencing can be employed. scRNA-seq enables genome-wide expression profiling of individual cells, uncovering cellular heterogeneity, rare populations and dynamic gene-regulatory networks (Pandey et al., 2023). In zebrafish neurobiology, scRNA-seq has already uncovered specific progenitor subtypes within the habenula region (Pandey et al., 2018, 2023).

Moreover, single-cell transcriptomics applied to injury models has revealed complex inflammatory responses and signalling cascades activated by tissue damage (Cortada et al., 2024). Applying scRNA-seq to an optimized adult PD model could similarly elucidate transcriptional programs driving dopaminergic neuron regeneration, highlighting candidate genes and pathways not previously linked to adult neurogenesis.

1.4 Current approaches for modelling DA neuron ablation in zebrafish

An optimal model for PD would include hallmark pathological features of PD, including the formation of Lewy bodies and selective degeneration of DA neurons, which manifests with both motor and non-motor symptoms mirroring the clinical presentation of PD. Zebrafish have been the object of extensive experimental studies to model the DA neuron loss associated with neurodegenerative diseases. Three main approaches have been used: gene-based models, chemical-based models and chemogenetic ablation models.

1.4.1 Gene-based models

Zebrafish gene-based modelling has progressed from broad, labour-intensive screens to pinpoint genome editing. Early studies relied on random mutagenesis followed by exhaustive phenotyping to locate informative lesions; this workflow was streamlined by TILLING, which couples mutagenesis with targeted sequencing to find mutations in predetermined loci. Subsequent loss-of-function methods introduced zinc-finger nucleases and antisense morpholinos for locus-specific cuts or transient knockdowns. Stable transgenesis then improved from low-efficiency plasmid injections (~5 % germ-line transmission) to the Tol2 transposase system, which raises transmission to 50-70 %. The current generation employs high-precision editors TALENs and,

most notably, CRISPR/Cas9-to create knock-out or knock-in lines in Parkinson-related genes such as Parkin (PRKN), PTEN-induced kinase 1 (PINK)1, DJ-1, Leucine-rich repeat kinase 2 (LRRK2) and SNCA (Doyle & Croll, 2022).

Mutations in the Parkin gene are the most common autosomal-recessive mutations in early-onset Parkinson's disease (EOPD). The Parkin gene encodes an E3 ubiquitin ligase, which is involved in the proteasome degradation system and may be involved in mitochondrial function. Zebrafish parkin has 62 % similarity with the human counterpart. A study by L. Flinn et al., 2009), using MOs caused a 20% decrease in the number of diencephalic DA neurons, the mutation reduced mitochondrial Complex 1 activity, similar to what is observed in human patients. The 20% decrease in diencephalic DA neurons did not translate into PD-like motor symptoms.

Mutations in the gene encoding PINK1 are the second most common cause of autosomal-recessive EOPD (Xi et al., 2011). Zebrafish pink1, which is 54% similar to human PINK1, is expressed ubiquitously in larvae but found only in the periventricular zones and in some diencephalic dopaminergic neurons of the adult fish brain (Anichtchik et al., 2008). A pink1−/− mutant zebrafish, identified using TILLING, showed loss of dopaminergic neurons, increased mitochondrial size and decreased mitochondrial Complex I and III activity in both larvae and adults (L. J. Flinn et al., 2013).

DJ-1 is a redox-sensitive chaperone that protects against oxidative stress. Mutations in the gene encoding DJ-1 (also known as PARK7) have been linked to autosomal-recessive EOPD, causing altered mitochondrial morphology and increased production of ROS (Cookson, 2005). The zebrafish Dj1 protein is 83% identical to the human version and is expressed throughout the brain, including in dopaminergic neurons in the CNS (specifically cell groups in the olfactory bulbs, diencephalon and telencephalon) (Bai et al., 2006). The CRISPR-Cas9 method was used to

produce a dj1-deficient zebrafish, which developed normally until the adult stage, at which point the fish began to exhibit low body mass and lower levels of TH. A proteomic analysis of the brains revealed a dysregulation in proteins involved with mitochondrial mitophagy, redox regulation, stress response and inflammation (Edson et al., 2019).

LRRK2: Mutations in the gene encoding LRRK2 are the most prevalent cause of autosomal dominant PD in humans. (Blandini & Armentero, 2012). Not much is known about the function of LRRK2, but it seems to be involved in neurodegeneration and kidney function (MacLeod et al., 2006). The zebrafish orthologue lrrk2 has a 38% similarity to its human counterpart (Sager et al., 2010). Evidence from MO knockdowns (Ren et al., 2011; Sheng et al., 2010) suggests that loss of lrrk2 function is associated with dopaminergic neuron loss, but the results present too much variation to be definitive.

Alpha-Synuclein (SNCA): Lewy bodies made of insoluble α-synuclein aggregates are a feature of PD and are thought to be caused by the dysregulation of α-synuclein, which is produced by the gene SNCA (Spillantini et al., 1998) In addition to α-synuclein, mammals also have β- and γ-synucleins, each encoded by its own gene (Clayton & George, 1998). In zebrafish, there is no evidence of a gene encoding α-synuclein. This gene may have been lost over time because of the overlapping function between the other synucleins (Chen et al., 2009). Zebrafish do possess β-synuclein and co-orthologues for γ-synuclein (γ1 and γ2), but only β and γ1 are expressed in the CNS (Sun & Gitler, 2008). An MO knockdown of β- or γ1-synuclein caused decreased motor activity, and knockdown of both β and γ1 caused delayed differentiation of dopaminergic neurons, reduced dopamine levels and impaired motor functions. Interestingly, expression of human α-synuclein can rescue this phenotype in zebrafish (Milanese et al., 2012).

1.4.2 Chemical-based models

Several PD models are based on the degeneration of dopaminergic neurons induced by local or systemic administration of neurotoxins such as MPTP, 6-OHDA, Pesticides and herbicides (Rotenone and Paraquat).

6-OHDA: The hydroxylated analogue of dopamine, 6-hydroxydopamine (6-OHDA), was used to create one of the first animal models of PD (Schober, 2004). It has a high affinity for the dopamine transporter, which carries 6-OHDA inside dopaminergic neurons where it accumulates and causes cell death (Blandini & Armentero, 2012). Administration in zebrafish via various delivery methods has resulted in locomotor defects and decreased dopamine levels in addition to increased oxidation throughout the brain.

MPTP: Administration of 1-methyl-4-phenyl-1,2,3,6-tetrahydropyridine (MPTP) has been a well-documented method of inducing dopaminergic neurodegeneration in a variety of animals (Dauer & Przedborski, 2003). The highly lipophilic MPTP crosses the blood brain barrier and is converted to the metabolite 1-methyl-4phenylpyridinium ion (MPP+) by monoamine oxidase B. MPP+ has a high affinity for the dopamine transporter and is carried into the dopaminergic neurons of the substantia nigra where it blocks mitochondrial Complex I activity It produces Parkinsonian-like symptoms in humans; however, it does not create the Lewy body-like inclusions that are present in PD(Blandini & Armentero, 2012). When exposed to MPTP, zebrafish exhibited loss of dopaminergic neurons and showed decreases in swimming responses after treatment with MPTP (Kalyn et al., 2019; Lam et al., 2005; Sallinen et al., 2009). Inhibition of monoamine oxidase B or the dopamine transporter mitigates the neuronal loss following administration of MPTP, which confirms the same mechanism of action as in mammals (Lam et al., 2005; McKinley et al., 2005).

Rotenone: Rotenone is widely used as both an insecticide and piscicide (fish toxin). It readily crosses the blood-brain barrier and is a high-affinity inhibitor of Complex I of the mitochondrial ETC (Sherer et al., 2003). Exposure of zebrafish to rotenone has resulted in moderate locomotor defects and a reduction in the number of dopaminergic neurons in the ventral diencephalon (Kalyn et al., 2019; Sherer et al., 2003).

Paraquat: Paraquat or N,N′-dimethyl-4-4′-bipiridinium is a widely used agricultural herbicide that subsequently becomes an aquatic contaminant due to run-off (Dinis-Oliveira et al., 2006). It is thought that paraquat impairs mitochondrial Complex I, leading to problems with the ETC and consequently the overproduction of ROS (X. H. Wang et al., 2018). It is very similar to the MPTP metabolite MPP+ and has specificity for the same dopamine transporter. Paraquat administration to zebrafish resulted in increased oxidative stress, upregulation of antioxidant genes and general apoptosis (Nellore & Nandita, 2015; Q. Wang et al., 2016). and reduction in the number of dopaminergic neurons in the ventral diencephalon of larval zebrafish (Kalyn et al., 2019).

1.4.3 Chemogenetic ablation models

Precise spatial and temporal control over dopaminergic-neuron ablation is essential for eliciting Parkinson-like phenotypes in experimental animals. Among several available approaches, chemogenetic ablation combines genetic targeting with pro-drug activation. In this strategy, a transgenic zebrafish line is engineered to express the Escherichia coli gene nfsB, which encodes nitroreductase, under the control of a cell-type-specific regulatory element. Coupled with the administration of chemicals or prodrugs in this case, cell-specific ablation is achieved. The NTR enzyme uses NADH or NADPH as cofactors to catalyze the reduction of nitro-heterocyclic

prodrugs (Christofferson & Wilkie, 2009). Through this reaction, NTR converts otherwise non-toxic compounds such as Metronidazole, Nifurpirinol, and Ronidazole into cytotoxic DNA-crosslinking metabolites that trigger apoptosis (Pisharath & Parsons, 2009). The result is highly selective, temporally controlled ablation of the targeted cells, as illustrated in Figure 6.

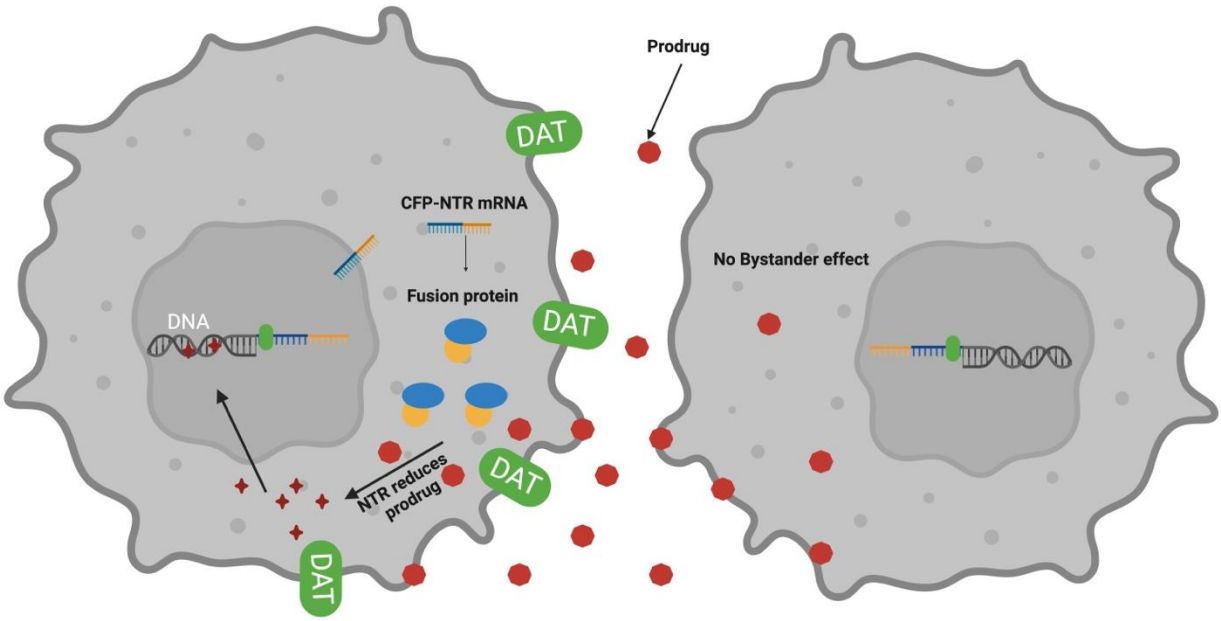

Figure 6. Nitroreductase mediates cell-specific ablation. Created in *https://BioRender.com*

Work by (Curado et al., 2007; Pisharath et al., 2007) launched the use of the ablation approach as a tool for cell-specific ablation and regenerative studies in zebrafish. Since then, the NTR-based approach has been used for the ablation of numerous zebrafish cell populations, ranging from skin cells to osteoblasts. Work by Godoy and colleagues (Godoy et al., 2015) created a transgenic zebrafish expressing NTR fused to cyan fluorescent protein under the control of

regulatory elements of the dopamine transporter. Administration of the anti-bacterial pro-drug metronidazole at 1 day post fertilization (dpf) resulted in loss of dopamine neurons at 5 dpf in addition to motor impairments. Some motor functions were re-established by 7 dpf when there was evidence of new dopamine cells. A follow-up study in adult transgenic zebrafish found that a 24 h exposure to metronidazole resulted in significant loss of dopaminergic neurons in the olfactory bulb and a decrease in the ability to smell (Godoy et al., 2020). The dopaminergic neuron ablation success varied across the brain, with the olfactory bulb having the most significant loss of DA neurons, followed by the telencephalon. These effects did not translate into locomotor impairment.

Given the significant loss of DA neurons observed in the olfactory bulb alone, in addition to behavioural effects being restricted to olfaction, the method of administration and the potency of MTZ stand out as potential explanations. To address the limitations of the NTR/MTZ ablation system, recent studies sought to explore other nitro-heterocyclic compounds as a substitute for MTZ. First, to address the commonly used 10 mM/24 hours treatment regimen, which appears not to be effective enough to efficiently ablate certain cell types. Additionally, a 10 mM concentration has proved to be toxic during such prolonged treatments, and this concentration is only 1.5 times inferior to its general toxic levels even after the 24-hour standard treatment. The observed toxicity could interfere with efforts to test pharmacological compounds in combination therapies for their impact on regeneration (Mathias et al., 2014). To that end, Bergemann et al., 2018) opted for Nifurpirinol as an alternative nitro-heterocyclic substrate for NTR. Its capacity for ablation was assessed in three different cell types, including dopaminergic neurons. As the use of NFP has never been described in zebrafish so far, they assessed its general toxicity on non-transgenic larvae and found NFP triggers cell-specific ablation at much lower concentrations than MTZ (2000 x) and at doses at least two-fold below its toxic concentrations. Similar to MTZ, the effect of NFP in NTR-

mediated cell ablations was only specific to target cells in transgenic larvae and did not show a bystander effect on neighboring cells. In Tg(dat:CFP-NTR) larvae treated with 5 μM NFP, dopaminergic neuron ablation was significantly greater compared to the MTZ and vehicle-treated groups. Results of this study addressed limitations posed by MTZ and suggest NFP to be a more potent substrate for NTR-mediated cell ablation.

In a recent effort to expand the list of nitro-heterocyclic compounds used in the NTR-mediated cell ablation system, Lai and colleagues (Lai et al., 2021) conducted a chemical screening of MTZ-like nitro-heterocyclic compounds from the US drug collection library to determine whether these nitro-heterocyclic derivatives show less toxicity and higher ablation efficiency. Among the 6 candidates, Ronidazole emerged as the superior prodrug. At 3 dpf, Tg(neurod1:Gal4FF; UAS:Eco.NfsB-mCherry) larvae were used to evaluate the spinal cord neuron ablation efficiency of Ronidazole and MTZ. Treatment with 2 mM Ronidazole or 8 mM MTZ led to a marked reduction in mCherry-positive neurons in the anterior spinal cord compared to the vehicle group. Ablation efficiency declined with lower prodrug concentrations, confirming a dose-dependent effect.

The zebrafish spinal cord transection and regeneration system was used to evaluate the potential toxicity of Ronidazole and MTZ. At 3 dpf, TgBAC(neurod1:EGFP) larvae underwent spinal cord transection and were treated with varying concentrations of Ronidazole or MTZ. Regeneration was assessed by axonal bridge formation at 2 dpi. While 79.9% of vehicle-treated larvae showed successful regeneration, high doses of Ronidazole (6 mM) and MTZ (8 mM) significantly reduced bridge formation (17.7% and 39.5%, respectively), indicating dose-dependent toxicity. Lower concentrations had no adverse effect. Given that 8 mM MTZ is commonly required for efficient cell ablation, its toxicity is concerning. In contrast, Ronidazole

effectively ablated spinal cord neurons at 2 mM without impairing regeneration, supporting its use as a safer and more effective alternative to MTZ in the NTR system (Lai et al., 2021). NFP's effect on axonal bridge formation was also assessed. Treatment with 4 μM NFP slightly reduced bridge formation, whereas 2 μM NFP had no effect. This supports NFP's ablation capacity in the NTR system but also indicates that higher concentrations may impair axon regeneration at or near its working concentration.

1.5 Drug administration route

In both larval and adult chemogenetic studies, bath immersion has traditionally been the standard method for delivering prodrugs. While immersion works reasonably well in larvae, its shortcomings become apparent in adults. For example, Godoy and colleagues (Godoy et al., 2020) achieved efficient dopaminergic ablation in the olfactory bulb but observed only limited loss in more caudal brain regions. Similar constraints are observed with other systemic delivery routes. Intraperitoneal (IP) injection requires passage through mesenteric vessels and is subject to first-pass hepatic metabolism, which often necessitates higher and potentially toxic doses (Turner et al., 2011). Intramuscular (IM) injection is also problematic, as zebrafish possess limited muscle mass and uneven vascularization of muscle tissue, resulting in unpredictable uptake and an elevated risk of local damage or necrosis (Abbate et al., 2018; Dowd, 2017). Immersion itself further lacks dose control, since absorption depends on factors such as body size, swimming activity, and gill-ventilation rate (Cassar et al., 2020).

To overcome these delivery bottlenecks, Kizil and colleagues introduced cerebroventricular micro-injection for adult zebrafish. CVMI is minimally invasive: under anesthesia, a tiny skull incision is made above the optic tectum, a fine glass capillary is inserted

into the cerebroventricular fluid (CVF), and ~500 nL of solution is pressure-injected directly into the CVF. Ventricular circulation then distributes the compound uniformly throughout fore-, mid- and hindbrain (Figure 8) while largely sparing peripheral tissues, providing a controlled, brain-wide exposure.

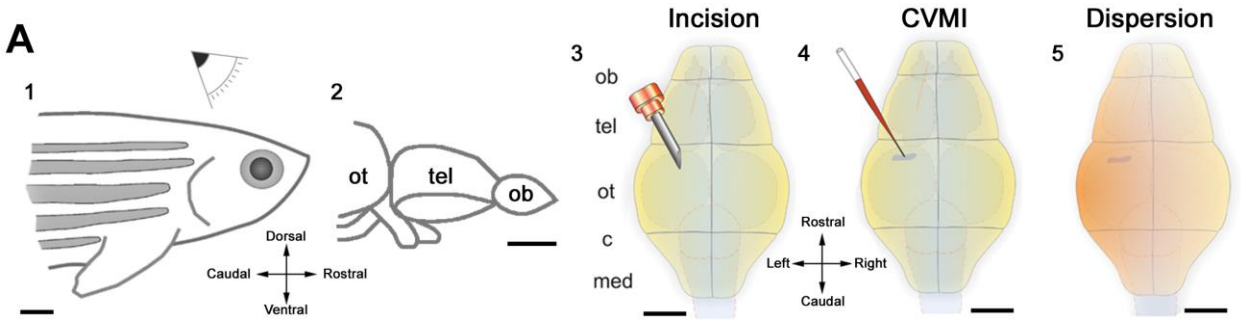

Figure 7. Overview of cerebroventricular microinjection (CVMI) paradigm. Adapted from (Kizil & Brand, 2011)

1.6 Statement of Purpose

Parkinson's disease is an incurable neurodegenerative disorder characterized by progressive loss of midbrain dopaminergic neurons and debilitating motor and non-motor symptoms. Current animal models, while invaluable, often fall short in replicating the full complexity of PD pathology, especially in adult stages. Zebrafish is widely recognized for its remarkable regenerative abilities in the adult brain and has emerged as a powerful model organism to study neuronal degeneration and regeneration. Chemogenetic ablation models of PD have relied on conventional drug delivery methods, which have translated into limited success in ablating dopaminergic neurons and ensuing PD-like phenotypes in adult zebrafish compared to larvae. The few attempts at adult zebrafish models have not fully recapitulated the extensive neuronal loss and robust PD-like symptoms necessary to study the ensuing regenerative response effectively.

This thesis addresses these critical gaps by optimizing an adult zebrafish PD model using two recent advancements: the identification of highly potent NTR-activated prodrugs (nifurpirinol and ronidazole), and the adaptation of cerebroventricular microinjection for precise, brain-wide delivery of prodrugs. Unlike conventional methods such as intraperitoneal injection, intramuscular injection, and immersion, each limited by uneven distribution and variable uptake, CVMI ensures uniform and reproducible dopaminergic neuron ablation throughout the adult zebrafish brain. By thoroughly validating dopaminergic neuron loss and associated PD-like motor and olfactory deficits, this work aims to establish a significantly improved chemogenetic ablation model, laying critical groundwork for future studies.

Establishing a robust adult zebrafish PD model is particularly significant because zebrafish possess an exceptional, inherent capacity to regenerate neurons lost due to injury or disease. Developing a model that reliably replicates PD pathology, including widespread neuron loss and

clear phenotypic consequences, is a necessary first step toward unravelling the cellular and molecular mechanisms of DA neuronal regeneration in the context of PD. To enable subsequent exploration of these regenerative processes, this thesis will also focus on developing an optimized adult brain dissociation protocol. High-quality single-cell preparations are essential for future single-cell RNA sequencing (scRNA-seq) studies, which hold promise for identifying novel genes, pathways, and factors involved in adult dopaminergic neurogenesis and regeneration. Thus, this thesis bridges a critical methodological gap, creating a robust experimental platform to advance our fundamental understanding of PD pathology and neuronal regeneration.

Aim 1: Establishment and Characterization of an Adult Zebrafish Chemogenetic PD Model

Aim 1.1: Optimize Cerebroventricular Microinjection of Advanced Prodrugs (MTZ, NFP, RON).

This aim focuses on defining prodrug concentrations and refining CVMI for precise, uniform prodrug delivery across the adult zebrafish brain. Phenol red, a visually traceable dye, will be co-injected with prodrugs to confirm complete and homogeneous distribution throughout rostral-caudal brain regions. Successful optimization will overcome limitations of immersion and conventional injection methods, ensuring reproducible, brain-wide dopaminergic neuron ablation.

Aim 1.2: Comprehensive Characterization of Dopaminergic Ablation and PD-Like Phenotypes.

Following optimized CVMI, dopaminergic neuron loss will be quantified by immunohistochemistry using TH and CFP markers. To validate functional consequences, motor

impairments will be evaluated using swim-tracking assays, alongside olfactory deficits assessed through behavioural avoidance tests. This characterization will demonstrate the model's fidelity in recapitulating key clinical aspects of PD.

Aim 2: Development of a Practical Protocol for Adult Zebrafish Brain Dissociation to Enable Single-Cell Analyses.

Aim 2.1: Establish a Reproducible Adult Brain Dissociation Workflow

To support future scRNA-seq studies of neuronal regeneration, this aim focuses on developing a reproducible and accessible protocol for generating viable single-cell suspensions from adult zebrafish brains. The objective is to refine enzymatic and mechanical dissociation methods, systematically evaluate cell viability, and provide a cost-effective workflow that does not rely on automated dissociation machinery.

2. Materials and Methods

2.1 Fish husbandry

The transgenic zebrafish lines used for this study are Tg(dat:eGFP) (Xi, Yu, et al., 2011) and Tg(dat:CFP-NTR) (Godoy et al., 2015). Experiments conducted in this thesis followed procedures approved by the Animal Care Committee at the University of Ottawa. Zebrafish were housed in tanks at 28.5 °C and maintained under a supervised light/dark (14h/10h) cycle. The transgenic zebrafish line used in all experiments in this thesis is the line. Adult fish (4-12 months old) were used for experiments. A combination of fluorescence microscopy and PCR was used to screen for transgenic zebrafish raised into adulthood.

2.2 Prodrug preparation and cerebroventricular microinjections in adult zebrafish

Metronidazole ($C_6H_9N_3O_3$, Product: PHR1052, CAS: 443-48-1, Sigma), Nifurpirinol ($C_{12}H_{10}N_2O_4$, Product: HY-135470, CAS: 13411-16-0, Medchemexpress) and Ronidazole ($C_6H_8N_4O_4$, Product: R7635, CAS: 7681-76-7, Sigma) were reconstituted in distilled water with 0.2% DMSO to a stock concentration of 27 mM, 0.58mM and 41μM and diluted to the working concentrations of 24 mM, 0.52 mM and 37 μM. Adult Tg(dat:CFP-NTR) zebrafish (~10-month-old) were anaesthetized with Tricaine. Following the procedure outlined in Kizil et al., a small incision of 200μm was then generated with a 30-gauge syringe (BD Ultra-fine II, BD Biosciences) in the cranium above the anterior portion of the optic tectum without damaging the brain. The prepared prodrug solutions diluted with 0.1% Phenol red (Sigma) were loaded into a thin glass capillary microinjecting needle (Sutter Instrument) to inject the contents through the incision into the cerebroventricular fluid surrounding the brain. Microinjections were performed using the IM-

300 vacuum pump microinjector station (Narishige) at a pressure range of 55-65 psi. Post injections, all the fish were placed in recovery tanks shielded from light.

2.3 Histology and cryosectioning

Adult zebrafish were euthanized by immersion in an ice bath for 10 minutes. Whole brains were rapidly dissected and submerged directly in 4% Paraformaldehyde (PFA) for 24 h at 4 °C for fixation. Brains were then washed three times with 1X Phosphate Buffered Saline (PBS) 15 minutes/wash. After the last wash with 1X PBS, brains were immersed in a 30% sucrose/PBS solution for 24h at 4°C. Brains were then oriented in cryomolds and fully submerged with Tissue-Tek OCT compound and frozen in liquid nitrogen for 1 minute before being stored at - 20°C. Frozen brains were then sectioned using the cryostat machine to obtain cryosections with a thickness of 16 µm. Tissue sections were stored at -20 °C for future experiments.

2.4 Immunohistochemistry

Brain sections were left to thaw at RT for 15 minutes before being washed with PBST (1X PBS with 0.5% Tween 20) for 15 minutes. Washed slides were incubated for 15 minutes at 85°C in an antigen retrieval solution containing 10 mM sodium citrate (pH 6.0) with 0.05% Tween-20. After the incubation period, the slides were left to cool down for 15 minutes, then washed for 15 minutes in PBST. The slides were then placed in 10 % fetal bovine serum (FBS) in PBST, blocking solution, for 2 hours at RT. 400µL of the primary antibody solution diluted (1:400) in PBST + 1% FBS was added to each slide, and the slides were incubated overnight at 4°C.. Slides were then washed three times in PBST (15 min/wash) at RT. After the last wash, 400 µL of the secondary antibody was added to each slide and incubated in the dark at RT for 2 hours. Slides were then washed three times in PBST (15 min/wash) at RT followed by a three minute wash with distilled water, after which 65 µL of VECTASHIELD® Antifade Mounting Media with DAPI (4',6-

diamidino-2-phenylindole) was applied to the slides and covered with a Microscope Cover Glass followed by sealing with nail polish. The slides were then stored at 4°C.

Table 1. Primary and secondary antibodies used for immunohistochemistry.

Primary antibody			
Host organism	**Target**	**Catalogue number**	**Antibody dilution**
Mouse	CFP	632381	1:400
Rabbit	TH	AB152	1:400
Secondary antibody			
Host organism	**Target**	**Supplier**	**Antibody dilution**
Goat Alexa 488	Mouse IgG (H+L)	Thermo Fisher Scientific	1:400
Goat Alexa 594	Rabbit IgG (H+L)	Thermo Fisher Scientific	1:400

2.5 Image analysis and cell counting

Images in this thesis were captured using the Zeiss AxioImager microscope. To account for all the cells present at the different depths of a tissue, only the composite image of the various Z-stacks was acquired. Images were then processed and analyzed using the Zen 2.3 (blue edition) software. To count the number of cells in a specific region of the brain, 6 subsequent tissues with similar characteristics were chosen. Two independent researchers manually counted the number of cells in each tissue, and the average number was used. Manual cell counts were done using ImageJ software.

2.6 Locomotion analysis

Before the start of the behavioural test, fish were placed individually in tanks filled with 1.5 L of system water. Fish were allowed to acclimate by keeping them in the testing chamber for at least 10 minutes before the start of the test. If fish displayed signs of stress by swimming

sporadically, the acclimatization period was prolonged by at least 15 minutes. Motor activity was tested at four key time points: 1,3,7, and 16dpt. Each trial lasted 10 minutes. Three different parameters were evaluated: total distance travelled, total time spent in a stationary state, and average velocity. Total distance was calculated by adding the inactive distance, small distance, and large distance. Distances were recorded in centimetres (cm). Total freezing time was determined by recording the inactive duration and was measured in seconds (s). Average velocity was calculated by dividing the total distance (cm) by the total trial time of 600 s. Tracking of the various parameters was done via Viewpoint ZebraLab tracking software.

2.7 Olfactory analysis

Olfactory function was tested according to Godoy and colleagues (Godoy et al., 2020). Briefly, tanks used for this experiment were customized and contained a mid-tank division, which divided the tank into a neutral zone, and left and right arms. Each adult zebrafish was allowed to swim freely in the tank for 3 minutes before the addition of the repulsive stimulus cadaverine (Sigma-Aldrich) (80 µL of 1 mM stock solution) to the arm where the fish was located. The time spent in each area was recorded for another 3 minutes. This elapsed time was sufficient to allow the stimulus to diffuse throughout one of the tank's arms without reaching a different tank area. The ratio of time spent in the stimulus arm was calculated post-stimulus by dividing the percentage of time spent in the stimulus by the total recording time. Cadaverine was delivered with a micropipette into the rearmost portion of the arm. Control animals received the same volume of system water.

2.8 Adult Zebrafish Brain Dissociation and Viability Staining Protocol

This protocol for manual enzymatic and mechanical dissociation of adult zebrafish brain tissue was adapted from the manufacturer's instructions for the Neural Tissue Dissociation Kit (P) (Miltenyi Biotec, Cat. 130-092-628) and work by Cosacak and colleagues (Cosacak et al., 2020)

2.8.1 Tissue Collection and Initial Dissociation

Adult zebrafish (4–12 months old) were euthanized by immersion in ice-cold water (ice bath) for 10 minutes. Whole brains were rapidly dissected out in ice-cold 1× phosphate-buffered saline (PBS) supplemented with 1:1000 β-mercaptoethanol (Thermo Fisher Cat# 21985023) to reduce oxidative damage. Dissected brains were immediately transferred into a 1.5 mL tube containing Buffer Mix-I (950 µL of Buffer X, 50 µL of Enzyme P, and 5.8 µL of 1:1000 β-mercaptoethanol) pre-warmed to 28 °C. Enzymatic digestion was initiated by incubating the brains in a 28 °C water bath for 10 minutes. Following this incubation, the tissue was gently triturated five times using a fire-polished glass Pasteur pipette (Sigma Cat# BR747725) to mechanically break up the brain. This 10-minute incubation plus gentle trituration cycle was repeated two more times (for a total of three cycles) to promote thorough tissue dissociation.

2.8.2 Enzymatic Digestion and Mechanical Trituration

After the initial dissociation cycles, a secondary enzyme mix was added to further dissociate the tissue. Specifically, 40 µL of Buffer Mix-II (comprised of 20 µL Enzyme A + 20 µL Buffer Y). Samples were returned to the 28 °C water bath and subjected to successive rounds of digestion and trituration: brains were incubated for another 10 minutes, then gently pipetted up and down five times. This digestion + trituration cycle was repeated three times in total. With each round, the bore of the pipette was narrowed (transitioning to P1000 plastic pipette tips with smaller

orifice diameters) as the tissue fragments became progressively smaller. This stepwise narrowing enhanced the mechanical shear and ensured that enzymes gained access to remaining tissue pieces, resulting in a homogeneous cell suspension.

2.8.3 Filtration and Cell Harvest

Once the brains were fully dissociated into a single-cell suspension (no visible large tissue), the mixture was sequentially filtered to remove debris and obtain a clean cell suspension. The cell suspension was first passed through a 70 μm nylon cell strainer and then through a 40 μm cell strainer to remove any remaining aggregates. Both strainers were pre-wetted and equilibrated with cold PBS containing 4% bovine serum albumin (BSA) to prevent cell adhesion to the filter and reduce shear stress. The filtrate was collected on ice. To reduce the BSA concentration from 4% to 2%, an equal volume of ice-cold 1× PBS (without BSA) was added to the cell suspension. Cells were then pelleted by gentle centrifugation at 300 × g for 8 minutes at 4 °C. The supernatant was carefully aspirated, and the cell pellet was resuspended in 10 mL of cold 2% BSA in PBS to wash. The suspension was centrifuged again under the same conditions. Finally, the washed cell pellet was gently resuspended in PBS + 2% BSA (ice-cold) to a small volume. The dissociated cells were kept on ice until further analysis.

2.8.4 Live/Dead Cell Viability Staining and Imaging

After dissociation, cell viability was assessed using both dye-exclusion and fluorescence-based live/dead staining methods. For rapid manual counting, a Trypan Blue exclusion test was performed: an aliquot of the cell suspension was mixed 1:1 with 0.4% Trypan Blue solution (final Trypan Blue concentration 0.2%). The cells were incubated in the dye for approximately 3–5 minutes at room temperature, then loaded onto a hemocytometer for microscopic examination. Viable cells exclude the Trypan Blue dye and remain unstained (clear), whereas non-viable cells

with compromised membranes take up the dye and appear blue. To avoid artifactual dye uptake upon prolonged exposure, count cells within 5 minutes of mixing.

For more detailed imaging-based viability analysis, fluorescent nucleic acid dyes were used to differentially label live and dead cells. In one approach, cells were stained with DAPI (4′,6-diamidino-2-phenylindole) at a final concentration of 0.5 µg/mL. The sample was incubated with DAPI for ~5 minutes on ice (protected from light). DAPI is a blue-fluorescent DNA-binding dye (excitation maximum ~358 nm, emission ~461 nm) that is impermeant to intact cell membranes. Thus, under these live cell staining conditions, DAPI is largely excluded from viable cells but readily enters non-viable cells with compromised membranes. After the short incubation, the cells can be observed under a fluorescence microscope with a DAPI filter set. Live cells remain DAPI-negative (no blue nuclear fluorescence), whereas dead cells show bright blue nuclear staining.

In a similar live/dead imaging assay, Hoechst 33342 was used as an alternative nuclear stain in combination with a counterstain for dead cells. Hoechst 33342 (a cell-permeant DNA dye) was added at 5 µg/mL and incubated for 5–10 minutes at room temperature. This dye permeates live cell membranes and binds to DNA, staining all nuclei (both live and dead) with blue fluorescence (excitation ~350 nm, emission ~461 nm). Because it labels all nucleated cells, Hoechst 33342 can be used to identify the total cell count and to visualize nuclear morphology. To specifically mark non-viable cells in this assay, Propidium Iodide (PI) was added at a final concentration of 1 µg/mL during the last 5 minutes of incubation. PI is a red-fluorescent viability dye: it is membrane-impermeable and therefore excluded by healthy live cells, but it readily enters cells with damaged membranes (dead or dying cells) and binds their DNA. When bound, PI fluoresces bright red (excitation ~535 nm, emission ~617 nm). After staining with Hoechst and PI, the cell suspension can be imaged using a fluorescence microscope with DAPI and Texas Red (or

TRITC) filter sets. Viability can be quantified by counting the number of PI-positive (red, dead) nuclei relative to the total number of Hoechst-positive nuclei.

Acridine Orange/Propidium Iodide dual staining was also employed as a rapid fluorescent live/dead assay. Acridine Orange (AO) is a cell-permeant nucleic acid dye that can penetrate all cells (live or dead). Cells were mixed with AO and PI at a final concentration of approximately 5–10 μg/mL each. No incubation period was required for AO/PI; staining occurs immediately upon mixing. Acridine Orange emits green fluorescence when bound to double-stranded DNA (excitation ~480–500 nm, emission ~525 nm), thereby labelling the nuclei of all cells. Propidium Iodide emits red fluorescence when bound to DNA in cells with compromised membranes. Because AO can enter all cells, whereas PI enters only non-viable cells, this combination yields two-colour viability data: under a fluorescence microscope (with appropriate FITC/GFP and Texas Red filters), live cells show green nuclear fluorescence (AO-stained DNA), and dead cells show red nuclear fluorescence (PI-stained DNA). Stained cells can be immediately visualized by fluorescence microscopy. Viability can be quantified by counting the number of PI-positive (red, dead) nuclei relative to the total number of Hoechst-positive nuclei.

All imaging-based viability assays were conducted on ice or at room temperature and protected from light to prevent photobleaching. Fluorescence filter sets used were: DAPI channel for DAPI and Hoechst 33342 (blue emission ~460 nm), FITC/GFP channel for Acridine Orange bound to DNA (green emission ~525 nm), and TRITC or Texas Red channel for Propidium Iodide (red emission ~617 nm). Table 2 below summarizes the excitation/emission characteristics and the viability indication for each dye.

Table 2. Key properties of live/dead staining dyes used in this protocol.

Viability Dye	Excitation/Emission (nm)	Stains Live Cells?	Stains Dead Cells?	Fluorescence Color
Trypan Blue	(Absorbance ~ in visible spectrum)	No (excluded by live)	Yes (enters dead cells)	Blue (non-fluorescent; bright-field imaging)
DAPI	358 / 461 (blue)	No (excluded by live)	Yes (binds DNA in dead nuclei)	Blue fluorescence
Hoechst 33342	350 / 461 (blue)	Yes (permeant; all nuclei)	Yes (stains all nuclei)	Blue fluorescence
Propidium Iodide (PI)	535 / 617 (red)	No (excluded by live)	Yes (binds DNA in dead nuclei)	Red fluorescence
Acridine Orange (AO)	~500 / 525 (green, DNA-bound)	Yes (permeant; stains DNA/RNA in all cells)	Yes (enters dead)	Green fluorescence in live (nuclear DNA);

2.9 Statistical analysis

Statistical analysis was done using GraphPad Prism 10 software. Dopaminergic neuron counts across treatment groups (vehicle, MTZ, NFP, RON) and time points were analyzed using two-way ANOVA (factors: treatment × time or treatment × cell type), followed by Tukey's multiple comparisons test. Locomotor activity and olfactory function were analyzed using one-way or two-way ANOVA, with Dunnett's multiple comparisons test applied where appropriate to compare each treatment group to vehicle controls. Statistical significance was set at $p < 0.05$, and results are reported as ns ($p > 0.05$), * ($p < 0.05$), ** ($p < 0.01$), *** ($p < 0.001$), and **** ($p < 0.0001$). All error bars represent the standard error of the mean (SEM) unless otherwise indicated, and exact sample sizes (n) for each experiment are provided in the corresponding figure legends.

3. Results

3.1 Optimization of CVMI and prodrug concentration

The goal of this experiment was to optimize CVMI conditions and prodrug concentrations in adult Tg(dat:CFP-NTR) zebrafish to maximize exposure of dopaminergic neurons and establish a reliable baseline for subsequent ablation. Cerebroventricular microinjection was performed in adult Tg(dat:CFP-NTR) zebrafish following Kizil and colleagues (Kizil & Brand, 2011). As an initial benchmark, we adopted prodrug doses commonly used in immersion paradigms. Metronidazole (MTZ) 10 mM, Nifurpirinol 5 μM, and Ronidazole 2 mM (Bergemann et al., 2018; Godoy et al., 2020b; Lai et al., 2021) and delivered five CVMIs every other day. Under this regimen, counts of CFP-positive neurons did not differ between vehicle and prodrug groups (data not shown). To increase intraventricular exposure, we then maximized prodrug concentration within aqueous solubility/tolerability limits and compressed dosing to five consecutive daily injections. The final CVMI working concentrations are summarized in Table 2, and the dosing timeline is shown in Figure 8. These optimized conditions were used in all subsequent experiments.

Table 3. Chemical structures, aqueous solubility, and injected concentrations of NTR Prodrugs used for CVMI in adult zebrafishs

Prodrug	Chemical Structure	Aqueous Solubility	Injected Concentration (CVMI)
Metronidazole	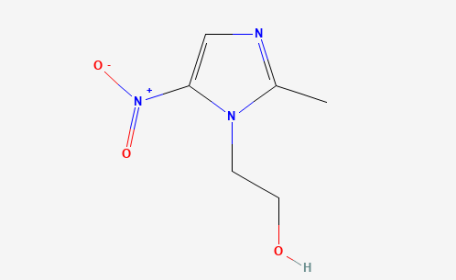	10 mg/mL	24mM
Ronidazole	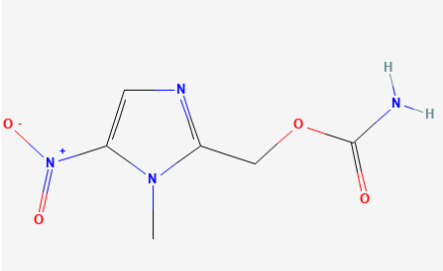	2.9 mg/mL	5mM
Nifurpirinol	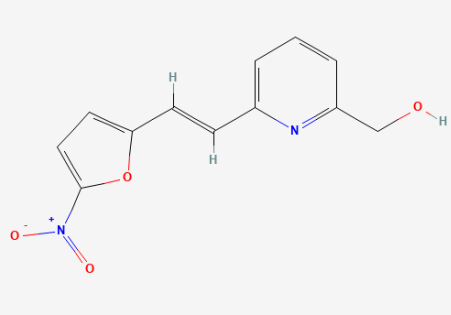	0.684 mg/mL	0.037mM

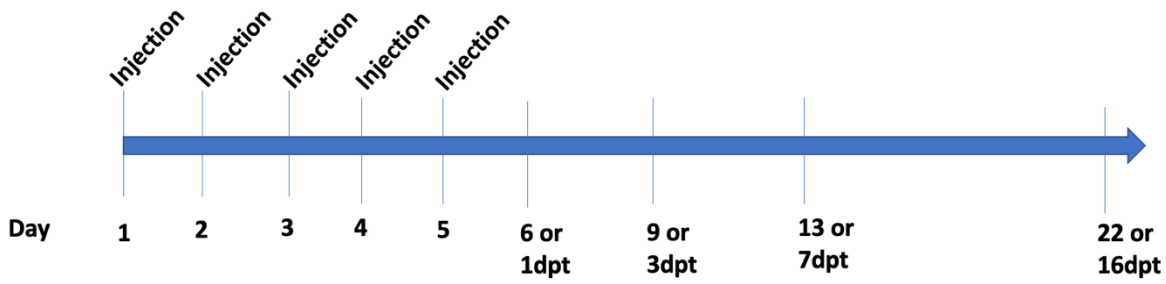

Figure 8. Prodrug dosing and treatment timeline for NTR ablation via CVMI.

Schedule of five once-daily cerebroventricular microinjections on days 1–5, followed by endpoint assessments at 1, 3, 7, and 16 days post-treatment, corresponding to days 6, 9, 13, and 22 from the first injection.

3.2 Dopaminergic Neuron Ablation (Histology)

To evaluate whether chemogenetic treatment ablated dopaminergic neurons, transgenic adult zebrafish (Tg(dat:CFP-NTR)) were treated with prodrugs or vehicle and then examined for TH and CFP-positive cells in key brain regions. Figure 8 outlines the treatment paradigm and confirms that daily cerebroventricular microinjections successfully delivered each prodrug (metronidazole, nifurpirinol, or ronidazole) into the brain ventricles over a 5-day course. This approach was expected to ensure a broad distribution of the drugs in the adult brain (Kizil & Brand, 2011). We quantified dopaminergic cell populations in the olfactory bulb, telencephalon, and diencephalon at 1 day post-treatment (1 dpt) and 7 dpt to detect any neuron loss.

In the olfactory bulb, there was no observable reduction in TH-positive or CFP-positive neuron counts in prodrug-treated fish compared to vehicle at 1 dpt (Figure 9C). Quantitative analysis revealed that treatment had no significant effect on neuron counts ($p>0.26$), nor was there a significant treatment × cell type interaction ($p>0.95$), meaning treatment did not differentially affect TH- vs. CFP-positive neurons. The only significant factor was cell type itself: overall, TH

counts were lower than CFP counts across all conditions ($p<0.0001$). Similarly, at 7 dpt (Figure 10), there were no significant differences in dopaminergic neuron counts in the OB between any prodrug group and the vehicle (two-way ANOVA, $p=0.59$ for treatment; no interaction, $p>0.996$). Across all prodrug treatments (MTZ, NFP, RON), the number of remaining OB TH neurons and CFP neurons was statistically indistinguishable from the DMSO-injected group (Tukey post-hoc tests, all adjusted $p>0.3$). Thus, no appreciable ablation of OB dopaminergic neurons was achieved by any prodrug when administered by CVMI.

In the telencephalon, the results were likewise negative for neuron ablation. At 1 dpt (Figure 11B), representative sections showed comparable TH and CFP immunofluorescence in prodrug-treated vs. vehicle brains. No significant loss of telencephalic dopaminergic neurons was detected (two-way ANOVA, $p=0.21$ for treatment; no interaction, $p=0.997$). By 7 dpt (Figure 12C), telencephalic TH and CFP cell counts remained similar across all groups (no treatment effect, $p=0.91$). In each case, the number of double-positive cells (CFP/TH) was also unchanged. These data indicate that our chemogenetic approach failed to ablate telencephalic dopaminergic neurons to any measurable extent when the prodrug was administered by CVMI.

In the diencephalon, specifically the ventral periventricular pretectal nucleus (PPV), where dense and easy-to-identify dopaminergic cell populations reside(Ma, 2003), we again found no significant neuron loss. At 1 dpt (Figure 13), diencephalic TH and CFP signals in treated fish were qualitatively intact. Cell counts showed no differences between treatments (two-way ANOVA, $p=0.95$ for treatment; $p>0.99$ for interaction), and even the overall cell type effect (TH vs. CFP) was not significant at this early time point. At 7 dpt (Figure 14C), a slight reduction in TH cell count was observed in some prodrug-treated fish; however, this did not reach statistical significance (two-way ANOVA, treatment $p=0.07$, n.s.). Post-hoc tests confirmed no reliable

differences between any prodrug group and controls (all adjusted $p>0.19$). The diencephalic dopaminergic nuclei thus showed no clear ablation, although the near-significant p value for treatment at 7 dpt suggests a possible small effect that did not achieve significance with the given sample size.

Overall, across all brain regions analyzed, the NTR-prodrug system did not produce a statistically significant loss of dopaminergic neurons in adult zebrafish. This result contrasts with expectations from larval studies and immersion-based lesion models, indicating that our adult PD model did not replicate the dopaminergic cell loss characteristic of Parkinson's disease.

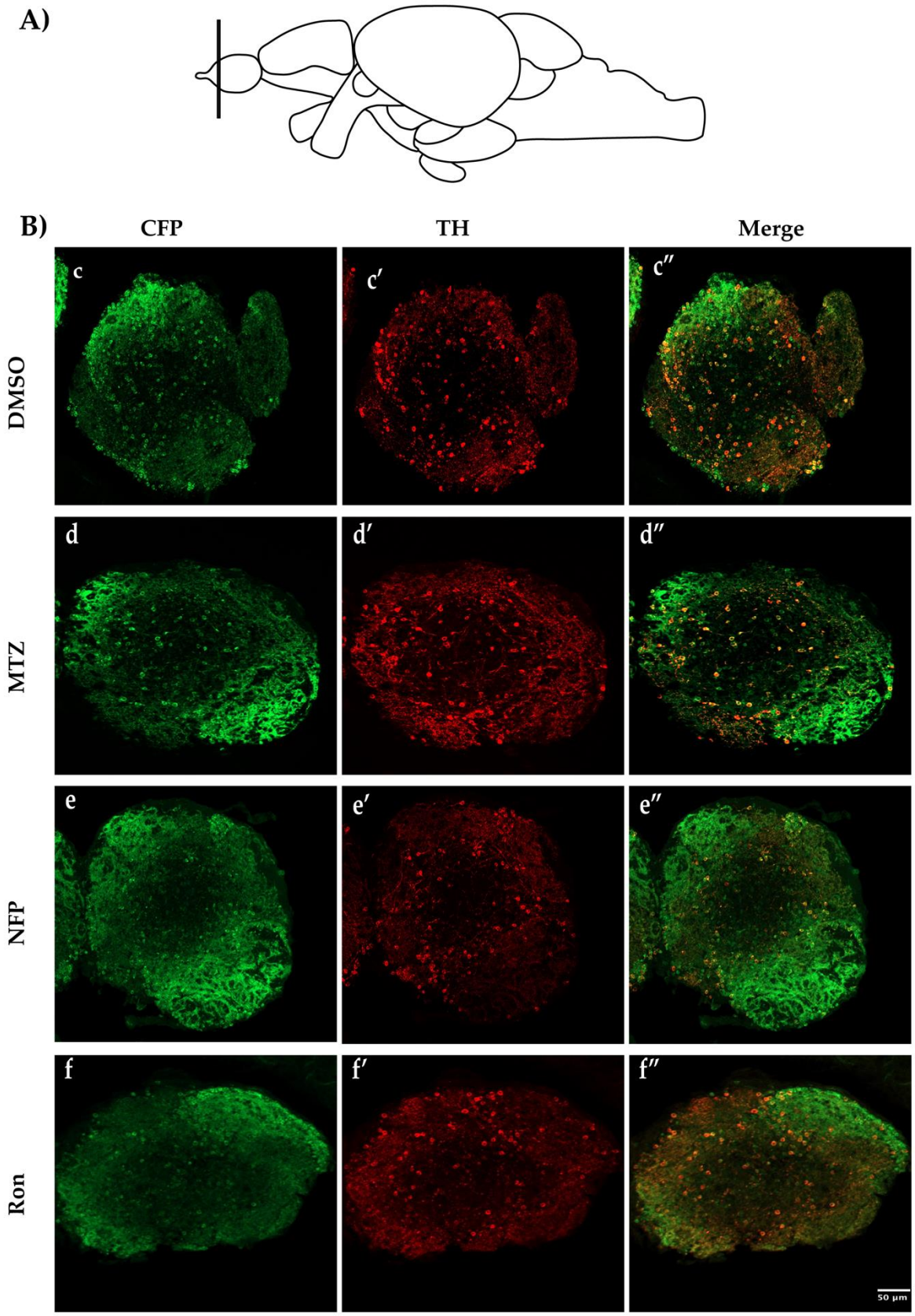
A)
B)
CFP
TH
Merge
DMSO
MTZ
NFP
Ron
c
c′
c″
d
d′
d″
e
e′
e″
f
f′
f″
50 µm

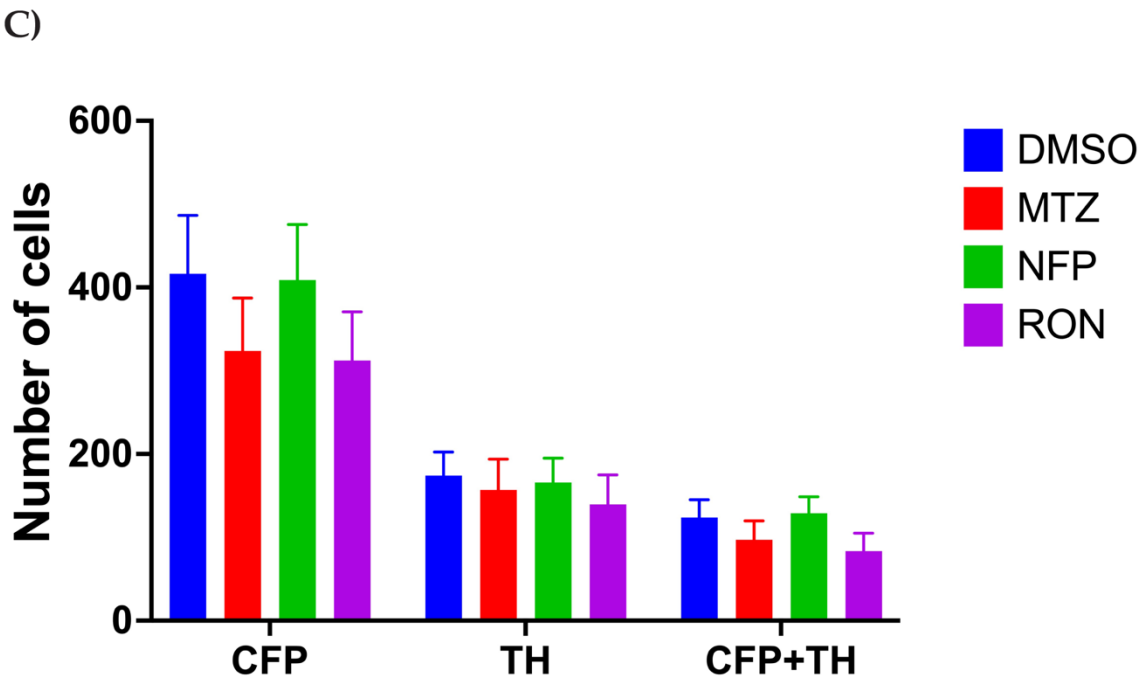

Figure 9. Dopaminergic neuron ablation in the olfactory bulb (1 dpt). (A) Schematic of the adult zebrafish brain showing the region that was analyzed. **(B)** Representative coronal sections from a vehicle (DMSO-injected) and a prodrug-treated adult zebrafish, immunostained for TH (red) and CFP (green). No obvious loss of TH/CFP cells is apparent. **(C)** Quantification at 1 dpt: a two-way ANOVA (factors: Cell type = CFP, TH, CFP+TH; Treatment = DMSO, MTZ, NFP, RON) showed no Cell type × Treatment interaction, $F(6,84)=0.26$, $p=0.953$, and no main effect of treatment, $F(3,84)=1.36$, $p=0.262$; Cell type differed overall, $F(2,84)=37.79$, $p<0.0001$. Tukey multiple comparison tests within each cell type found no differences between any prodrug and DMSO (all adjusted $p>0.35$). Bars show mean±SEM; n per treatment per cell type: DMSO=9, MTZ=8, NFP=8, RON=7. (Scale bar = 50 μm).

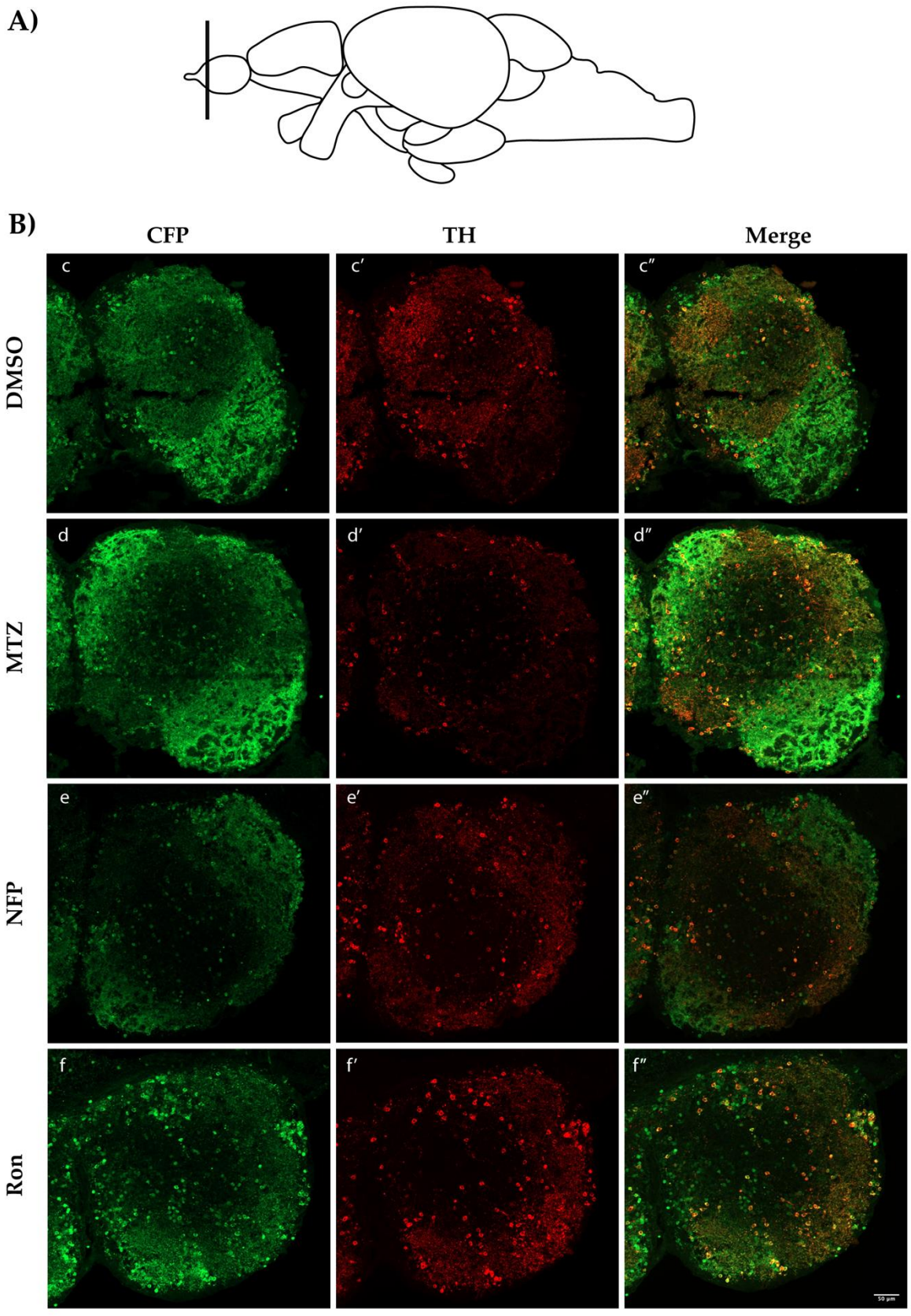
A)
B)
CFP
TH
Merge
DMSO
MTZ
NFP
Ron
c
c′
c″
d
d′
d″
e
e′
e″
f
f′
f″
50 µm

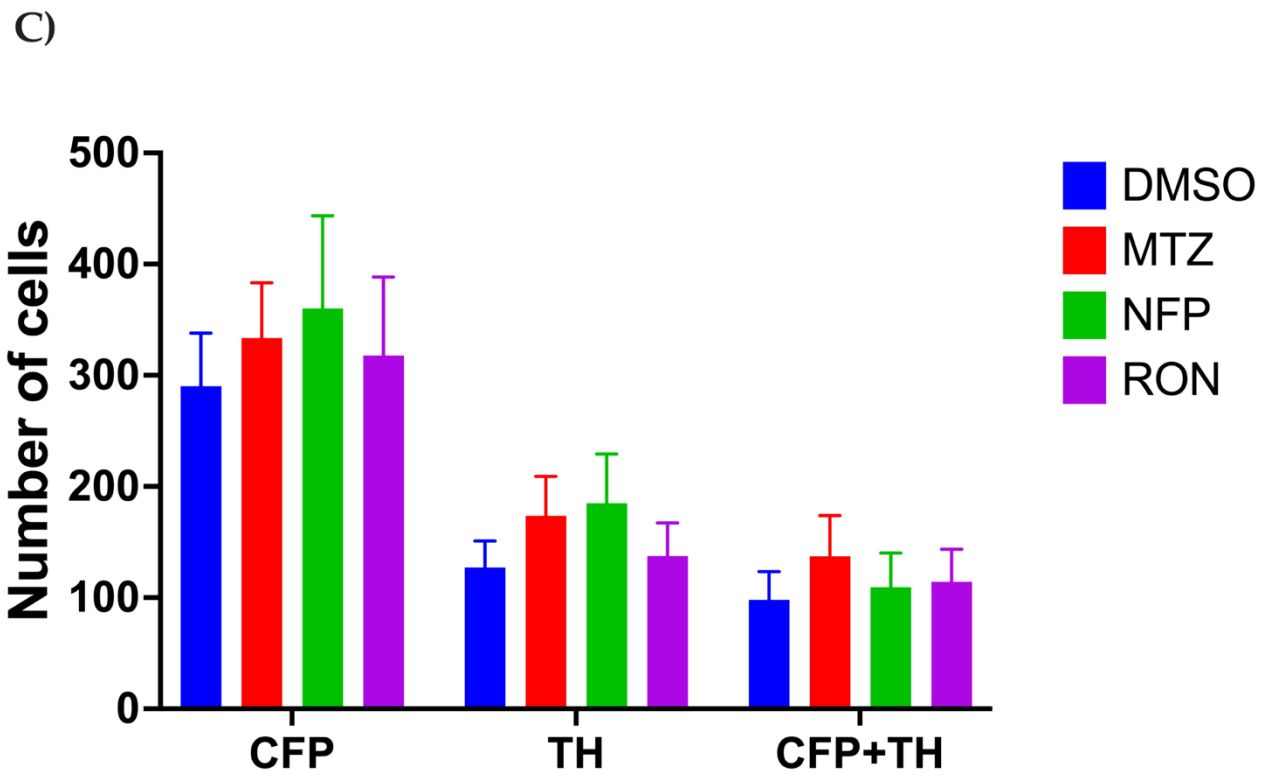

Figure 10. Dopaminergic neurons in the olfactory bulb (7 dpt). (A) Schematic of the adult zebrafish brain showing the region that was analyzed. **(B)** TH (red) and CFP (green) immunofluorescence in vehicle and prodrug-treated fish. **(C)** Quantification at 7 dpt: a two-way ANOVA (factors: Cell type = CFP, TH, CFP+TH; Treatment = DMSO, MTZ, NFP, RON) showed no Cell type × Treatment interaction, $F(6,86)=0.10$, $p=0.996$, a significant main effect of Cell type, $F(2,86)=20.78$, $p<0.0001$, and no main effect of treatment, $F(3,86)=0.64$, $p=0.590$. Tukey multiple comparison tests within each cell type detected no differences between any prodrug and DMSO (all adjusted $p>0.69$). Bars show mean±SEM; n per treatment per cell type: DMSO=10 (CFP, TH), 9 (CFP+TH); MTZ=5; NFP=8; RON=10. (Scale bar = 50 µm)

A)

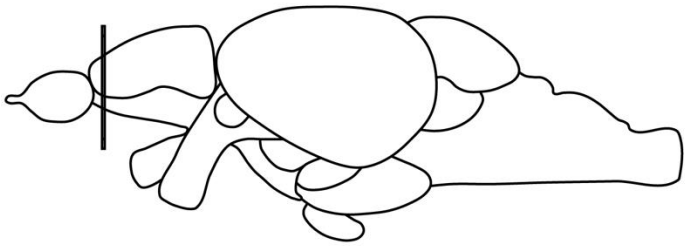

B)

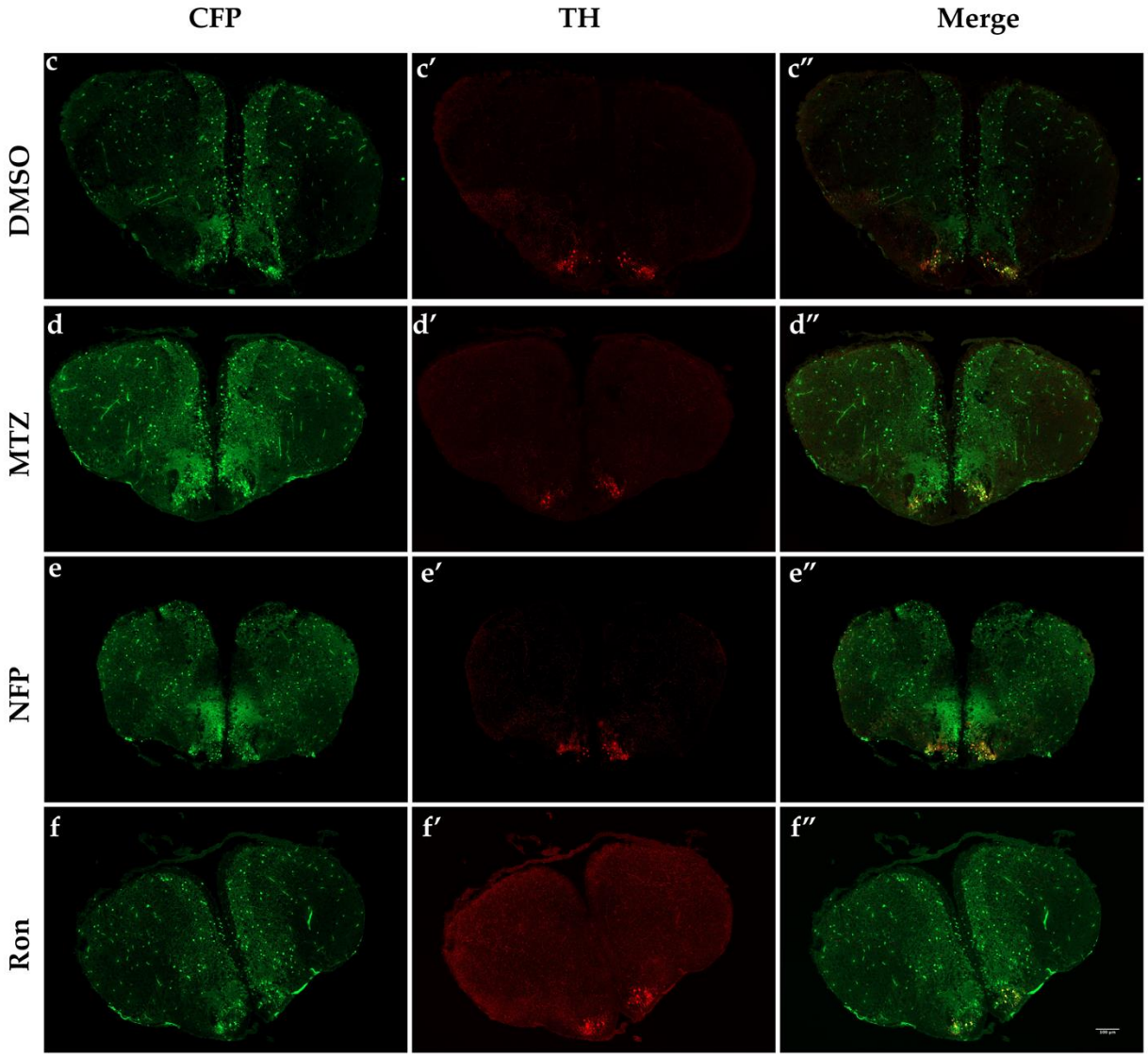

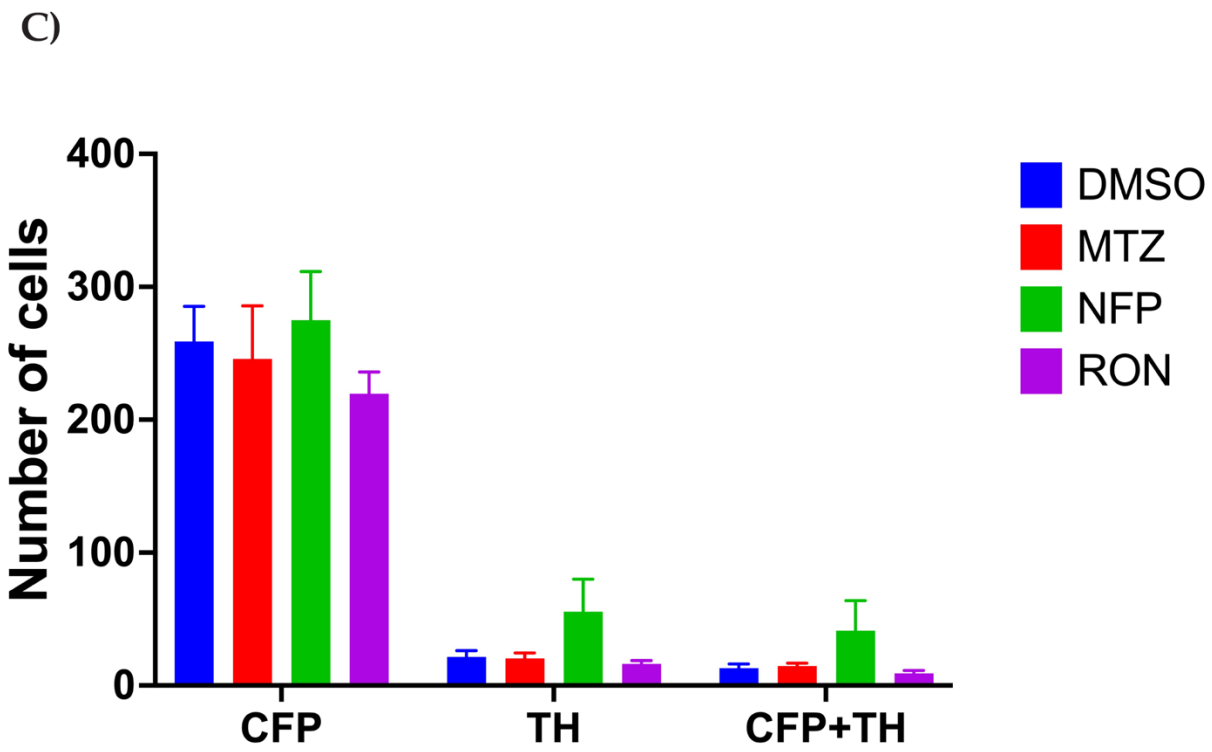

Figure 11.Dopaminergic neuron ablation in the telencephalon (1 dpt). (A) Schematic of the adult zebrafish brain showing the region that was analyzed. **(B)** TH (red) and CFP (green) label*l*ing in the telencephalic region of vehicle vs. prodrug-treated fish. **(C)** Quantification at 1 dpt: a two-way ANOVA (factors: Cell type = CFP, TH, CFP+TH; Treatment = DMSO, MTZ, NFP, RON) showed no Cell type × Treatment interaction, $F(6,54)=0.093$, $p=0.997$; a main effect of Cell type, $F(2,54)=105.5$, $p<0.0001$; and no main effect of Treatment, $F(3,54)=1.57$, $p=0.208$. Tukey multiple comparison tests within each cell type found no differences between any prodrug and DMSO (all adjusted $p>0.44$). Bars show mean±SEM; n per treatment per cell type: DMSO=4, MTZ=8, NFP=6, RON=4. (Scale bar = 100 µm)

A)

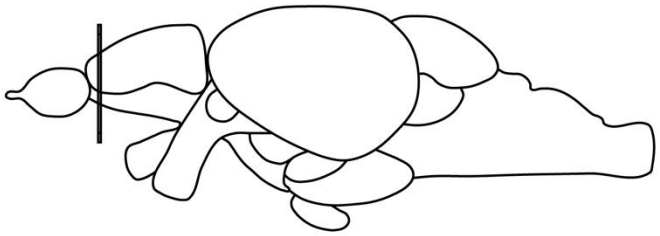

B)

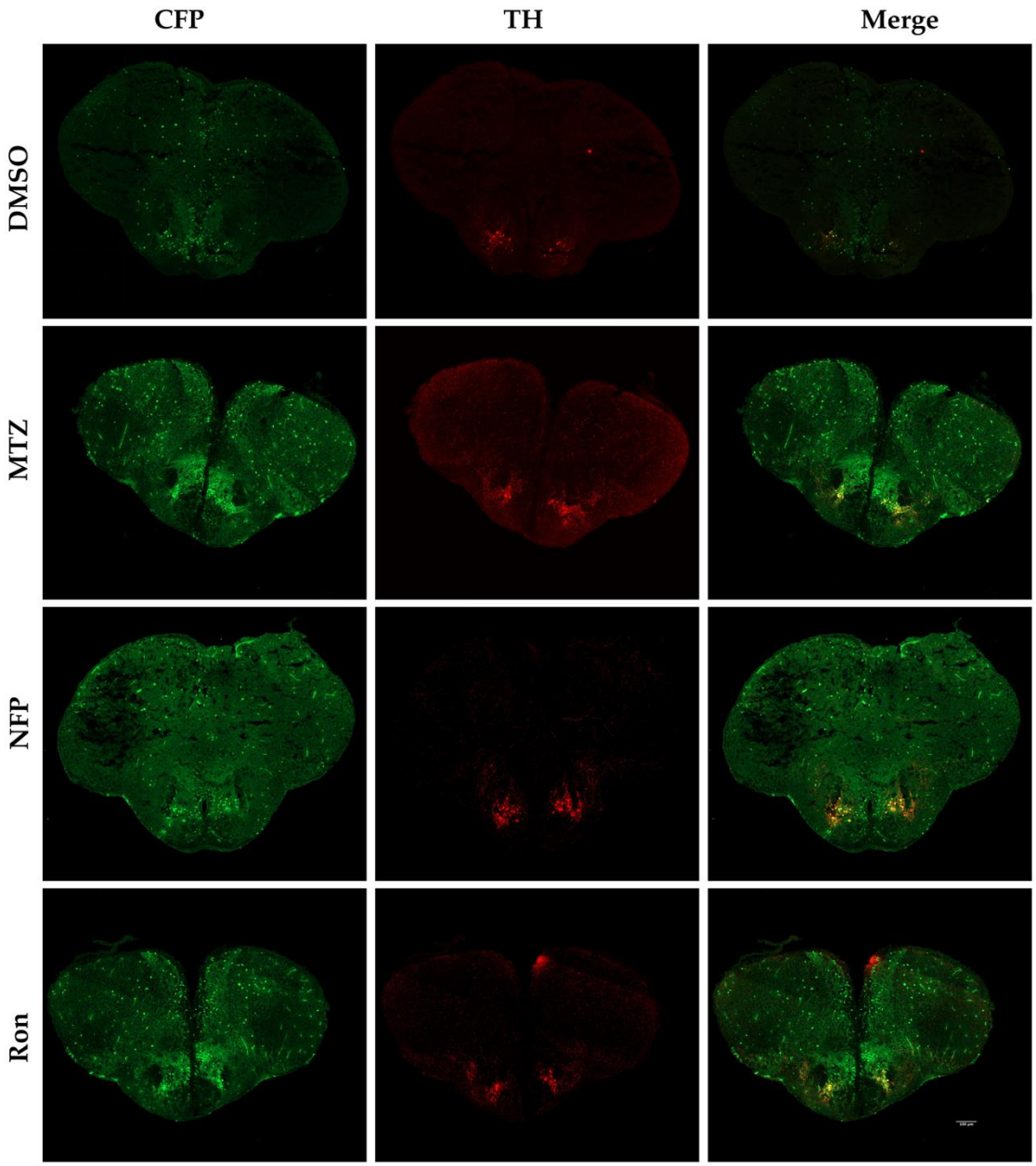

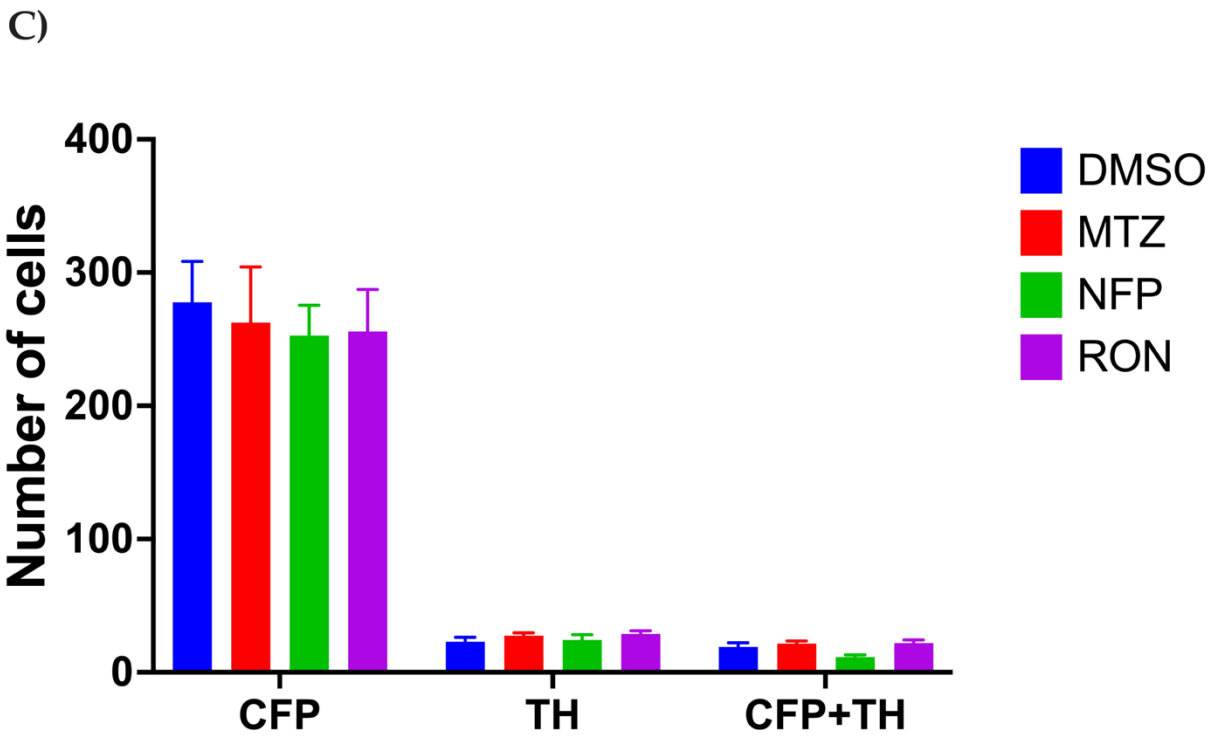

Figure 12. Dopaminergic neurons ablation in the telencephalon (7 dpt). (A) Schematic of the adult zebrafish brain showing the region that was analyzed. **(B)** TH (red) and CFP (green) co-staining in vehicle and prodrug-treated fish. **(C)** Quantification at 7 dpt: a two-way ANOVA (factors: Cell type = CFP, TH, CFP+TH; Treatment = DMSO, MTZ, NFP, RON) found no Cell type × Treatment interaction, $F(6,90)=0.17$, $p=0.985$; a main effect of Cell type, $F(2,90)=214.6$, $p<0.0001$; and no main effect of treatment, $F(3,90)=0.18$, $p=0.912$. Tukey multiple comparison tests within each cell type showed no differences between any prodrug and DMSO (all adjusted $p\geq0.75$). Bars show mean±SEM; n per treatment per cell type: DMSO=11, MTZ=6, NFP=8, RON=9. (Scale bar = 100 µm)

A)

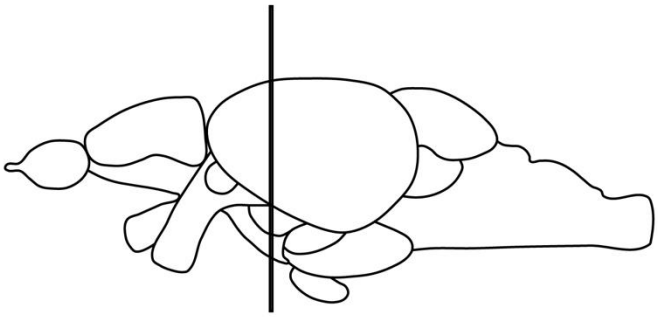

B)

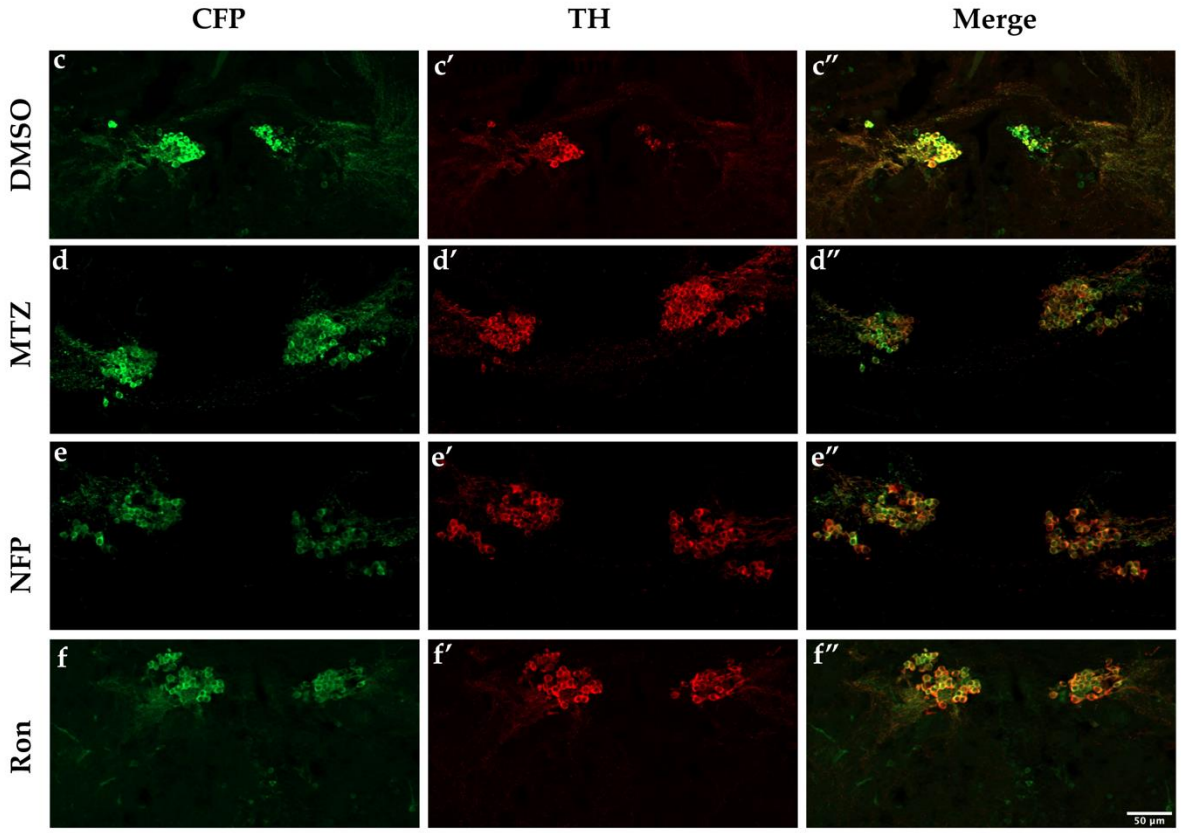

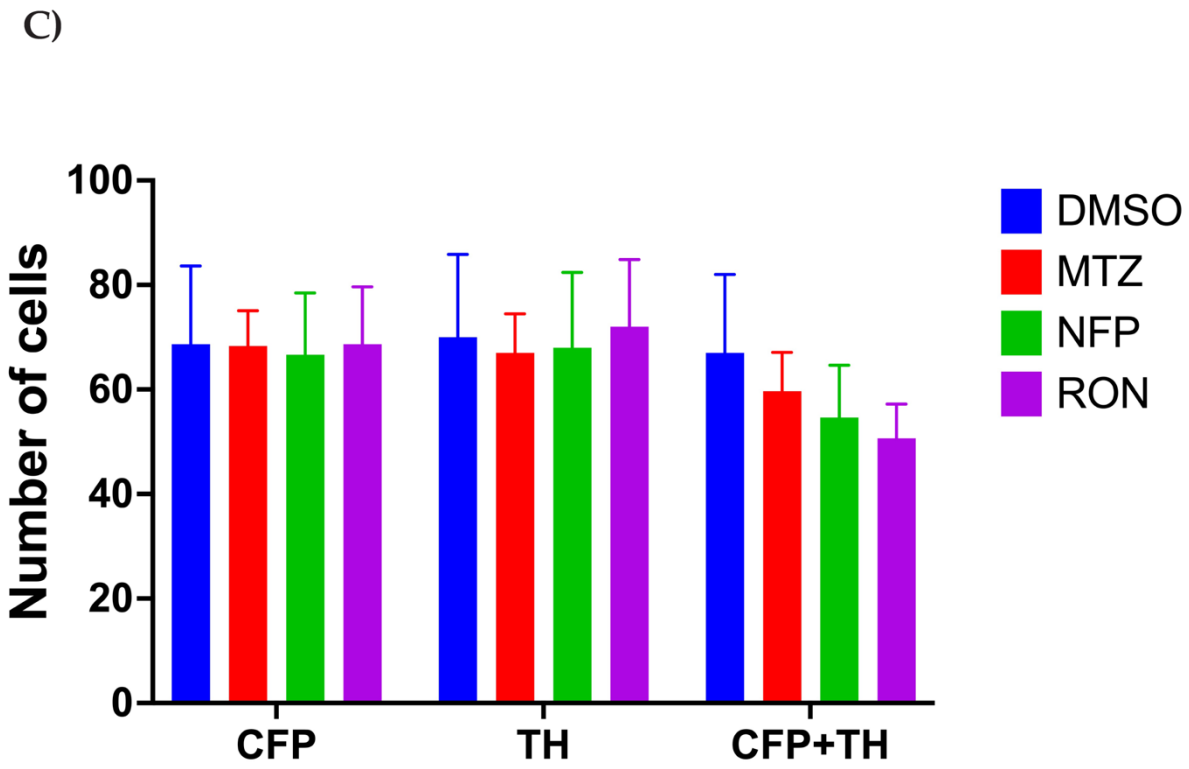

Figure 13. Dopaminergic neurons ablation in the diencephalon (1 dpt). (A) Schematic of the adult zebrafish brain showing the region that was analyzed. **(B)** TH (red) and CFP (green) immunostaining in the diencephalic region PPV of vehicle and prodrug-treated fish. **(C)** Quantification at 1 dpt: a two-way ANOVA (factors: Cell type = CFP, TH, CFP+TH; Treatment = DMSO, MTZ, NFP, RON) showed no Cell type × Treatment interaction, $F(6,42)=0.106$, $p=0.995$; no main effect of Cell type, $F(2,42)=0.846$, $p=0.436$; and no main effect of Treatment, $F(3,42)=0.115$, $p=0.951$. Tukey multiple comparison tests within each cell type detected no differences between any prodrug and DMSO (all adjusted $p\geq0.83$). Bars show mean±SEM; n per treatment per cell type: DMSO=6, MTZ=6, NFP=3, RON=3. (Scale bar = 50 µm).

A)

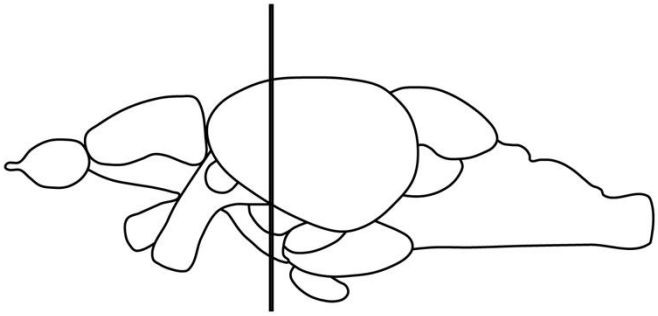

B)

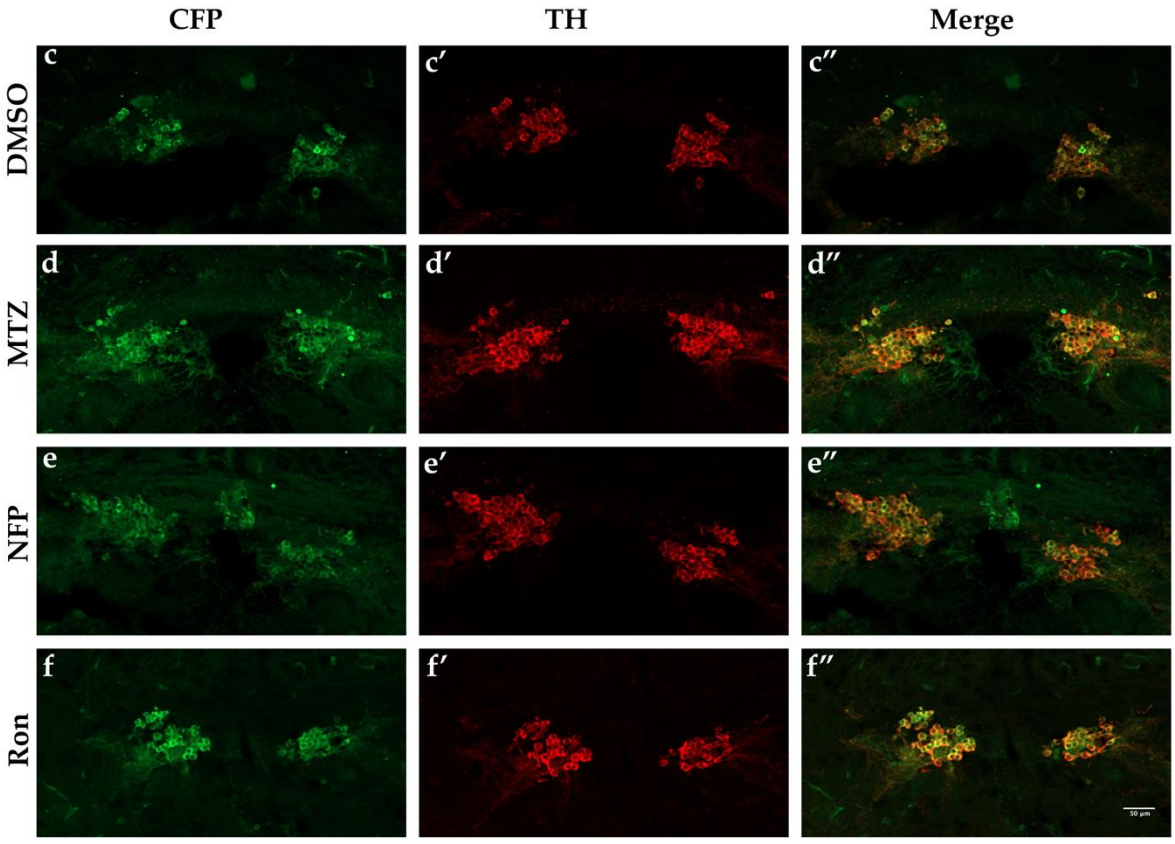

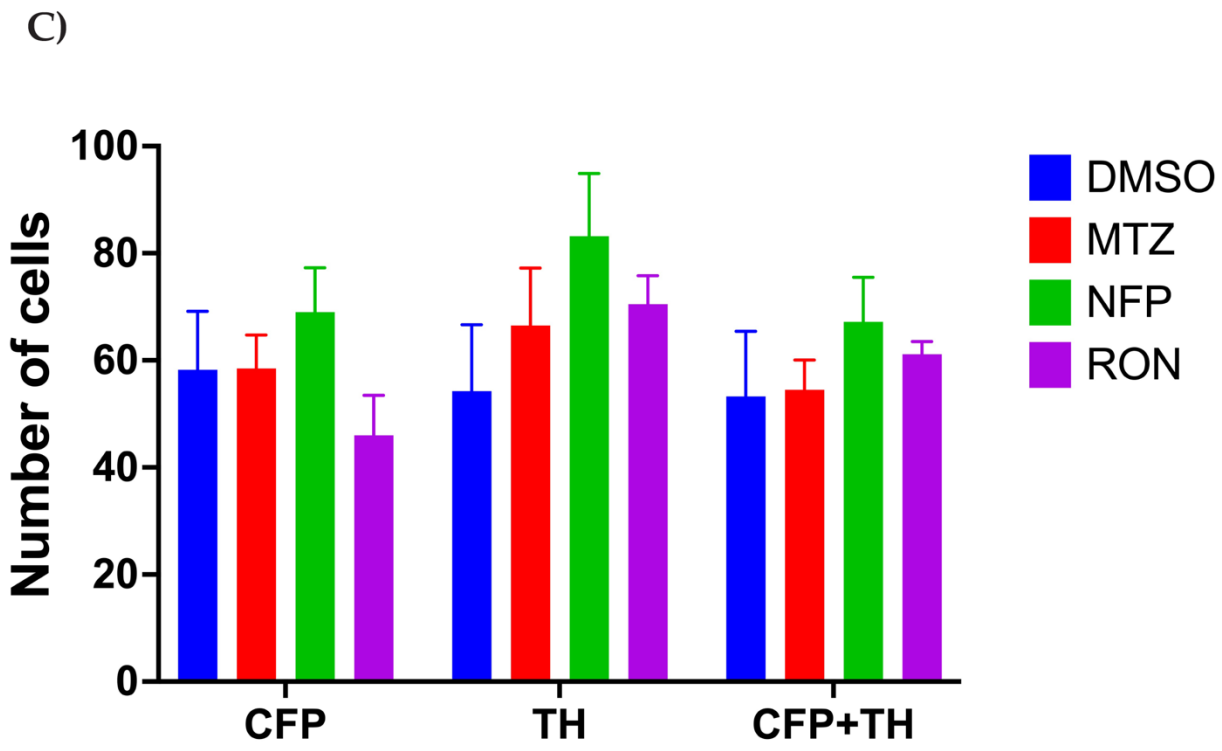

Figure 14. Dopaminergic neurons ablation in the diencephalon (7 dpt). (A) Schematic of the adult zebrafish brain showing the region that was analyzed. **(B)** TH (red) and CFP (green) labelling in vehicle and prodrug-treated fish. **(C)** Quantification at 7 dpt: a two-way ANOVA (factors: Cell type = CFP, TH, CFP+TH; Treatment = DMSO, MTZ, NFP, RON) showed no Cell type × Treatment interaction, $F(6,45)=0.65$, $p=0.691$; no main effect of Cell type, $F(2,45)=1.85$, $p=0.169$; and a non-significant trend for Treatment, $F(3,45)=2.52$, $p=0.070$. Tukey multiple comparison tests within each cell type detected no differences between any prodrug and DMSO (all adjusted $p\geq0.19$). Bars show mean±SEM; n per treatment per cell type: DMSO=4, MTZ=4, NFP=5, RON=6. (Scale bar = 50 µm).

3.3 Effects of prodrug administration on olfactory function

We next assessed whether the treated fish exhibited PD-like behavioural deficits, even in the absence of overt neuron loss. Two behavioural domains were tested: olfactory function and motor (locomotor) activity. Olfactory deficits are a known non-motor symptom of PD (Merhi et al., 2021), so we performed an odour avoidance assay using cadaverine, which has been previously shown to induce a repulsive behaviour in zebrafish (Hussain et al., 2013), to probe olfaction. In this test, fish were allowed to explore a tank freely. After acclimatization, the fish movement was recorded before cadaverine introduction. Then cadaverine was introduced to the arm in which the fish was located. The recording proceeded post-cadaverine addition, and the time spent in the odour zone before and after cadaverine addition was measured. Figure 15 summarizes the olfactory assay results. At both 1 dpt and 7 dpt, no significant differences were found in olfactory avoidance behaviour between vehicle-injected fish and any of the prodrug-injected groups. All fish, regardless of treatment, showed a robust aversion to the cadaverine side, spending very little time in the odour zone after stimulus introduction. The ratio of time spent in the cadaverine zone (post- vs. pre-odour introduction) was similar for vehicle and prodrug-treated fish (mean ± SEM overlaps between groups). Thus, chemogenetic treatment did not induce an olfactory impairment under our testing conditions. This contrasts with PD models in adult zebrafish, which have reported measurable olfactory deficits(Godoy et al., 2020; Razali et al., 2024). Our negative result is consistent with the lack of dopaminergic neuron loss in the olfactory bulbs across vehicle and prodrug-treated fish.

A)

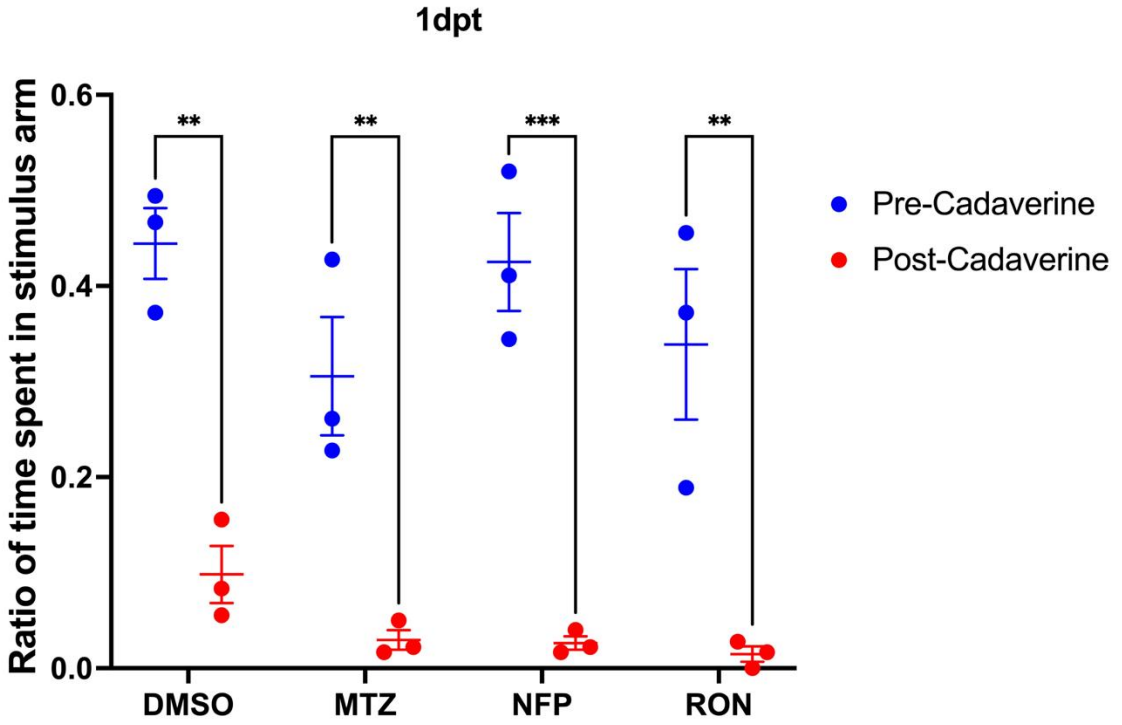
1dpt
Ratio of time spent in stimulus arm
0.6
0.4
0.2
0.0
**
**
***
**
DMSO
MTZ
NFP
RON
Pre-Cadaverine
Post-Cadaverine

B)

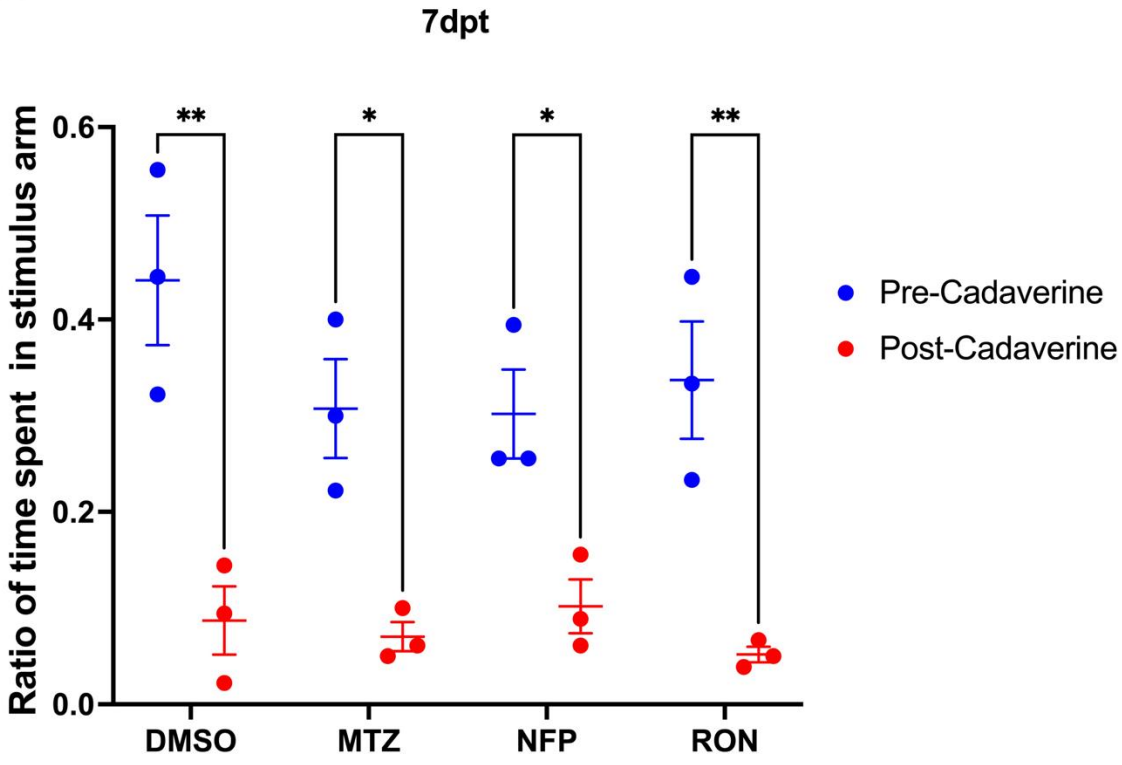
7dpt
Ratio of time spent in stimulus arm
0.6
0.4
0.2
0.0
**
*
*
**
DMSO
MTZ
NFP
RON
Pre-Cadaverine
Post-Cadaverine

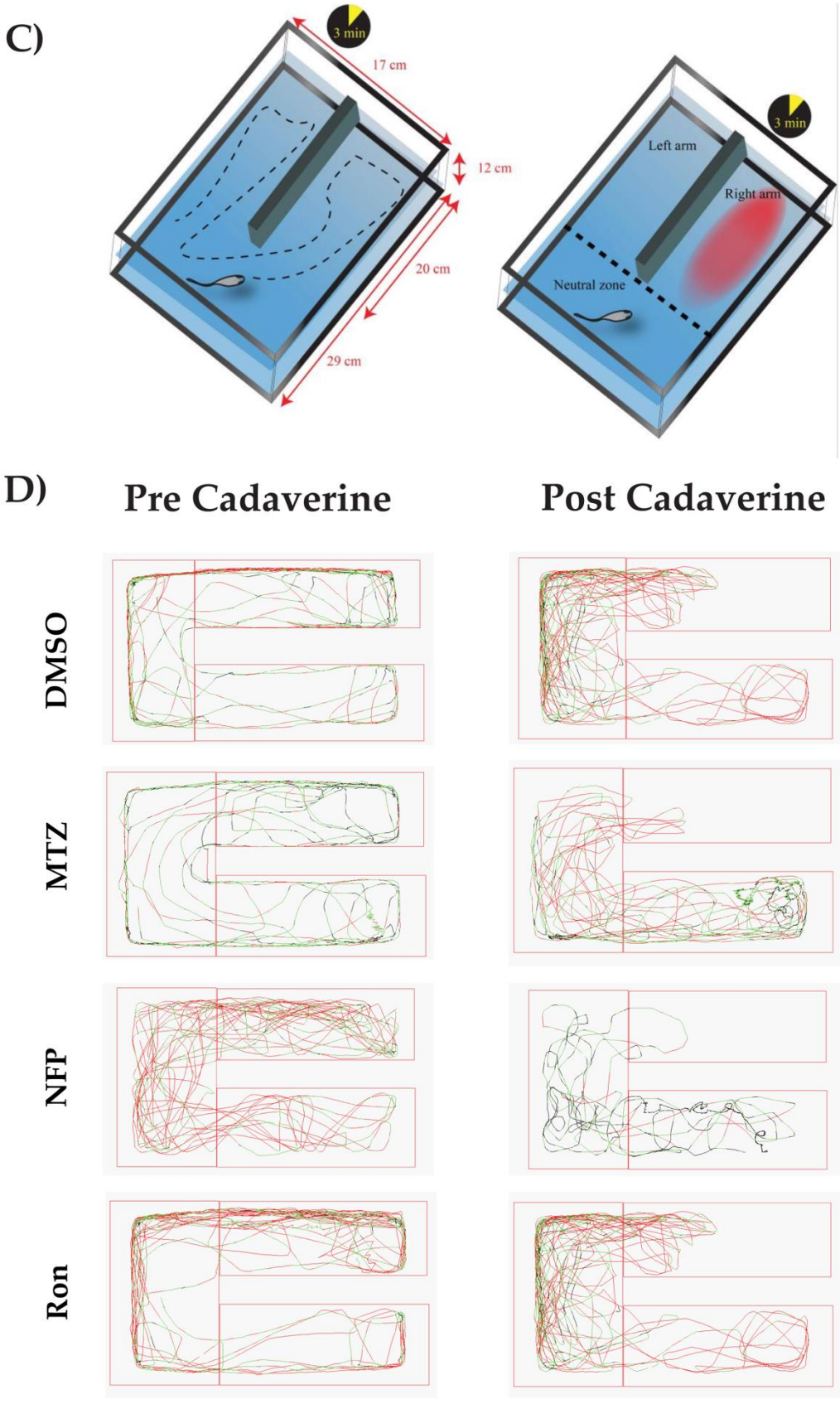
C)
3 min
17 cm
12 cm
20 cm
29 cm
3 min
Left arm
Right arm
Neutral zone
D)
Pre Cadaverine
Post Cadaverine
DMSO
MTZ
NFP
Ron

Figure 15. Olfactory behavioural assay at 1 and 7dpt. Olfactory function was assessed in an odour-avoidance task at 1 dpt and 7 dpt. **(A-B)** show the ratio of time spent in the stimulus arm before and after cadaverine addition. **(C)**, Schematic representation of the tank designed to address the OB phenotype. The tank contained a mid-tank wall separating space into 3 areas: left arm, right arm and neutral zone. Animals were allowed to swim freely for 3 min before the addition of the repulsive stimulus cadaverine. Animal response to the stimulus was recorded for 3 additional minutes. **(D)** shows swimming path images. Data are mean±SEM. (A): Two-way repeated-measures ANOVA (within-subject factor: Condition = pre vs. post cadaverine; between-subject factor: Treatment = DMSO, MTZ, NFP, RON) found no Condition × Treatment interaction, $F(3,8)=0.78$, $p=0.538$, and no main effect of Treatment, $F(3,8)=2.18$, $p=0.168$; Condition was significant, $F(1,8)=135.5$, $p<0.0001$. Across all treatments, pre- and post-cadaverine differences were significant (Šídák multiple comparison tests, adjusted $p=0.0005–0.0056$), confirming task sensitivity. n=12 fish total (3 per treatment). (B): Results were similar: no Condition × Treatment interaction, $F(3,8)=1.33$, $p=0.330$, and no Treatment effect, $F(3,8)=1.11$, $p=0.402$; Condition remained significant, $F(1,8)=87.56$, $p<0.0001$. Within each treatment, pre- and post-cadaverine differences were again significant (Šídák multiple comparison tests, adjusted $p=0.0011–0.0329$). These analyses indicate no olfactory deficit due to prodrug treatment at either time point.

3.4 Motor impact following prodrug administration

We also evaluated locomotor activity to detect any motor impairments analogous to PD bradykinesia or akinesia. At 1 dpt, we tracked spontaneous swimming in an open field arena for each fish. Figure 16(A-C) shows quantitative comparisons of total distance travelled, average swim velocity, and time spent stationary during a 10-minute trial. There were no significant locomotor differences among the four groups at 1 dpt (one-way ANOVAs for distance, speed, and stationary time: all $p > 0.25$). For example, mean distances moved ranged widely among individuals, but the group averages for MTZ, NFP, and RON were not significantly reduced compared to the DMSO group ($p>0.26$ for all pairwise comparisons). Representative swim trajectories (Figure 16D–G) illustrate that treated fish explored the tank similarly to controls. By 7 dpt, locomotor behaviour remained largely normal in all groups (Figure 17). Treated fish did not exhibit the reduced movement or freezing behaviour that would indicate Parkinsonian bradykinesia. Their swim paths and activity levels were comparable to DMSO-injected fish, reinforcing that no motor deficit emerged following the prodrug treatments.

Finally, we monitored locomotor activity over a longer term to see if any subtle changes developed at an intermediary or later time point. Figures 18–20 present the time course of three activity metrics (total distance travelled, swim velocity, and stationary duration) measured at 1-, 3-, 7-, and 16-days post-treatment. This longitudinal tracking also failed to reveal any treatment-related effects. A two-way ANOVA at each time course showed no main effect of treatment on distance travelled (Figure 18; $p=0.812$), swim speed (Figure 19; $p=0.785$), or inactivity time (Figure 20; $p=0.891$). There was also no treatment × time interaction in any measure, indicating that the trajectories of behavioural recovery or change were parallel across groups. All fish showed a slight reduction in activity at 7 dpt (likely due to handling or age), but this occurred similarly in

vehicle and prodrug-treated fish. By 16 dpt, activity levels had stabilized without significant group differences. In summary, none of the prodrugs induced motor impairments in adult zebrafish, in agreement with the histological finding that dopaminergic neurons were largely intact. The absence of behavioural phenotypes suggests that our chemogenetic ablation approach did not produce a Parkinson-like condition in these adult fish.

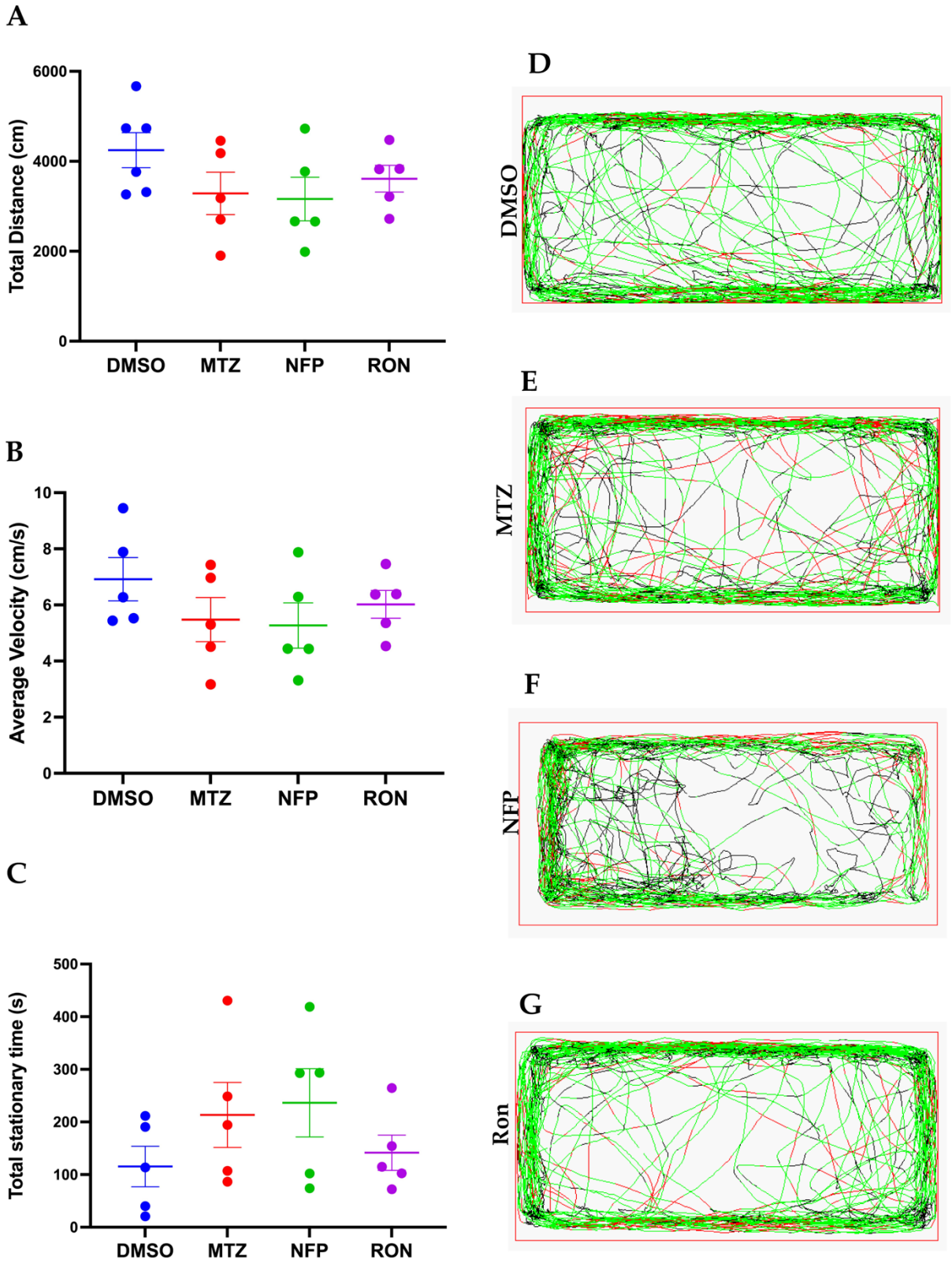
A
Total Distance (cm)
6000
4000
2000
0
DMSO
MTZ
NFP
RON
B
Average Velocity (cm/s)
10
8
6
4
2
0
DMSO
MTZ
NFP
RON
C
Total stationary time (s)
500
400
300
200
100
0
DMSO
MTZ
NFP
RON
D
DMSO
E
MTZ
F
NFP
G
Ron

Figure 16. Locomotor behaviour at 1 day post-treatment (1 dpt*).* (A-C) Quantification of locomotor activity at 1 dpt. **(D-G)** Example 5-min swim trajectories from a control and a prodrug-treated fish; individual paths vary, but group-level analyses showed no treatment effects. One-way ANOVAs across treatments found no differences in total distance travelled, $F(3,17)=1.45$, $p=0.263$; average velocity, $F(3,16)=1.02$, $p=0.408$; or total stationary time, $F(3,16)=1.25$, $p=0.326$. Dunnett's tests versus DMSO showed no pairwise differences (distance: adjusted $p=0.19–0.58$; velocity: 0.29–0.72; stationary time: 0.26–0.97). Data are mean±SEM; n (distance): DMSO=6, MTZ=5, NFP=5, RON=5; n (velocity and stationary time): 5 per group.

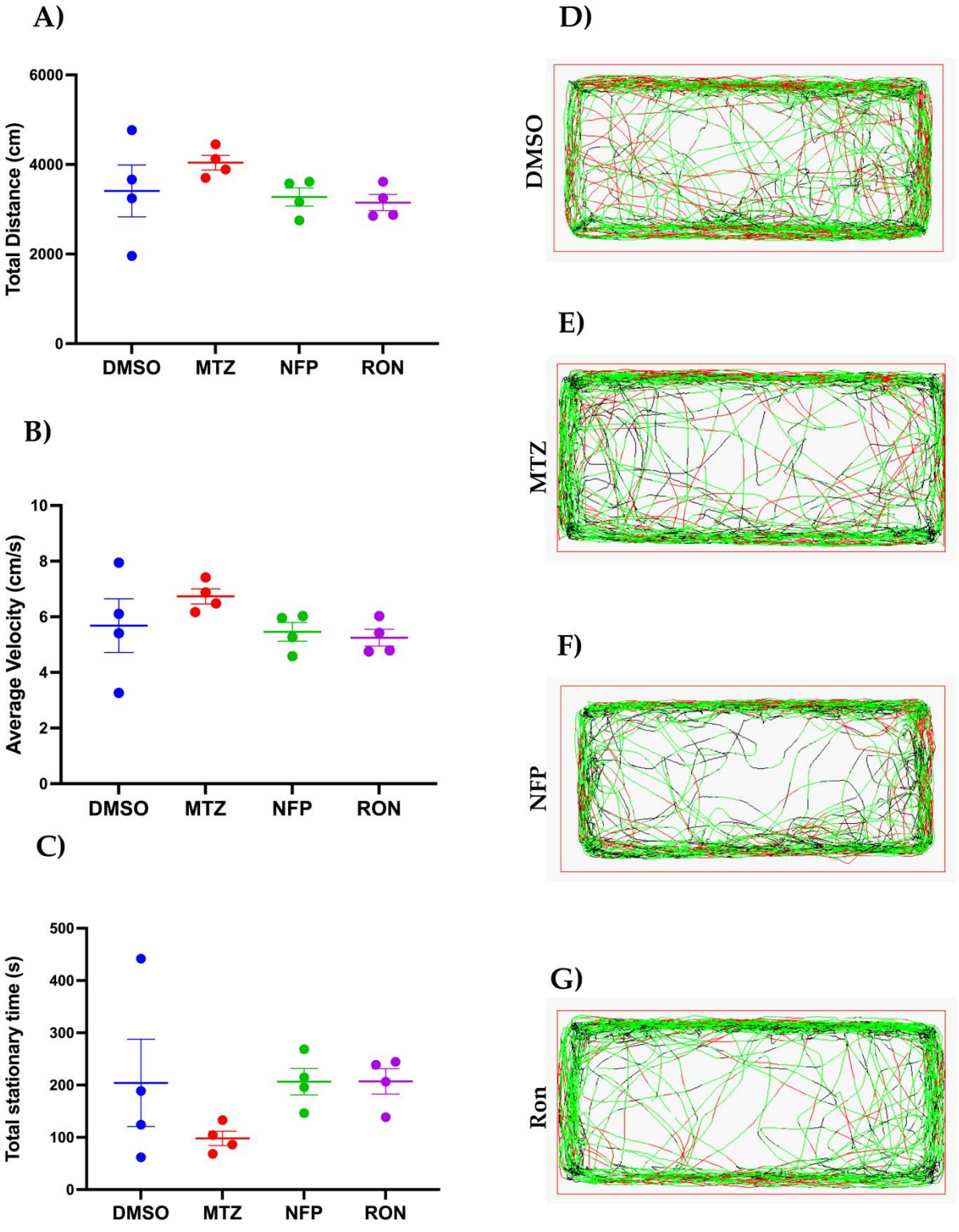
A)
Total Distance (cm)
6000
4000
2000
0
DMSO
MTZ
NFP
RON
B)
Average Velocity (cm/s)
10
8
6
4
2
0
DMSO
MTZ
NFP
RON
C)
Total stationary time (s)
500
400
300
200
100
0
DMSO
MTZ
NFP
RON
D)
DMSO
E)
MTZ
F)
NFP
G)
Ron

Figure 17. Locomotor behaviour at 7 days post-treatment (7 dpt). (A-C) Quantification of locomotor activity at 7 dpt. **(D-G)** Representative 5-minute swim paths from control and prodrug-treated fish show broadly similar exploratory activity. One-way ANOVAs across treatments detected no differences in total distance, $F(3,12)=1.44$, $p=0.281$; average velocity, $F(3,12)=1.44$, $p=0.281$; or total stationary time, $F(3,12)=1.39$, $p=0.292$. Dunnett's tests vs DMSO showed no pairwise differences (distance: adjusted $p=0.42–0.98$; velocity: 0.42–0.98; stationary time: 0.28–>0.9999). Data are mean±SEM; n=4 fish per treatment.

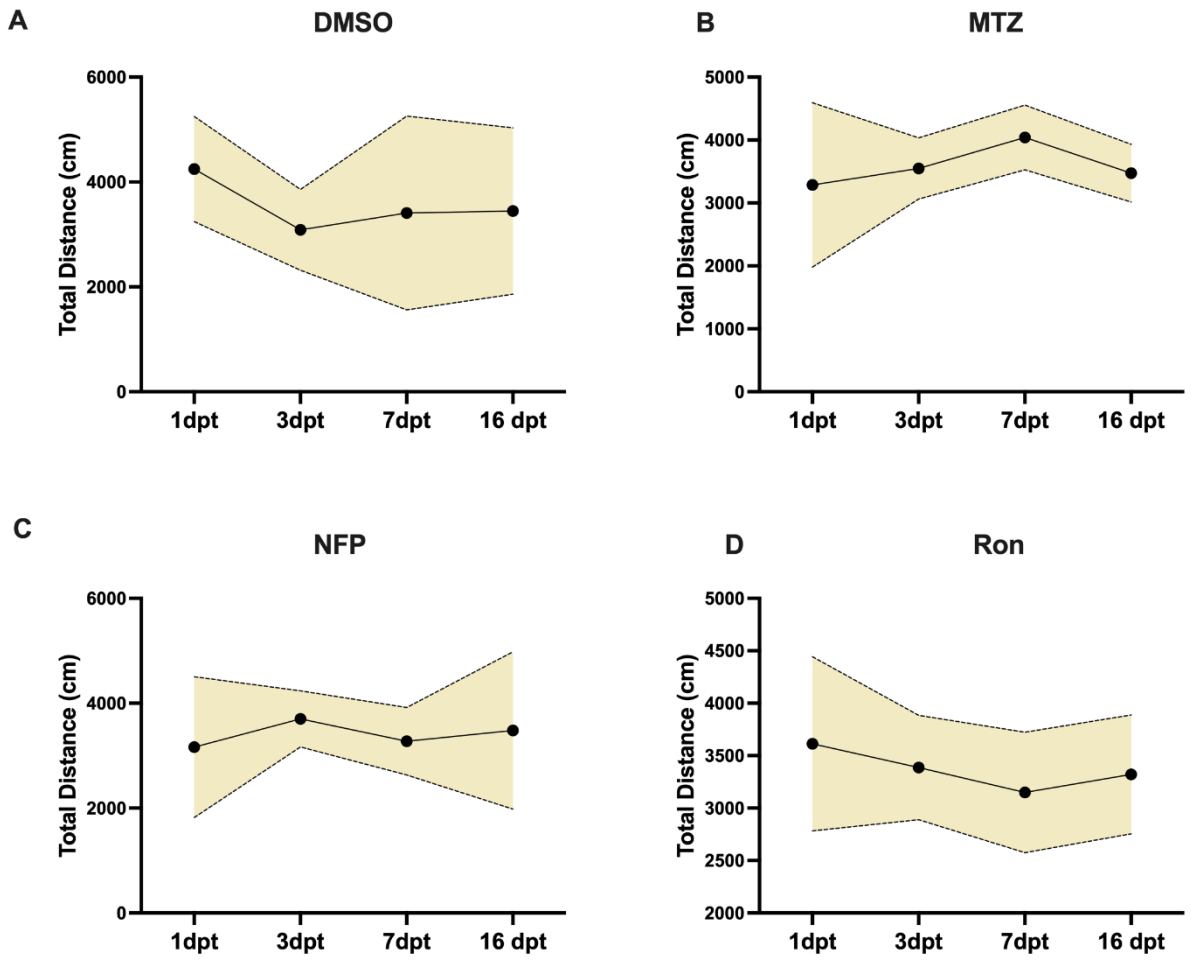

Figure 18. Time course of locomotor activity (total distance travelled). Mean total distance travelled at 1,3,7, and 16 dpt for vehicle and prodrug-treated fish. A two-way ANOVA (factors: Time point = 1, 3, 7, 16 dpt; Treatment = DMSO, MTZ, NFP, RON) detected no main effect of Time, $F(3,74)=0.24$, $p=0.867$, and no main effect of Treatment, $F(3,74)=0.32$, $p=0.812$. Tukey multiple comparison tests showed no pairwise differences between any prodrug and DMSO (all adjusted $p \geq 0.87$). The black line tracks the group mean over time. Shaded ribbons are the 95 % confidence intervals. Sample sizes per treatment: 1 dpt=5 each; 3 dpt=6 each; 7 dpt=4 each; 16 dpt: DMSO=3, MTZ=6, NFP=5, RON=6.

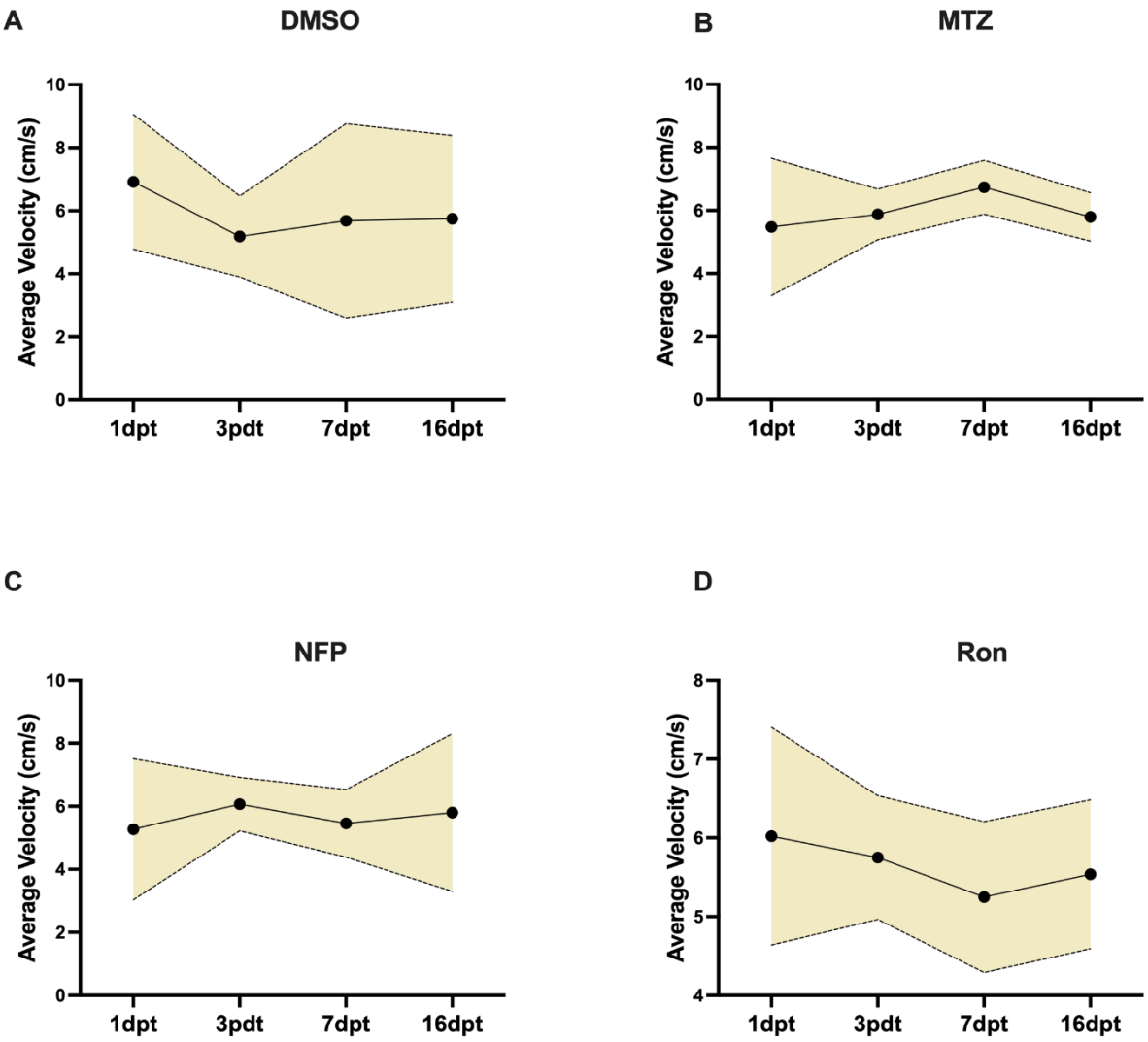

Figure 19. Time course of locomotor activity (average swim velocity). Mean swim speed (cm/s) at 1,3,,7 and 16 dpt for vehicle and prodrug-treated fish. Two-way ANOVA (Time point × Treatment) showed no interaction, $F(9,64)=1.09$, $p=0.381$, and no main effects of Time point, $F(3,64)=0.12$, $p=0.947$, or Treatment, $F(3,64)=0.356$, $p=0.785$. Tukey multiple comparison tests found no differences between any prodrug and DMSO (1 dpt: adjusted $p=0.27$–0.99; 3 dpt: 0.61–0.99; 7 dpt: 0.34–0.99; 16 dpt: ≥0.98). The black line tracks the group mean over time. Shaded ribbons are the 95 % confidence intervals. Sample sizes per treatment: 1 dpt=5 each; 3 dpt=6 each; 7 dpt=4 each; 16 dpt: DMSO=3, MTZ=6, NFP=5, RON=6.

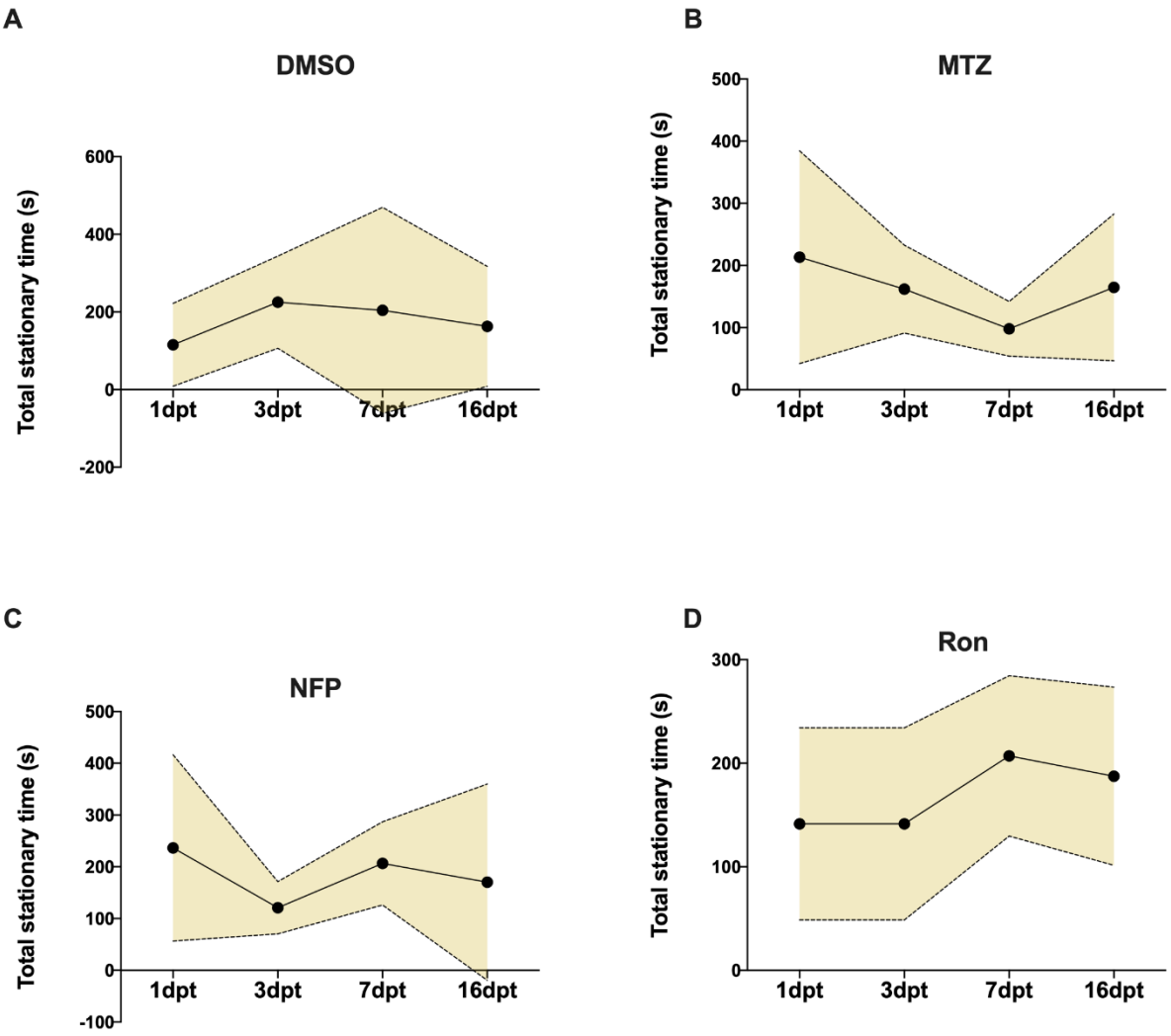

Figure 20. Time course of locomotor inactivity (stationary time). Mean stationary duration at 1,3,7, and 16 dpt for vehicle and prodrug-treated fish. Two-way ANOVA (Time × Treatment) showed no interaction, $F(9,61)=1.373$, $p=0.220$; no main effect of Time, $F(3,61)=0.116$, $p=0.951$; and no main effect of Treatment, $F(3,61)=0.208$, $p=0.891$. Tukey tests within each time point found no differences between any prodrug and DMSO (1 dpt: adjusted $p=0.217$–0.98; 3 dpt: 0.262–0.99; 7 dpt: 0.399–>0.9999; 16 dpt: 0.984–>0.9999). The black line tracks the group mean over time. Shaded ribbons are the 95 % confidence intervals. n per treatment: 1 dpt=5, 3 dpt=6, 7 dpt=4, 16 dpt: DMSO=3, MTZ=4, NFP=5, RON=6.

3.5 Development of an Adult Zebrafish Brain Dissociation Protocol (Single-Cell Preparation)

One of the aims of this study was to develop a practical and reproducible protocol for generating viable single-cell suspensions from adult zebrafish brains for downstream single-cell RNA sequencing. Although dissociation of adult brains has been achieved, the literature lacks detailed, cost-effective workflows, particularly methods that avoid reliance on automated or expensive machinery.

To begin addressing this gap, we evaluated cell viability after dissociating adult zebrafish brain tissue, and an initial Trypan Blue exclusion assay was performed under brightfield microscopy. This traditional method, in which dead cells uptake the blue dye while live cells exclude it, indicated that many cells were released (Figure 21), but poor uptake of trypan blue, poor contrast and the abundance of debris made viability estimates unreliable. Therefore, a more refined fluorescence-based strategy was pursued for clearer visualization and quantification of live and dead cells.

In the next step, we used the nuclear dye DAPI to stain the dissociated cells (Figure 22). DAPI brightly labels DNA but is membrane-impermeant, meaning it penetrates only cells with compromised membranes. As shown in Figure 22, DAPI staining revealed a uniform distribution of nuclei of various sizes, indicating successful dissociation into single cells. However, because DAPI stains only cells that are already non-viable or permeabilized, it cannot, by itself, distinguish live cells in a mixed population. In other words, DAPI nuclei represent dead or membrane-damaged cells, while viable cells remain unlabelled by DAPI and thus invisible to this stain. This limitation made it clear that DAPI alone is not suitable for a comprehensive viability assessment. An additional method was needed to visualize all cells (live and dead) simultaneously.

To achieve this, we refined our approach by using cell-permeant nuclear dyes in combination with a dead-cell indicator, allowing all nuclei to be visualized while specifically marking non-viable cells. In practice, we tested Hoechst 33342 and acridine orange as live-cell-permeant DNA stains, together with propidium iodide as a membrane-impermeant dead-cell stain. Both Hoechst 33342 and acridine orange readily penetrate live cell membranes and stain nuclear DNA (Hoechst emits blue fluorescence; AO emits green), whereas PI intercalates nucleic acids only in cells with compromised membranes (emitting red). Co-staining dissociated cells with these dyes enabled a dual readout: total nuclei (from Hoechst or AO) versus dead cells (PI-positive). Figure 23 illustrates the outcome of this double-staining viability assay. In Figure 23A, cells stained with Hoechst 33342 (blue) and PI (red) show predominantly purple nuclei in the merged image, indicating that many nuclei were co-stained by PI. Similarly, Figure 23B shows acridine orange (green) combined with PI (red), yielding a yellow overlap in most nuclei. The extensive co-localization of PI with the nuclear dyes in both panels suggests that a substantial fraction of cells was non-viable post-dissociation. In other words, many cells had compromised membranes that allowed PI entry, likely due to the staining process, mechanical or enzymatic stress from the dissociation protocol. This observation implies that the dissociation procedure or staining protocol strained the cells, resulting in a high proportion of membrane-damaged (PI-positive) cells.

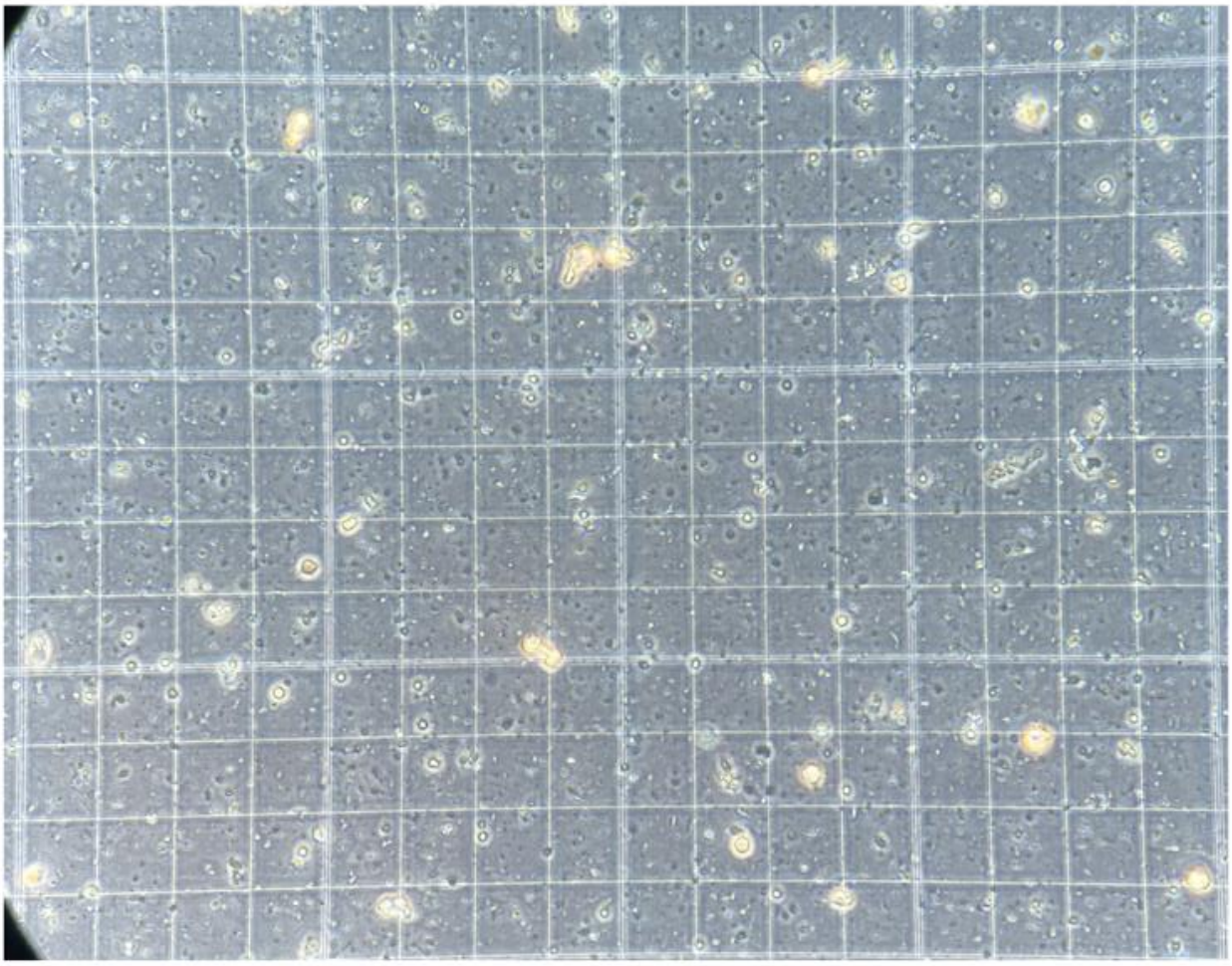

Figure 21. Trypan Blue Visualization of Dissociated Adult Zebrafish Brain Cells. Representative image showing cell suspension following enzymatic and mechanical dissociation of adult zebrafish brain tissue, stained with trypan blue. Although numerous cells are present, accurate assessment of cell viability was limited by low contrast and poor resolution under light microscopy, complicating the distinction between viable cells, dead cells, and debris. (Magnification 40X).

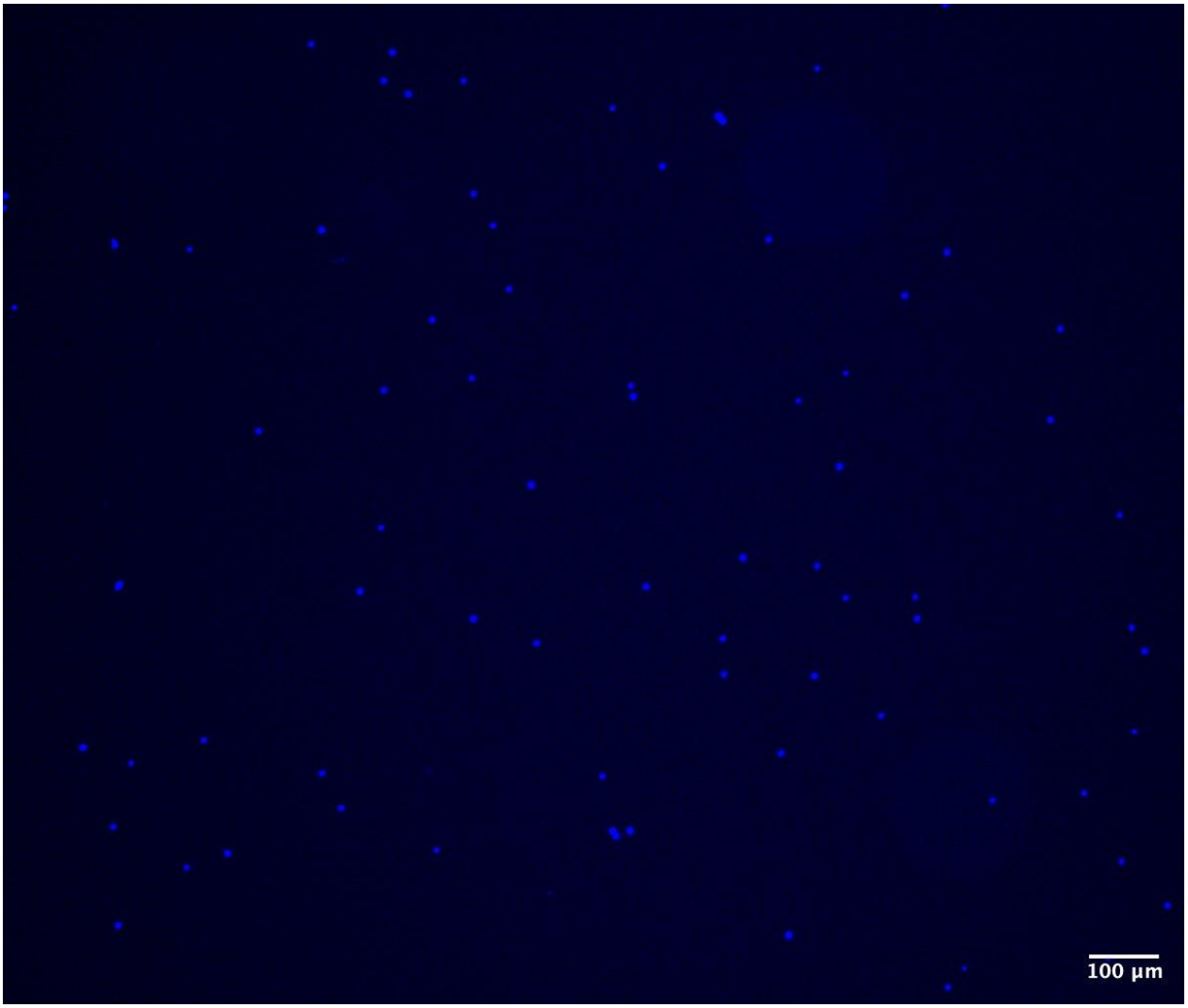

Figure 22. Representative epifluorescence image of dissociated adult zebrafish brain cells stained with DAPI (blue). Nuclei are uniformly dispersed and of variable size.

A)

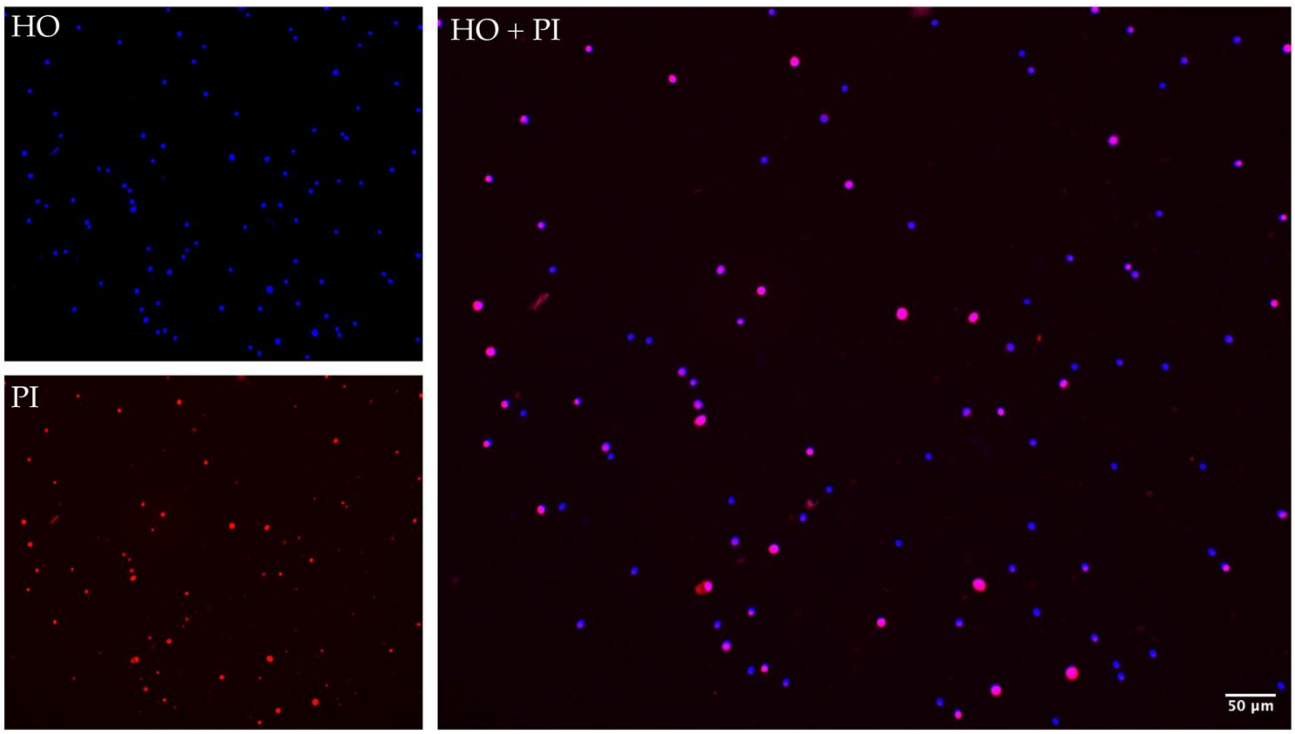

B)

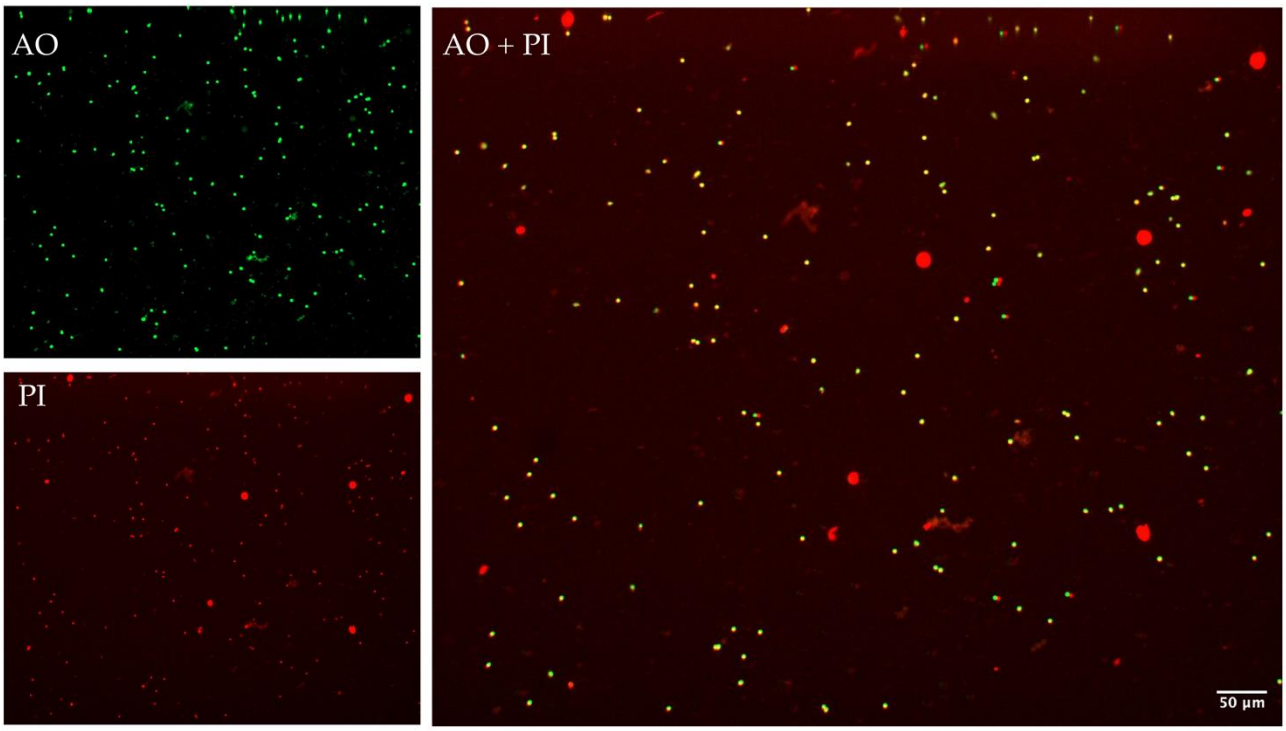

Figure 23. Post-dissociation cell viability assay. Live/dead fluorescent staining of dissociated adult zebrafish brain cells to assess viability for single-cell sequencing. **(A)** Cells were co-stained with Hoechst 33342 (nuclei, blue) and propidium iodide (dead-cell indicator, red). **(B)** Cells were co-stained with acridine orange (nuclei, green) and propidium iodide. The merged fluorescence image (A) shows predominantly blue/red cells, indicating most cells are not viable post-dissociation. The merged fluorescence image (B) shows a similar profile, indicating low viability post-dissociation.

4. Discussion

The results of the first half of this study were unexpectedly negative in terms of achieving dopaminergic neurodegeneration in adult zebrafish. Despite using a targeted chemogenetic ablation strategy, we observed no significant loss of dopaminergic neurons in the olfactory bulb, telencephalon, or diencephalon, and correspondingly no Parkinsonian behavioural deficits. In this section, we reflect on potential reasons for these negative findings and discuss improvements for future work to develop a robust adult zebrafish PD model.

4.1 Potential Factors Limiting Dopaminergic Neuron Ablation

Several factors may have contributed to the absence of detectable dopaminergic neuron ablation in our study. While the NTR-prodrug system has proven effective in larval zebrafish, its translation to adults introduces additional challenges. Differences in drug solubility, delivery, and distribution, the intrinsic catalytic efficiency of the enzyme, the regenerative potential of adult neurons, and technical limitations in imaging and quantification could each have played a role. The following sections will explore each of these constraints in detail.

4.1.1 Prodrug Solubility and Bioavailability

Several factors could explain why the NTR-prodrug system failed to ablate dopaminergic neurons in adult zebrafish. A major limitation relates to aqueous solubility and bioavailability, both of which directly determine whether sufficient prodrug concentrations can be achieved at the target neurons. According to the United States Pharmacopeia solubility classifications, all three compounds tested here are only sparingly soluble in water. Specifically, MTZ dissolves at ~10

mg/mL, RON at ~2.9 mg/mL, NFP at ~0.684 mg/mL (Table 3). Because cerebroventricular microinjection (CVMI) delivers compounds in very small volumes (hundreds of nanoliters), these low solubility limits imposed a ceiling concentration, beyond which the compounds could not be safely prepared or injected. Even though NFP and RON are intrinsically more potent substrates for NTR than MTZ (Bergemann et al., 2018; Lai et al., 2021), their poor solubility likely prevented sufficient drug accumulation in adult brain tissue to trigger ablation.

Beyond solubility, bioavailability further constrained effective dosing. Prodrugs were dissolved in 0.2% DMSO for injection, and any precipitation or instability during preparation or delivery could have reduced the amount of compound available in solution. In addition, diffusion from the ventricular space into deeper brain regions is inherently limited and declines with distance, while the complex extracellular architecture and increased myelination in adult zebrafish further restrict penetration (Jung et al., 2010; Siems et al., 2021; Syková & Nicholson, 2008). Thus, the bioavailable fraction of the injected dose may have been substantially lower than the nominal concentrations shown in Table 3. Indeed, while Table 3 indicates the doses prepared for injection, we did not directly measure drug levels in brain tissue. Future pharmacokinetic measurements will be essential to confirm whether effective prodrug concentrations reach dopaminergic neuron regions. Uneven distribution could also contribute; for example, if anterior regions such as the olfactory bulb received proportionally lower drug exposure, this could explain the lack of ablation in those cells.

4.1.2 Enzyme Efficiency and NTR Variant Constraints

Another critical factor is enzyme efficiency. While the *Tg(dat:CFP-NTR)* transgenic line robustly expresses the NTR enzyme in adult dopaminergic clusters, including the olfactory bulb,

telencephalon, preoptic area, pretectum, and diencephalon, evidence from (Godoy et al., 2020) confirms widespread colocalization of CFP-NTR with TH in these regions. This supports that the expression is not a limiting factor. Instead, the modest catalytic activity of NTR 1.0 appears to be central. First-generation NTR requires millimolar doses of prodrug and prolonged exposure to achieve ablation (Curado et al., 2007, 2008; Mathias et al., 2014), and even then, often shows cell-type variability and incomplete or resistant ablation (Sharrock et al., 2022). The lack of detectable dopaminergic neuron loss in our adult experiments likely reflects these constraints on enzyme efficacy, rather than expression ceiling. Notably, recent advances have resulted in an engineered NTR 2.0, a variant of NfsB with enhanced enzymatic efficacy, which provides ~100-fold higher MTZ-mediated ablation efficiency and enables sub-millimolar dosing, including in cell types previously described as hard to ablate (Sharrock et al., 2022). Accordingly, the use of NTR 1.0 is likely the most significant limiting factor in our ablation outcomes, reinforcing the recommendation to transition to NTR 2.0 for robust adult PD modelling (Mulligan & Mumm, 2024).

4.1.3 Timing of Ablation and Neuronal Regeneration

Drug activation timing and regenerative response might have also played a role. We examined fish at 1 and 7 days post-treatment, assuming that any neuron death would be evident by those times. It's possible that cell ablation was only partial or delayed, and that surviving neurons or neural progenitors quickly compensated. Adult zebrafish have a remarkable capacity for neuronal regeneration (Bhattarai et al., 2016; Reimer et al., 2009). If a fraction of dopaminergic neurons were damaged by the treatment but not immediately lost, they might recover function or be replaced by new neurons rapidly, especially by 7 dpt (Caldwell et al., 2019; Godoy et al., 2020).

Our observation of no significant dopaminergic cell loss even at 1 dpt suggests the initial injury was minimal, but we cannot rule out transient sub-lethal damage. It's conceivable that some DA neurons had reduced function or dopamine levels that we could not detect by counting cells. A more sensitive readout (such as measuring dopamine or TH protein levels via western blot or HPLC) might reveal subtle effects of prodrug treatment that our immunofluorescence cell counts missed. Additionally, suboptimal imaging (e.g., non-specific antibody signal and low signal-to-background in CFP-labelled sections) could bias the quantification, leading to an underestimation of neuronal loss. However, given that behavioural results were also negative, it appears unlikely that a substantial ablation occurred undetected.

4.1.4 Imaging and Quantification Limitations

Imaging and quantification limitations require careful consideration. We relied on manual counting of TH and CFP-labelled cells in brain sections. A significant drawback is that our counts may not fully capture neuron loss if the signal-to-noise ratio is low or if dying neurons lose TH immunoreactivity. For instance, neurons under stress might downregulate TH expression but still be present (Alam et al., 2017; Feng et al., 2014). We partially mitigated this issue by also counting CFP-positive cells, which label DA neurons regardless of their TH status. The absence of a drop in CFP-positive cells suggests it's unlikely that neurons were still present but lost TH. However, the precision of our cell counts was limited in crowded brain regions like the olfactory bulb, medial ventral telencephalon, and certain diencephalic clusters, where to signal-to-noise ratio made it difficult to detect subtle or moderate neuron loss. The signal-to-noise limitation is apparent in our histological images (Figure 9-12B), where background autofluorescence often competes with the true neuronal signal. While our 16 µm cryosections minimize scattering compared to thicker

vibratome sections (Adolf et al., 2006), autofluorescence from adult brain tissue remains a significant confounder. Such autofluorescence, arising from pigments, lipofuscin, or fixation-related artifacts, has been well documented in zebrafish and can reduce contrast in fluorescence microscopy (Billinton & Knight, 2001; Rajput et al., 2024). Recent improvements such as tissue clearing (e.g., TSA-PACT) have demonstrated >2-fold increases in signal-to-noise ratio in adult zebrafish brains (K. Wang et al., 2023), suggesting similar strategies, such as incorporating semi-automated image-analysis pipelines such as the open-source tools CellProfiler (Carpenter et al., 2006) or ilastik (Berg et al., 2019), would allow automated segmentation and quantification of fluorescently labelled neurons, reducing operator bias and improving throughput in cell quantification. Furthermore, improving imaging resolution or using transgenic reporters for cell death (e.g., activated caspase) could help detect subtle cell loss that our current methods may have missed.

In summary, the lack of detectable dopaminergic neuron ablation in adult zebrafish may reflect a combination of factors rather than a single limitation. Low aqueous solubility and restricted bioavailability of the prodrugs likely limited the concentrations that could be achieved by CVMI, while diffusion barriers and the architecture of the adult brain may have further reduced penetration into deeper regions. In addition, the modest catalytic activity of NTR 1.0 may have required higher exposure levels than could realistically be delivered, leaving neurons less responsive to ablation. It is also possible that transient or partial injury was masked by the rapid regenerative capacity of adult zebrafish neurons. Finally, technical considerations such as background autofluorescence and reliance on manual quantification could have reduced sensitivity to subtle changes. Together, these factors suggest that while the NTR–prodrug approach has been effective in larvae, its application in adults will likely require optimization of multiple components,

including enzyme variants (e.g., NTR 2.0), prodrug chemistry, delivery methods, and more sensitive readouts to achieve robust and interpretable outcomes in adult PD models.

4.2 Interpretation of Behavioural Results

Given that we did not ablate dopaminergic neurons, it follows that we also did not see classic PD-like behaviours. The treated adult fish showed normal olfactory responses and locomotor activity. In toxin-based adult zebrafish PD models, dopaminergic neuron loss typically leads to measurable phenotypes such as reduced swimming endurance or altered odour preference (Anichtchik et al., 2004; Vaz et al., 2018). Our behavioural assays were designed to detect such changes, yet all metrics remained comparable to the vehicle group. This consistency between histology and behaviour strengthens the conclusion that our interventions did not induce neurodegeneration.

One might wonder if the behavioural tests were sensitive enough. Prior studies have demonstrated its sensitivity to dopaminergic neuron loss. For example, (Godoy et al., 2020) showed that ablation of dopaminergic neurons in the olfactory bulb reduced zebrafish avoidance of cadaverine, while (Merhi et al., 2021) reported that loss of *parla* function similarly impaired olfactory bulb dopaminergic populations and resulted in diminished avoidance behaviour. In our case, all fish avoided the odour strongly, indicating intact olfaction. The locomotor assay was similarly sufficient to detect even subtle hypoactivity. We measured multiple parameters (distance, velocity, inactivity) and even tracked changes over more than two weeks. The consistency of normal behaviour across these measures provides confidence that no mild motor deficit was overlooked. It appears that unless there is actual dopaminergic cell loss or dysfunction, adult zebrafish do not develop PD-like symptoms spontaneously. This reinforces that achieving a loss-of-function at the neuronal level is a prerequisite for a valid disease model. It also highlights the

resilience or redundancy in the adult zebrafish motor system; partial lesions might be behaviorally compensated for by remaining circuits or by intrinsic plasticity. For example, even when ~50% of certain dopaminergic populations are lesioned by 6-OHDA, adult zebrafish show only transient or modest motor deficits (Vijayanathan et al., 2017). Our fish likely maintained full motor function because the dopaminergic system was essentially unperturbed by the treatments.

4.3 Future Directions and Improvements

While this study did not yield evidence of dopaminergic neuron ablation, the results highlight several clear avenues for methodological improvement. These future directions focus on enhancing the efficacy of the NTR-prodrug system, refining drug delivery approaches, optimizing treatment paradigms, and broadening behavioural assays to capture subtle phenotypes better. Together, these strategies aim to establish a more reliable and sensitive adult zebrafish model of Parkinson's disease.

4.3.1 Enhancing Enzyme Efficiency

Despite the negative results, this project has illuminated clear next steps to realize an improved adult zebrafish PD model. A top priority is to increase the efficacy of chemogenetic ablation. One approach is to utilize the aforementioned NTR 2.0 enzyme. This rationally engineered NTR variant has shown substantially enhanced cell-killing efficiency, enabling ablation of previously resistant cell types (Sharrock et al., 2022). We propose to generate a new transgenic zebrafish line, Tg(dat:CFP-NTR 2.0), where dopaminergic neurons express the NTR 2.0 enzyme. Such a line could be created by Tol2-mediated transgenesis, replacing the original nfsB sequence with the improved variant (Sharrock et al., 2022). With NTR 2.0, even the standard

prodrug metronidazole, a 5-nitroimidazole, yields far greater ablation than with first-generation NTR. By contrast, NTR 2.0 does not enhance activity with nifurpirinol (NFP), a 5-nitrofuran with a distinct heterocyclic scaffold and redox cycling mechanism, underscoring that structural class strongly influences enzyme compatibility (Bergemann et al., 2018; Maya et al., 2003; Sharrock et al., 2022). Ronidazole, like MTZ, is also a nitroimidazole, differing mainly in side-chain substitutions as shown in Table 3. Given this structural similarity and evidence that RON outperforms MTZ in zebrafish larvae at lower, less toxic concentrations (Lai et al., 2021), pairing RON with NTR 2.0 may achieve the ablation we originally sought. We will need to validate that the new transgenic expresses NTR 2.0 in all relevant dopaminergic neurons and that the enzyme is stable in adult fish (some prior attempts noted expression stability issues with certain NTR variants; Sharrock et al., 2022). If successful, the next experiments would treat Tg(dat:NTR2.0) fish with RON via CVMI and assess neuron loss and behaviour as done here. We anticipate a much higher likelihood of observing dopaminergic cell ablation with this upgraded system. Another improvement relates to drug delivery and distribution.

4.3.2 Optimizing Prodrug Delivery and Dosing

While CVMI proved feasible and presumably gave broad ventricular distribution, we could refine the technique to ensure maximal prodrug exposure. For example, administering a larger volume or using multiple injection sites (forebrain and midbrain ventricles) might help reach anterior regions like the olfactory bulb more effectively. Additionally, performing injections under conditions that prolong prodrug contact (such as temporarily reducing cerebrospinal fluid turnover or using a gelling agent to slow diffusion) (Hasanzadeh et al., 2023) could be explored. We will also consider the treatment schedule; our 5-day dosing might be optimized by extending to more

days or higher frequency, balanced against fish health. Any future protocol will include verifying actual brain concentrations of the prodrug or its active metabolite to confirm that sufficient dosing is achieved.

4.3.4 Expanding Behavioural Assessments

For the behavioural assessment, future studies should include additional tests to capture subtle phenotypes. In this thesis, we used straightforward locomotor and olfactory assays. Other groups have examined anxiety-like behaviour (light/dark preference, novel tank diving) and social behaviour (shoaling, startle response) in zebrafish PD models (Caldwell et al., 2019; Kysil et al., 2017). Incorporating such assays might reveal deficits that total distance swum does not. Moreover, if we successfully induce partial neuron loss in the future, we might expect only mild motor impairments that require more sensitive detection (e.g., altered gait or fine movement analysis). Coupling behavioural tests with pharmacological challenges such as levodopa rescue (Feng et al., 2014) could strengthen the characterization of any PD-like state.

4.4 Future Optimization of the Brain Dissociation Protocol

In summary, aim 2 (establishing an adult brain dissociation protocol) was only partially achieved. While we successfully dissociated adult zebrafish brains into single cells, we encountered limitations in assessing cell viability with standard fluorescent dyes. These issues highlight the need for more robust, quantitative viability assays to validate and optimize the health of dissociated cells. We therefore plan to implement a flow cytometry-based viability assay using the same dyes (Hoechst 33342 or Acridine Orange, propidium iodide, and Calcein-AM) to accurately distinguish live vs. dead cells and quantitatively assess viable cell yield in adult brain

cell suspensions. Flow cytometry will allow us to gate single cells, exclude debris, and obtain precise live/dead cell counts (Wlodkowic et al., 2011). By calibrating the instrument with appropriate control samples (e.g., fully killed cells vs. healthy cells), we can set fluorescence thresholds to define viability, providing a reliable metric for how gentle and effective our dissociation protocol is. We will also optimize enzymatic conditions (e.g., varying enzyme concentrations) and mechanical trituration to maximize cell yield while preserving cell integrity. Once a high-viability single-cell suspension is achieved, we can proceed with single-cell RNA sequencing to examine gene expression changes after dopaminergic cell ablation. Ultimately, combining an improved ablation model (with NTR 2.0 and potent prodrugs) with a robust single-cell analysis pipeline will enable us to probe the mechanisms of adult brain regeneration in response to dopamine neuron loss. The groundwork laid by this thesis, which identified the shortcomings of the first-generation model and established tools for cell collection, is guiding these future directions

5. Conclusion

This thesis represents an important step toward developing an adult zebrafish model of Parkinson's disease, even though the expected dopaminergic neuron ablation was not achieved. Using a chemogenetic approach combining nitroreductase (NTR) and prodrug activation with cerebroventricular microinjection, we observed no significant loss of dopaminergic neurons across key brain regions and no associated behavioural deficits.

Our findings suggest that the lack of ablation reflects a combination of limitations rather than a single failure. The sparing solubility and restricted bioavailability of the prodrugs limited the concentrations achievable within the small injection volumes, while the modest catalytic efficiency of the first-generation NTR (NTR 1.0) further reduced the likelihood of effective ablation. Additional factors, such as uneven drug distribution, rapid neuronal regeneration in adult zebrafish, and technical constraints of fluorescence imaging and manual quantification, may also have masked subtle neuronal loss.

Despite the absence of detectable ablation, these results provide meaningful insight. They underscore the differences between adult and larval PD models, clarify the shortcomings of current tools, and identify key areas requiring optimization. Importantly, this work establishes a foundation for improved strategies, including the adoption of more potent enzyme variants such as NTR 2.0, refined prodrug delivery and dosing, rigorous pharmacokinetic validation, and enhanced imaging and analysis workflows. Parallel efforts to optimize brain dissociation protocols for single-cell RNA sequencing will further enable mechanistic studies of adult dopaminergic neuron regeneration.

In summary, while the first-generation NTR/prodrug system proved insufficient for robust ablation in adult zebrafish, this thesis defines both the limitations, and the future directions needed

to establish a reliable adult PD model. By highlighting where current approaches fall short and laying out methodological pathways forward, this work contributes to the long-term goal of harnessing the zebrafish's regenerative capacity to better understand and eventually treat neurodegenerative diseases.

References

Abbate, A., Almasio, P. L., Mongitore, M., Vita, G. Di, & Patti, R. (2018). Necrotizing Soft Tissue Fasciitis after Intramuscular Injection. *Case Reports in Surgery*, *2018*, 3945497. https://doi.org/10.1155/2018/3945497

Adolf, B., Chapouton, P., Lam, C. S., Topp, S., Tannhäuser, B., Strähle, U., Götz, M., & Bally-Cuif, L. (2006). Conserved and acquired features of adult neurogenesis in the zebrafish telencephalon. *Developmental Biology*, *295*(1), 278–293. https://doi.org/10.1016/J.YDBIO.2006.03.023

Alam, G., Edler, M., Burchfield, S., & Richardson, J. R. (2017). Single Low Doses of MPTP Decrease Tyrosine Hydroxylase Expression in the Absence of Overt Neuron Loss. *Neurotoxicology*, *60*, 99. https://doi.org/10.1016/J.NEURO.2017.03.008

Anichtchik, O., Diekmann, H., Fleming, A., Roach, A., Goldsmith, P., & Rubinsztein, D. C. (2008). Loss of PINK1 Function Affects Development and Results in Neurodegeneration in Zebrafish. *Journal of Neuroscience*, *28*(33), 8199–8207. https://doi.org/10.1523/JNEUROSCI.0979-08.2008

Anichtchik, O. V., Kaslin, J., Peitsaro, N., Scheinin, M., & Panula, P. (2004). Neurochemical and behavioural changes in zebrafish Danio rerio after systemic administration of 6-hydroxydopamine and 1-methyl-4-phenyl-1,2,3,6-tetrahydropyridine. *Journal of Neurochemistry*, *88*(2), 443–453. https://doi.org/10.1111/J.1471-4159.2004.02190.X,

Antony, P. M. A., Diederich, N. J., Krüger, R., & Balling, R. (2013). The hallmarks of Parkinson's disease. *The FEBS Journal*, *280*(23), 5981–5993. https://doi.org/10.1111/FEBS.12335

Bai, Q., Mullett, S. J., Garver, J. A., Hinkle, D. A., & Burton, E. A. (2006). Zebrafish DJ-1 is evolutionarily conserved and expressed in dopaminergic neurons. *Brain Research*, *1113*(1), 33–44. https://doi.org/10.1016/J.BRAINRES.2006.07.057

Berg, S., Kutra, D., Kroeger, T., Straehle, C. N., Kausler, B. X., Haubold, C., Schiegg, M., Ales, J., Beier, T., Rudy, M., Eren, K., Cervantes, J. I., Xu, B., Beuttenmueller, F., Wolny, A., Zhang, C., Koethe, U., Hamprecht, F. A., & Kreshuk, A. (2019). ilastik: interactive machine learning for (bio)image analysis. *Nature Methods*, *16*(12), 1226–1232. https://doi.org/10.1038/S41592-019-0582-9;SUBJMETA=114,1305,1564,631,794;KWRD=IMAGE+PROCESSING,MACHINE+LEARNING,SOFTWARE

Bergemann, D., Massoz, L., Bourdouxhe, J., Carril Pardo, C. A., Voz, M. L., Peers, B., & Manfroid, I. (2018). Nifurpirinol: A more potent and reliable substrate compared to metronidazole for nitroreductase-mediated cell ablations. *Wound Repair and Regeneration : Official Publication of the Wound Healing Society [and] the European Tissue Repair Society*, *26*(2), 238–244. https://doi.org/10.1111/WRR.12633

Bhattarai, P., Thomas, A. K., Cosacak, M. I., Papadimitriou, C., Mashkaryan, V., Froc, C., Reinhardt, S., Kurth, T., Dahl, A., Zhang, Y., & Kizil, C. (2016). IL4/STAT6 Signaling Activates Neural Stem Cell Proliferation and Neurogenesis upon Amyloid-β42 Aggregation in Adult Zebrafish Brain. *Cell Reports*, *17*(4), 941–948. https://doi.org/10.1016/j.celrep.2016.09.075

Billinton, N., & Knight, A. W. (2001). Seeing the Wood through the Trees: A Review of Techniques for Distinguishing Green Fluorescent Protein from Endogenous

Autofluorescence. *Analytical Biochemistry*, *291*(2), 175–197. https://doi.org/10.1006/ABIO.2000.5006

Björklund, A., & Dunnett, S. B. (2007). Dopamine neuron systems in the brain: an update. *Trends in Neurosciences*, *30*(5), 194–202. https://doi.org/10.1016/J.TINS.2007.03.006

Björklund, A., & Lindvall, O. (1984). Dopamine-containing systems in the CNS. *Handbook of Chemical Neuroanatomy*, *2*(Part 1), 55–122.

Blaess, S., Stott, S. R. W., & Ang, S. L. (2020). The generation of midbrain dopaminergic neurons. *Patterning and Cell Type Specification in the Developing CNS and PNS: Comprehensive Developmental Neuroscience, Second Edition*, 369–398. https://doi.org/10.1016/B978-0-12-814405-3.00017-5

Blandini, F., & Armentero, M. T. (2012). Animal models of Parkinson's disease. *The FEBS Journal*, *279*(7), 1156–1166. https://doi.org/10.1111/J.1742-4658.2012.08491.X

Braak, H., Del Tredici, K., Rüb, U., De Vos, R. A. I., Jansen Steur, E. N. H., & Braak, E. (2003). Staging of brain pathology related to sporadic Parkinson's disease. *Neurobiology of Aging*, *24*(2), 197–211. https://doi.org/10.1016/S0197-4580(02)00065-9

Braak, H., Ghebremedhin, E., Rüb, U., Bratzke, H., & Del Tredici, K. (2004). Stages in the development of Parkinson's disease-related pathology. *Cell and Tissue Research*, *318*(1), 121–134. https://doi.org/10.1007/S00441-004-0956-9

Caldwell, L. J., Davies, N. O., Cavone, L., Mysiak, K. S., Semenova, S. A., Panula, P., Armstrong, J. D., Becker, C. G., & Becker, T. (2019). Regeneration of Dopaminergic Neurons in Adult Zebrafish Depends on Immune System Activation and Differs for Distinct Populations. *The Journal of Neuroscience*, *39*(24), 4694. https://doi.org/10.1523/JNEUROSCI.2706-18.2019

Carpenter, A. E., Jones, T. R., Lamprecht, M. R., Clarke, C., Kang, I. H., Friman, O., Guertin, D. A., Chang, J. H., Lindquist, R. A., Moffat, J., Golland, P., & Sabatini, D. M. (2006). CellProfiler: Image analysis software for identifying and quantifying cell phenotypes. *Genome Biology*, *7*(10), 1–11. https://doi.org/10.1186/GB-2006-7-10-R100/FIGURES/4

Cassar, S., Adatto, I., Freeman, J. L., Gamse, J. T., Iturria, I., Lawrence, C., Muriana, A., Peterson, R. T., Van Cruchten, S., & Zon, L. I. (2020). Use of Zebrafish in Drug Discovery Toxicology. *Chemical Research in Toxicology*, *33*(1), 95–118. https://doi.org/10.1021/ACS.CHEMRESTOX.9B00335,

Chen, Y. C., Cheng, C. H., Chen, G. Der, Hung, C. C., Yang, C. H., Hwang, S. P. L., Kawakami, K., Wu, B. K., & Huang, C. J. (2009). Recapitulation of zebrafish sncga expression pattern and labeling the habenular complex in transgenic zebrafish using green fluorescent protein reporter gene. *Developmental Dynamics : An Official Publication of the American Association of Anatomists*, *238*(3), 746–754. https://doi.org/10.1002/DVDY.21877

Cheng, H. C., Ulane, C. M., & Burke, R. E. (2010). Clinical Progression in Parkinson's Disease and the Neurobiology of Axons. *Annals of Neurology*, *67*(6), 715. https://doi.org/10.1002/ANA.21995

Chinta, S. J., & Andersen, J. K. (2005). Dopaminergic neurons. *The International Journal of Biochemistry & Cell Biology*, *37*(5), 942–946. https://doi.org/10.1016/J.BIOCEL.2004.09.009

Christofferson, A., & Wilkie, J. (2009). Mechanism of CB1954 reduction by Escherichia coli nitroreductase. *Biochemical Society Transactions*, *37*(Pt 2), 413–418. https://doi.org/10.1042/BST0370413

Clayton, D. F., & George, J. M. (1998). The synucleins: a family of proteins involved in synaptic function, plasticity, neurodegeneration and disease. *Trends in Neurosciences*, *21*(6), 249–254. https://doi.org/10.1016/S0166-2236(97)01213-7

Cookson, M. R. (2005). The biochemistry of Parkinson's disease. *Annual Review of Biochemistry*, *74*, 29–52. https://doi.org/10.1146/ANNUREV.BIOCHEM.74.082803.133400

Cortada, E., Yao, J., Xia, Y., Dündar, F., Zumbo, P., Yang, B., Rubio-Navarro, A., Perder, B., Qiu, M., Pettinato, A. M., Homan, E. A., Stoll, L., Betel, D., Cao, J., & Lo, J. C. (2024). Cross-species single-cell RNA-seq analysis reveals disparate and conserved cardiac and extracardiac inflammatory responses upon heart injury. *Communications Biology 2024 7:1*, *7*(1), 1–20. https://doi.org/10.1038/s42003-024-07315-x

Cosacak, M. I., Bhattarai, P., & Kizil, C. (2020). Protocol for Dissection and Dissociation of Zebrafish Telencephalon for Single-Cell Sequencing. *STAR Protocols*, *1*(1), 100042. https://doi.org/10.1016/j.xpro.2020.100042

Curado, S., Anderson, R. M., Jungblut, B., Mumm, J., Schroeter, E., & Stainier, D. Y. R. (2007). Conditional targeted cell ablation in zebrafish: a new tool for regeneration studies. *Developmental Dynamics : An Official Publication of the American Association of Anatomists*, *236*(4), 1025–1035. https://doi.org/10.1002/DVDY.21100

Curado, S., Stainier, D. Y. R., & Anderson, R. M. (2008). Nitroreductase-mediated cell/tissue ablation in zebrafish: A spatially and temporally controlled ablation method with applications in developmental and regeneration studies. *Nature Protocols*, *3*(6), 948–954. https://doi.org/10.1038/NPROT.2008.58,

Dauer, W., & Przedborski, S. (2003). Parkinson's disease: Mechanisms and models. *Neuron*, *39*(6), 889–909. https://doi.org/10.1016/S0896-6273(03)00568-3

Dinis-Oliveira, R. J., Remião, F., Carmo, H., Duarte, J. A., Navarro, A. S., Bastos, M. L., & Carvalho, F. (2006). Paraquat exposure as an etiological factor of Parkinson's disease. *Neurotoxicology*, *27*(6), 1110–1122. https://doi.org/10.1016/J.NEURO.2006.05.012

Dowd, F. J. (2017). Pharmacokinetics: The Absorption, Distribution, and Fate of Drugs. *Pharmacology and Therapeutics for Dentistry: Seventh Edition*, 15–43. https://doi.org/10.1016/B978-0-323-39307-2.00002-3

Doyle, J. M., & Croll, R. P. (2022). A Critical Review of Zebrafish Models of Parkinson's Disease. *Frontiers in Pharmacology*, *13*, 835827. https://doi.org/10.3389/FPHAR.2022.835827/BIBTEX

Edson, A. J., Hushagen, H. A., Frøyset, A. K., Elda, I., Khan, E. A., Di Stefano, A., & Fladmark, K. E. (2019). Dysregulation in the Brain Protein Profile of Zebrafish Lacking the Parkinson's Disease-Related Protein DJ-1. *Molecular Neurobiology*, *56*(12), 8306–8322. https://doi.org/10.1007/S12035-019-01667-W

Feng, C. W., Wen, Z. H., Huang, S. Y., Hung, H. C., Chen, C. H., Yang, S. N., Chen, N. F., Wang, H. M., Hsiao, C. Der, & Chen, W. F. (2014). Effects of 6-Hydroxydopamine Exposure on Motor Activity and Biochemical Expression in Zebrafish (Danio Rerio) Larvae. *Zebrafish*, *11*(3), 227. https://doi.org/10.1089/ZEB.2013.0950

Flinn, L. J., Keatinge, M., Bretaud, S., Mortiboys, H., Matsui, H., De Felice, E., Woodroof, H. I., Brown, L., McTighe, A., Soellner, R., Allen, C. E., Heath, P. R., Milo, M., Muqit, M. M. K., Reichert, A. S., Köster, R. W., Ingham, P. W., & Bandmann, O. (2013). TigarB causes

mitochondrial dysfunction and neuronal loss in PINK1 deficiency. *Annals of Neurology*, *74*(6), 837–847. https://doi.org/10.1002/ANA.23999

Flinn, L., Mortiboys, H., Volkmann, K., Kster, R. W., Ingham, P. W., & Bandmann, O. (2009). Complex I deficiency and dopaminergic neuronal cell loss in parkin-deficient zebrafish (Danio rerio). *Brain : A Journal of Neurology*, *132*(Pt 6), 1613–1623. https://doi.org/10.1093/BRAIN/AWP108

Gasiorowska, A., Wydrych, M., Drapich, P., Zadrozny, M., Steczkowska, M., Niewiadomski, W., & Niewiadomska, G. (2021). The Biology and Pathobiology of Glutamatergic, Cholinergic, and Dopaminergic Signaling in the Aging Brain. *Frontiers in Aging Neuroscience*, *13*, 391. https://doi.org/10.3389/FNAGI.2021.654931/BIBTEX

Godoy, R., Hua, K., Kalyn, M., Cusson, V. M., Anisman, H., & Ekker, M. (2020). Dopaminergic neurons regenerate following chemogenetic ablation in the olfactory bulb of adult Zebrafish (Danio rerio). *Scientific Reports*, *10*(1). https://doi.org/10.1038/S41598-020-69734-0

Godoy, R., Noble, S., Yoon, K., Anisman, H., & Ekker, M. (2015). Chemogenetic ablation of dopaminergic neurons leads to transient locomotor impairments in zebrafish larvae. *Journal of Neurochemistry*, *135*(2), 249–260. https://doi.org/10.1111/JNC.13214

Grattan, D. R. (2015). 60 YEARS OF NEUROENDOCRINOLOGY: The hypothalamo-prolactin axis. *The Journal of Endocrinology*, *226*(2), T101–T122. https://doi.org/10.1530/JOE-15-0213

Hasanzadeh, E., Seifalian, A., Mellati, A., Saremi, J., Asadpour, S., Enderami, S. E., Nekounam, H., & Mahmoodi, N. (2023). Injectable hydrogels in central nervous system: Unique and novel platforms for promoting extracellular matrix remodeling and tissue engineering. *Materials Today Bio*, *20*, 100614. https://doi.org/10.1016/J.MTBIO.2023.100614

Hussain, A., Saraiva, L. R., Ferrero, D. M., Ahuja, G., Krishna, V. S., Liberles, S. D., & Korsching, S. I. (2013). High-affinity olfactory receptor for the death-associated odor cadaverine. *Proceedings of the National Academy of Sciences of the United States of America*, *110*(48), 19579–19584. https://doi.org/10.1073/PNAS.1318596110/-/DCSUPPLEMENTAL

Jung, S., Kim, S., Chung, A., Kim, H., So, J., Ryu, J., Park, H., & Kim, C. (2010). Visualization of myelination in GFP-transgenic zebrafish. *Developmental Dynamics*, *239*(2), 592–597. https://doi.org/10.1002/DVDY.22166'))

Kalyn, M., Hua, K., Noor, S. M., Wong, C. E. D., & Ekker, M. (2019). Comprehensive Analysis of Neurotoxin-Induced Ablation of Dopaminergic Neurons in Zebrafish Larvae. *Biomedicines*, *8*(1). https://doi.org/10.3390/BIOMEDICINES8010001

Kizil, C., & Brand, M. (2011). Cerebroventricular Microinjection (CVMI) into Adult Zebrafish Brain Is an Efficient Misexpression Method for Forebrain Ventricular Cells. *PLoS ONE*, *6*(11). https://doi.org/10.1371/JOURNAL.PONE.0027395

Kouli, A., Torsney, K. M., & Kuan, W.-L. (2018). Parkinson's Disease: Etiology, Neuropathology, and Pathogenesis. *Parkinson's Disease: Pathogenesis and Clinical Aspects*, 3–26. https://doi.org/10.15586/CODONPUBLICATIONS.PARKINSONSDISEASE.2018.CH1

Kysil, E. V., Meshalkina, D. A., Frick, E. E., Echevarria, D. J., Rosemberg, D. B., Maximino, C., Lima, M. G., Abreu, M. S., Giacomini, A. C., Barcellos, L. J. G., Song, C., & Kalueff, A. V. (2017). Comparative Analyses of Zebrafish Anxiety-Like Behavior Using Conflict-Based Novelty Tests. *Zebrafish*, *14*(3), 197–208. https://doi.org/10.1089/ZEB.2016.1415,

Lai, S., Kumari, A., Liu, J., Zhang, Y., Zhang, W., Yen, K., & Xu, J. (2021). Chemical screening reveals Ronidazole is a superior prodrug to Metronidazole for nitroreductase-induced cell ablation system in zebrafish larvae. *Journal of Genetics and Genomics = Yi Chuan Xue Bao*, *48*(12), 1081–1090. https://doi.org/10.1016/J.JGG.2021.07.015

Lam, C. S., Korzh, V., & Strahle, U. (2005). Zebrafish embryos are susceptible to the dopaminergic neurotoxin MPTP. *European Journal of Neuroscience*, *21*(6), 1758–1762. https://doi.org/10.1111/J.1460-9568.2005.03988.X

Ma, P. M. (2003). Catecholaminergic systems in the zebrafish. IV. Organization and projection pattern of dopaminergic neurons in the diencephalon. *Journal of Comparative Neurology*, *460*(1), 13–37. https://doi.org/10.1002/CNE.10544

MacLeod, D., Dowman, J., Hammond, R., Leete, T., Inoue, K., & Abeliovich, A. (2006). The familial Parkinsonism gene LRRK2 regulates neurite process morphology. *Neuron*, *52*(4), 587–593. https://doi.org/10.1016/J.NEURON.2006.10.008

Mathias, J. R., Zhang, Z., Saxena, M. T., & Mumm, J. S. (2014). Enhanced cell-specific ablation in zebrafish using a triple mutant of escherichia coli nitroreductase. *Zebrafish*, *11*(2), 85–97. https://doi.org/10.1089/ZEB.2013.0937,

Maya, J. D., Bollo, S., Nuñez-Vergara, L. J., Squella, J. A., Repetto, Y., Morello, A., Périé, J., & Chauvière, G. (2003). Trypanosoma cruzi: effect and mode of action of nitroimidazole and nitrofuran derivatives. *Biochemical Pharmacology*, *65*(6), 999–1006. https://doi.org/10.1016/S0006-2952(02)01663-5

McKinley, E. T., Baranowski, T. C., Blavo, D. O., Cato, C., Doan, T. N., & Rubinstein, A. L. (2005). Neuroprotection of MPTP-induced toxicity in zebrafish dopaminergic neurons.

Brain Research. Molecular Brain Research, *141*(2), 128–137. https://doi.org/10.1016/J.MOLBRAINRES.2005.08.014

Merhi, R., Kalyn, M., Zhu-Pawlowsky, A., & Ekker, M. (2021). Loss of parla Function Results in Inactivity, Olfactory Impairment, and Dopamine Neuron Loss in Zebrafish. *Biomedicines*, *9*(2), 205. https://doi.org/10.3390/BIOMEDICINES9020205

Milanese, C., Sager, J. J., Bais, Q., Farrells, T. C., Cannons, J. R., Greenamyre, J. T., & Burtons, E. A. (2012). Hypokinesia and reduced dopamine levels in zebrafish lacking β- and γ1-synucleins. *The Journal of Biological Chemistry*, *287*(5), 2971–2983. https://doi.org/10.1074/JBC.M111.308312

Mulligan, T. S., & Mumm, J. S. (2024). Selective Cell Ablation Using an Improved Prodrug-Converting Nitroreductase. *Methods in Molecular Biology*, *2707*, 223–234. https://doi.org/10.1007/978-1-0716-3401-1_15,

Musacchio, J. M. (1975). Enzymes Involved in the Biosynthesis and Degradation of Catecholamines. *Biochemistry of Biogenic Amines*, 1–35. https://doi.org/10.1007/978-1-4684-3171-1_1

Nellore, J., & Nandita, P. (2015). Paraquat exposure induces behavioral deficits in larval zebrafish during the window of dopamine neurogenesis. *Toxicology Reports*, *2*, 950–956. https://doi.org/10.1016/J.TOXREP.2015.06.007

Nummenmaa, L., Seppälä, K., & Putkinen, V. (2022). Molecular Imaging of the Human Emotion Circuit. *Social and Affective Neuroscience of Everyday Human Interaction: From Theory to Methodology*, 3–21. https://doi.org/10.1007/978-3-031-08651-9_1

Pandey, S., Moyer, A. J., & Thyme, S. B. (2023). A single-cell transcriptome atlas of the maturing zebrafish telencephalon. *Genome Research*, *33*(4), 658–671. https://doi.org/10.1101/GR.277278.122/-/DC1

Pandey, S., Shekhar, K., Regev, A., & Schier, A. F. (2018). Comprehensive Identification and Spatial Mapping of Habenular Neuronal Types Using Single-Cell RNA-Seq. *Current Biology*, *28*(7), 1052-1065.e7. https://doi.org/10.1016/j.cub.2018.02.040

Pisharath, H., & Parsons, M. J. (2009). Nitroreductase-mediated cell ablation in transgenic zebrafish embryos. *Methods in Molecular Biology (Clifton, N.J.)*, *546*, 133–143. https://doi.org/10.1007/978-1-60327-977-2_9

Pisharath, H., Rhee, J. M., Swanson, M. A., Leach, S. D., & Parsons, M. J. (2007). Targeted ablation of beta cells in the embryonic zebrafish pancreas using E. coli nitroreductase. *Mechanisms of Development*, *124*(3), 218–229. https://doi.org/10.1016/J.MOD.2006.11.005

Rajput, N., Parikh, K., Squires, A., Fields, K. K., Wong, M., Kanani, D., & Kenney, J. W. (2024). Whole-brain mapping in adult zebrafish and identification of a novel tank test functional connectome. *BioRxiv*, 2024.08.16.607981. https://doi.org/10.1101/2024.08.16.607981

Razali, K., Kumar, J., & Mohamed, W. M. Y. (2024). Characterizing the adult zebrafish model of Parkinson's disease: a systematic review of dynamic changes in behavior and physiology post-MPTP administration. *Frontiers in Neuroscience*, *18*, 1432102. https://doi.org/10.3389/FNINS.2024.1432102/BIBTEX

Razali, K., Othman, N., Mohd Nasir, M. H., Doolaanea, A. A., Kumar, J., Ibrahim, W. N., Mohamed Ibrahim, N., & Mohamed, W. M. Y. (2021). The Promise of the Zebrafish Model

for Parkinson's Disease: Today's Science and Tomorrow's Treatment. *Frontiers in Genetics*, *12*, 553. https://doi.org/10.3389/FGENE.2021.655550/BIBTEX

Reimer, M. M., Kuscha, V., Wyatt, C., Sörensen, I., Frank, R. E., Knüwer, M., Becker, T., & Becker, C. G. (2009). Sonic hedgehog is a polarized signal for motor neuron regeneration in adult zebrafish. *Journal of Neuroscience*, *29*(48), 15073–15082. https://doi.org/10.1523/JNEUROSCI.4748-09.2009,

Ren, G., Xin, S., Li, S., Zhong, H., & Lin, S. (2011). Disruption of LRRK2 does not cause specific loss of dopaminergic neurons in zebrafish. *PloS One*, *6*(6). https://doi.org/10.1371/JOURNAL.PONE.0020630

Sager, J. J., Bai, Q., & Burton, E. A. (2010). Transgenic zebrafish models of neurodegenerative diseases. *Brain Structure & Function*, *214*(2–3), 285–302. https://doi.org/10.1007/S00429-009-0237-1

Sallinen, V., Torkko, V., Sundvik, M., Reenilä, I., Khrustalyov, D., Kaslin, J., & Panula, P. (2009). MPTP and MPP+ target specific aminergic cell populations in larval zebrafish. *Journal of Neurochemistry*, *108*(3), 719–731. https://doi.org/10.1111/J.1471-4159.2008.05793.X

Schober, A. (2004). Classic toxin-induced animal models of Parkinson's disease: 6-OHDA and MPTP. *Cell and Tissue Research*, *318*(1), 215–224. https://doi.org/10.1007/S00441-004-0938-Y

Sharrock, A. V., Mulligan, T. S., Hall, K. R., Williams, E. M., White, D. T., Zhang, L., Emmerich, K., Matthews, F., Nimmagadda, S., Washington, S., Le, K. D., Meir-Levi, D., Cox, O. L., Saxena, M. T., Calof, A. L., Lopez-Burks, M. E., Lander, A. D., Ding, D., Ji, H., … Mumm, J. S. (2022). NTR 2.0: a rationally engineered prodrug-converting enzyme

with substantially enhanced efficacy for targeted cell ablation. *Nature Methods*, *19*(2), 205–215. https://doi.org/10.1038/S41592-021-01364-4,

Sheng, D., Qu, D., Kwok, K. H. H., Ng, S. S., Lim, A. Y. M., Aw, S. S., Lee, C. W. H., Sung, W. K., Tan, E. K., Lufkin, T., Jesuthasan, S., Sinnakaruppan, M., & Liu, J. (2010). Deletion of the WD40 domain of LRRK2 in Zebrafish causes Parkinsonism-like loss of neurons and locomotive defect. *PLoS Genetics*, *6*(4). https://doi.org/10.1371/JOURNAL.PGEN.1000914

Sherer, T. B., Betarbet, R., Testa, C. M., Seo, B. B., Richardson, J. R., Kim, J. H., Miller, G. W., Yagi, T., Matsuno-Yagi, A., & Greenamyre, J. T. (2003). Mechanism of Toxicity in Rotenone Models of Parkinson's Disease. *Journal of Neuroscience*, *23*(34), 10756–10764. https://doi.org/10.1523/JNEUROSCI.23-34-10756.2003

Siems, S. B., Jahn, O., Hoodless, L. J., Jung, R. B., Hesse, D., Möbius, W., Czopka, T., & Werner, H. B. (2021). Proteome Profile of Myelin in the Zebrafish Brain. *Frontiers in Cell and Developmental Biology*, *9*, 640169. https://doi.org/10.3389/FCELL.2021.640169/XML

Spillantini, M. G., Crowther, R. A., Jakes, R., Hasegawa, M., & Goedert, M. (1998). alpha-Synuclein in filamentous inclusions of Lewy bodies from Parkinson's disease and dementia with lewy bodies. *Proceedings of the National Academy of Sciences of the United States of America*, *95*(11), 6469–6473. https://doi.org/10.1073/PNAS.95.11.6469

Sun, Z., & Gitler, A. D. (2008). Discovery and characterization of three novel synuclein genes in zebrafish. *Developmental Dynamics : An Official Publication of the American Association of Anatomists*, *237*(9), 2490–2495. https://doi.org/10.1002/DVDY.21569

Sveinbjornsdottir, S. (2016). The clinical symptoms of Parkinson's disease. *Journal of Neurochemistry*, *139*, 318–324. https://doi.org/10.1111/JNC.13691

Syková, E., & Nicholson, C. (2008). Diffusion in brain extracellular space. *Physiological Reviews*, *88*(4), 1277–1340. https://doi.org/10.1152/PHYSREV.00027.2007,

Turner, P. V., Brabb, T., Pekow, C., & Vasbinder, M. A. (2011). Administration of Substances to Laboratory Animals: Routes of Administration and Factors to Consider. *Journal of the American Association for Laboratory Animal Science : JAALAS*, *50*(5), 600. https://pmc-ncbi-nlm-nih-gov.proxy.bib.uottawa.ca/articles/PMC3189662/

Tysnes, O. B., & Storstein, A. (2017). Epidemiology of Parkinson's disease. *Journal of Neural Transmission 2017 124:8*, *124*(8), 901–905. https://doi.org/10.1007/S00702-017-1686-Y

Van den Heuvel, D. M. A., & Pasterkamp, R. J. (2008). Getting connected in the dopamine system. *Progress in Neurobiology*, *85*(1), 75–93. https://doi.org/10.1016/J.PNEUROBIO.2008.01.003

Vaz, R. L., Outeiro, T. F., & Ferreira, J. J. (2018). Zebrafish as an Animal Model for Drug Discovery in Parkinson's Disease and Other Movement Disorders: A Systematic Review. *Frontiers in Neurology*, *9*(JUN), 1. https://doi.org/10.3389/FNEUR.2018.00347

Vijayanathan, Y., Lim, F. T., Lim, S. M., Long, C. M., Tan, M. P., Majeed, A. B. A., & Ramasamy, K. (2017). 6-OHDA-Lesioned Adult Zebrafish as a Useful Parkinson's Disease Model for Dopaminergic Neuroregeneration. *Neurotoxicity Research*, *32*(3), 496–508. https://doi.org/10.1007/S12640-017-9778-X,

Wang, K., Yu, Y., Xu, Y., Yue, Y., Zhao, F., Feng, W., Duan, Y., Duan, W., Yue, J., Liao, Z., Fei, P., Sun, H., & Xiong, B. (2023). TSA-PACT: a method for tissue clearing and immunofluorescence staining on zebrafish brain with improved sensitivity, specificity and stability. *Cell and Bioscience*, *13*(1), 1–15. https://doi.org/10.1186/S13578-023-01043-1/FIGURES/8

Wang, Q., Liu, S., Hu, D., Wang, Z., Wang, L., Wu, T., Wu, Z., Mohan, C., & Peng, A. (2016). Identification of apoptosis and macrophage migration events in paraquat-induced oxidative stress using a zebrafish model. *Life Sciences*, *157*, 116–124. https://doi.org/10.1016/J.LFS.2016.06.009

Wang, X. H., Souders, C. L., Zhao, Y. H., & Martyniuk, C. J. (2018). Paraquat affects mitochondrial bioenergetics, dopamine system expression, and locomotor activity in zebrafish (Danio rerio). *Chemosphere*, *191*, 106–117. https://doi.org/10.1016/J.CHEMOSPHERE.2017.10.032

Wlodkowic, D., Telford, W., Skommer, J., & Darzynkiewicz, Z. (2011). Apoptosis and Beyond: Cytometry in Studies of Programmed Cell Death. *Methods in Cell Biology*, *103*, 55. https://doi.org/10.1016/B978-0-12-385493-3.00004-8

Xi, Y., Noble, S., & Ekker, M. (2011). Modeling neurodegeneration in zebrafish. *Current Neurology and Neuroscience Reports*, *11*(3), 274–282. https://doi.org/10.1007/S11910-011-0182-2

Xi, Y., Yu, M., Godoy, R., Hatch, G., Poitras, L., & Ekker, M. (2011). Transgenic zebrafish expressing green fluorescent protein in dopaminergic neurons of the ventral diencephalon. *Developmental Dynamics*, *240*(11), 2539–2547. https://doi.org/10.1002/dvdy.22742